

**EXPLORATORY DEVELOPMENT OF VARIM PROCESS FOR  
MANUFACTURING HIGH TEMPERATURE POLYMER MATRIX  
COMPOSITES**

---

A Dissertation presented to  
the Faculty of the Graduate School  
University of Missouri-Columbia

---

In Partial Fulfillment  
of the Requirements for the Degree  
Doctor of Philosophy

---

by

AHMED KHATTAB

Dr. A. Sherif El-Gizawy, Dissertation Supervisor

JULY 2005

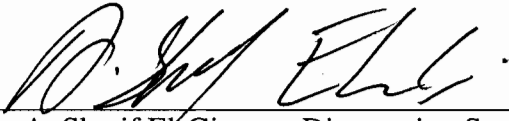
The undersigned, appointed by the Dean of the Graduate School, have examined  
the dissertation entitled

**EXPLORATORY DEVELOPMENT OF VARIM PROCESS FOR  
MANUFACTURING HIGH TEMPERATURE POLYMER MATRIX  
COMPOSITES**

presented by Ahmed Khattab

a candidate for the degree of Doctor of Philosophy

and hereby certify that in their opinion it is worth of acceptance



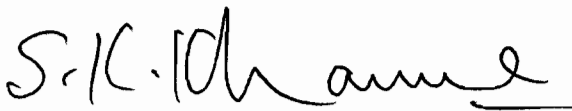
---

Dr. A. Sherif El-Gizawy, Dissertation Supervisor



---

Dr. Uee Wan Cho



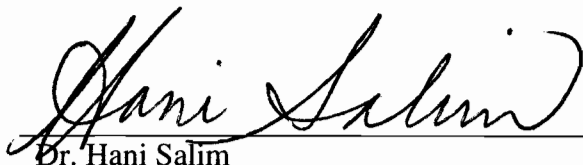
---

Dr. Sanjeev Khanna



---

Dr. Hongbin Ma



---

Dr. Hani Salim

Dedicated to my dear wife Eman

## ACKNOWLEDGMENTS

All Praise is due to the almighty God; the most Gracious and the most Merciful.

I would like to thank The Boeing Company for its financial support to this project. Also, I'd like to extend my special gratitude to Mr. Gregg Bogucki, of the Boeing Company, for his advice about the mechanical testing procedures.

I would like to thank Dr. Donald Adams at the University of Wyoming, Dr. Rajesh Shende at the University of Missouri-Columbia, and Dr. James Bryan at the University of Missouri-Columbia for their advices and their useful suggestions.

Also, I extend my gratitude to the entire staff of the Department of Mechanical and Aerospace Engineering at the University of Missouri-Columbia. The technical support of engineering workshop's crew, Mr. Richard Oberto, Mr. Brian Samuels, and Mr. Rix Gish, during my experiments is highly appreciated.

I would like to acknowledge all the members of my Ph.D. committee, Dr. Uee Wan Cho, Dr. Sanjeev Khanna, Dr. Hongbin Ma, and Dr. Hani Salim for reading the dissertation and for their constructive remakes.

I would like to express my deepest gratitude to my advisor, Dr. Sherif El-Gizawy, for his advice, guidance, and encouragement throughout my Ph.D. program.

I would like to express my special and deepest gratitude to my parents who are pushing me towards the success.

Last but not least, I would like to thank my dear wife, Eman, for her patience, support, sacrifices, and encouragement during the years of my study. Also, I'd like to express my love for my two sons, Karim and Khaled, who give me the smile and hope for the whole life.

## ABSTRACT

This research focuses on an exploratory development of vacuum assisted resin infusion molding (VARIM) process for manufacturing high temperature polymer matrix composites for high speed civil transport. The present study involves development of a comprehensive process virtual model and a physical model to relate the process conditions to the evolved properties and defects in the molded composites. The virtual model consists of three modules: the resin infusion stage; the resin cure stage; and the cure dependant mechanical properties. The physical model investigates the feasibility of VARIM for fabricating high temperature polymer composites and the behavior of the process with the change in its parameters. Characterization of properties, defects, and internal structure of produced composites is the major thrust in this study.

A virtual model for simulating the polymer flow behavior during the infusion stage was developed and verified experimentally, with capabilities for prediction of flow pattern, under the vacuum bagging, and evolved defects. The developed model of thermal and cure analysis was used to get a complete temperature and cure histories of the molded composites. The mechanical properties as functions of degree of cure and time were determined for 5250-4-RTM resin and eight-harness carbon fiber mats.

Based on the developed virtual model and with the appropriate mold design, sound panels, with internal voids content less than 1%, were successfully molded. Thus, the

VARIM process was found to be feasible for fabrication of high temperature polymer composites. The experimental investigation shows that post cure time and maximum cure temperature are the most significant parameters. Heating rate has a little effect on the process. As the maximum cure temperature decreases the material strength increases. Increasing post cure time from zero to five hours helps to increase the strength under high humidity and high temperature condition. The study shows that, within the range used for each parameter in the experimental design, a maximum cure temperature of 183°C, a post cure time of 5 hours at 227°C, and a heating rate of 1.67°C/min are the optimum process conditions for high-temperature and high-humidity applications. These curing conditions would maximize the mechanical properties of composites molded by VARIM.

The findings of this research will help in developing a science based technology for the VARIM process for understanding of the process behavior and the effects of various process parameters on the properties and integrity of the produced composites.

# TABLE OF CONTENTS

ACKNOWLEDGMENTS .....	ii
ABSTRACT .....	iv
LIST OF TABLES .....	x
LIST OF FIGURES .....	xii
LIST OF NOMENCLATURE .....	xvi
Chapter 1: INTRODUCTION.....	1
1.1 Problem Statement .....	1
1.2 Objectives .....	2
Chapter 2: LITERATURE REVIEW.....	4
2.1 Vacuum Assisted Resin Infusion Molding (VARIM) Process.....	4
2.2 Resin Flow Behavior.....	6
2.3 Resin Cure.....	10
Chapter 3: Investigation Approach.....	13
3.1 Process Modeling.....	13
3.1.1 Virtual Flow Module.....	13
3.1.2 Thermal and Cure Analysis Module .....	13
3.1.3 Cure Dependant Mechanical Properties Module .....	14
3.2 Experimental Evaluation of VARIM Process.....	14
3.2.1 Materials .....	14
3.2.2 Fabrication Process .....	15
3.2.3 Evaluation of Process-induced Properties .....	15



3.2.4 Experimental Design.....	16
Chapter 4: MODELING OF VARIM PROCESS.....	17
4.1 Virtual Flow Module.....	17
4.1.1 Numerical Modeling.....	18
4.1.2 Visual Presentation and Animation of the Results .....	23
4.1.3 Case Studies.....	23
4.2 Thermal and Resin Cure Analysis .....	29
4.3 Cure Dependant Mechanical Properties.....	32
4.3.1 Fiber Mat Structure.....	32
4.3.2 Shape Function Formulation.....	35
4.3.3 Stiffness Matrix Formulation.....	38
4.4 Discussion of Cure Modeling Results.....	43
4.4.1 Thermal and Cure Analysis Results.....	43
4.4.2 Composite Mechanical Properties Results.....	51
Chapter 5: EXPERIMENTAL INVESTIGATION OF VARIM PROCESS .....	60
5.1 Introduction.....	60
5.2 Materials .....	60
5.3 Experimental Procedure.....	63
5.4 Experimental Design.....	67
5.5 Specimens Preparation.....	69
5.6 Conditioning Chamber.....	71
Chapter 6: CHARACTERIZATION OF PROPERTIES OF COMPOSITES	
MOLDED BY VARIM.....	74

6.1 Introduction.....	74
6.2 Internal Structure of Molded Panels .....	75
6.3 Characterization of Room-Temperature Tensile Properties .....	77
6.3.1 Test Procedure .....	77
6.3.2 Data Collection .....	79
6.3.3 Response Analysis .....	84
6.4 Characterization of Compressive Properties of the Molded Materials under Different Environmental Conditions .....	90
6.4.1 Room Temperature Compression Test .....	90
6.4.1.1 Test Procedure .....	90
6.4.1.2 Data Collection .....	91
6.4.1.3 Response Analysis .....	93
6.4.2 High Temperature- Dry Compression Test.....	96
6.4.2.1 Test Procedure .....	96
6.4.2.2 Data Collection .....	98
6.4.2.3 Response Analysis .....	102
6.4.3 High Temperature- Wet Compression Test.....	107
6.4.3.1 Test Procedure .....	107
6.4.3.2 Data Collection .....	108
6.4.3.3 Response Analysis .....	111
6.5 Discussion of Experimental Results .....	114
6.6 Empirical Model of VARIM Process .....	119
6.7 Comparison of Properties of Composites Produced by .....	129

## VARIM and other Molding Techniques

Chapter 7: CONCLUSIONS AND RECOMMENDATIONS .....	131
7.1 Introduction.....	131
7.2 Conclusions.....	132
7.3 Recommendations.....	134
APPENDIX A.....	135
APPENDIX B.....	141
APPENDIX C.....	144
APPENDIX D.....	150
REFERENCES .....	153
VITA.....	159

## LIST OF TABLES

Table	Page
4.1 Kinetic parameters for 5250-4-RTM resin .....	43
4.2 Some case studies used to produce composite panel by VARIM .....	44
4.3 Elastic properties of the carbon fiber AS4 and 5250-4-RTM resin.....	51
4.4 Cure dependent properties for carbon fiber/5250-4-RTM resin.....	57
5.1 Control factor levels corresponding to their coded levels .....	68
5.2 Three parameter central composite design .....	68
6.1 Percentage of voids obtained by image analysis for some samples produced by VARIM .....	76
6.2 Process parameters effect on ultimate tensile strength for each case .....	82
6.3 Process parameters effect on tensile modulus for each case .....	83
6.4 Analysis of variance for ultimate tensile strength .....	87
6.5 Analysis of variance for tensile modulus at room temperature .....	89
6.6 Process parameters effect on compressive strength at room temperature .....	92
6.7 Analysis of variance for max compressive strength at room temperature.....	95
6.8 Process parameters effect on the compressive strength for high temp-dry .....	100
6.9 Process parameters effect on the compressive modulus for each case .....	101
6.10 Analysis of variance for compressive strength at high temperature-dry .....	104
6.11 Analysis of variance for compressive modulus at high temperature-dry .....	107
6.12 Percentage of weight gain after condoning and at time of test.....	108
6.13 Process parameters effect on the compressive strength for high temp-wet.....	110

6.14	Analysis of variance for compressive strength at high temperature-wet.....	113
6.15	Analysis of variance for compressive strength at high temperature-wet.....	120
6.16	Predicted strength and corresponding percent error of model for each case...	121
6.17	Optimum process parameters and the model predicted response.....	122
6.18	Response polynomial coefficients for maximum compressive strength .....	123
6.19	Predicted strength and corresponding percent error of model for each case...	124
6.20	Optimum process parameters and the model predicted response.....	125
6.21	Response polynomial coefficients for maximum compressive strength .....	126
6.22	Predicted strength and corresponding percent error of model for each case...	127
6.23	Optimum process parameters and the model predicted response.....	128

## LIST OF FIGURES

Figure	Page
4.1 Schematic diagram of the experimental setup.....	20
4.2 Resin flow front during infusion stage .....	26
4.3 The thick white line represents the actual resin flow front.....	26
4.4 Resin flow front with the effect of race-tracking during resin infusion .....	27
4.5 Race-tracking effect, (a) the flow front during infusion and (b) macro-void due to race-tracking effect at the end of mold filling .....	27
4.6 Macro-void due to race-tracking effect, (a) the simulation result and (b) the actual part (the thick white line surrounds an air void) .....	28
4.7 Resin flow front during infusion stage, a) experimental, b) simulation results, c) actual flow front near the end of infusion stage.....	28
4.8 Schematic of a top view of eight-harness carbon fiber mat .....	33
4.9 Geometry of a cross section of eight-harness carbon fiber mat, (a) a CAD drawing (b) a picture obtained by optical microscope for sample produced by VARIM.....	34
4.10 Geometry of eight-harness carbon fiber mat. Each section represents a cross section of the mat along the y-direction .....	34
4.11 Geometry of a cross section of eight-harness carbon fiber mat.....	35
4.12 Geometrical relation between the fill yarn and the warp yarn of 8H fiber mat .....	35
4.13 Variation of resin elastic modulus and Poisson's ratio with cure.....	41
4.14 Cure and temperature histories for case 1 .....	46
4.15 Distribution of degree of cure through the panel thickness along the length ....	47
4.16 Distribution of degree of cure through the panel thickness along the width.....	47
4.17 Distribution of temperature through the panel thickness along the length.....	48

4.18	Distribution of degree of cure through the panel thickness along the length ....	48
4.19	Cure and temperature histories for case 2 .....	49
4.20	Cure history comparison for cases 1 and 2 .....	49
4.21	Cure history comparison for cases 3 and 4 .....	50
4.22	Distribution of Young's modulus for section A-A at the end of cure cycle.....	52
4.23	Distribution of Young's modulus at an area with fiber undulation .....	53
4.24	Average of Young's modulus through the thickness and along the length .....	54
4.25	Average of Young's modulus through the thickness and along the length .....	54
4.26	Average of Young's modulus through the thickness and along the length for the 8 sections of the unit cell of a one-layer laminate.....	55
4.27	A laminate with six layers of carbon fiber randomly distributed .....	56
4.28	Average of Young's modulus through the thickness and along the length for the 8 sections of the unit cell of a six-layer laminate.....	56
4.29	Variation of Young's modulus with resin degree of cure .....	57
4.30	Variation of extensional stiffness with resin degree of cure .....	58
4.31	Variation of bending-extension stiffness with resin degree of cure .....	59
4.32	Variation of bending stiffness with resin degree of cure.....	59
5.1	Chemical structures of 5250-4 RTM resin components, taken from .....	62
5.2	Chemical structure of the combined 3-component 5250-4 RTM resin .....	62
5.3	Schematic diagram of the experimental setup .....	65
5.4	VARIM experimental setup-carbon fiber at the top of the mold .....	66
5.5	VARIM experimental setup-vacuum bag covers the mold .....	66
5.6	VARIM experimental setup.....	66
5.7	Machining of composite specimen using a special fixture.....	69

5.8	Lateral lines being cut in the composite panel .....	70
5.9	Machining of the edges of carbon fiber composite sample .....	70
5.10	Environmentally controlled chamber .....	72
5.11	Setup of conditioning chamber .....	73
5.12	Composite specimens loaded in the conditioning chamber.....	73
6.1	Scanning electron micrograph of composite material produced by VARIM....	75
6.2	Image analysis micrograph report showing the low micro-voids contents (average 0.25%).....	76
6.3	Dimensions in millimeter of coupon used in tensile test.....	78
6.4	Tension test setup for composite sample.....	78
6.5	Stress-strain curve of tensile test for one of the cases .....	79
6.6	Scatter plot of tensile strength for each case shown in table 6-2.....	82
6.7	Scatter plot of tensile modulus for each case shown in table 6-3.....	83
6.8	Average main effect of post cure time on ultimate tensile strength .....	84
6.9	Average main effect of max cure temperature on ultimate tensile strength.....	85
6.10	Average main effect of heating rate on ultimate tensile strength .....	85
6.11	Average main effect of heating rate on tensile modulus .....	88
6.12	Average main effect of post cure time on tensile modulus .....	88
6.13	Average main effect of max cure temperature on tensile modulus .....	89
6.14	Combined loading compressive test fixture .....	91
6.15	Scatter plot of tensile modulus for each case shown in table 6-6.....	92
6.16	Average main effect of post cure time on compressive strength.....	93
6.17	Average main effect of heating rate on compressive strength.....	94
6.18	Average main effect of max cure temperature on compressive strength .....	94



6.19	Combined load compression (CLC) modified fixture.....	96
6.20	One half of the CLC modified fixture showing the heating system.....	97
6.21	The specimen with the strain gage used in the compression test.....	98
6.22	Stress-strain curve for compression test of one of the cases.....	99
6.23	Scatter plot of compressive modulus for each case shown in table 6-8.....	100
6.24	Scatter plot of compressive modulus for each case shown in table 6-9.....	101
6.25	Average main effect of post cure time on compressive strength.....	102
6.26	Average main effect of max cure temperature on compressive strength.....	103
6.27	Average main effect of heating rate on compressive strength.....	103
6.28	Average main effect of max cure temperature on compressive modulus.....	105
6.29	Average main effect of post cure time on compressive modulus.....	105
6.30	Average main effect of heating rate on compressive modulus.....	106
6.31	Scatter plot of compressive modulus for each case shown in table 6-13.....	110
6.32	Average main effect of post cure time on compressive strength.....	111
6.33	Average main effect of max cure temperature on compressive strength.....	112
6.34	Average main effect of heating rate on compressive strength.....	112
6.35	Comparison between the measured and the predicted tensile strength.....	121
6.36	Predicted tensile strength versus measured tensile strength.....	122
6.37	Comparison between the measured and the predicted compressive strength..	124
6.38	Predicted compressive strength versus measured compressive strength.....	125
6.39	Comparison between the measured and the predicted compressive strength..	127
6.40	Predicted compressive strength versus measured compressive strength.....	128
6.41	Comparison between the VARIM, RTM and prepreg molding technique.....	130

## LIST OF NOMENCLATURE

- $A_{1, 2}$  : Arrhenius constants (1/s)
- $A_{ij}$  : Extensional stiffnesses (N/m)
- $B_{ij}$  : Bending-extension coupling stiffnesses (Pa m<sup>2</sup>)
- $C_A$  : Local concentration of the uncured resin
- $C_1$  : Initial concentration of uncured resin
- $c_p$  : Specific heat (J/kg K)
- $c_{pf}$  : Specific heat of fiber (J/kg K)
- $c_{pr}$  : Specific heat of resin (J/kg K)
- $D_{ij}$  : Bending stiffnesses (Pa m<sup>2</sup>)
- $E_m$  : Tensile modulus of matrix (GPa)
- $E_f$  : Tensile modulus of fiber (GPa)
- $E_k$  : Activation energy (J/mole)
- $G_m$  : Shear modulus of matrix (GPa)
- $G_f$  : Shear modulus of fiber (GPa)
- $H$  : Height (m)
- $h_t$  : Thickness of matrix top layer (m)
- $h_z$  : Yarn thickness (m)
- $K_{\text{eff}}$  : Effective permeability (m<sup>2</sup>)
- $K_{\text{race}}$  : Equivalent race tracking permeability (m<sup>2</sup>)

$K_{1, 2}$  : Reaction rate constants  
 $k$  : Thermal conductivity (W/m K)  
 $k_f$  : Thermal conductivity of fiber (W/m K)  
 $k_r$  : Thermal conductivity of resin (W/m K)  
 $n$  : Order of the reaction  
 $P$  : Pressure (N/m<sup>2</sup>)  
 $R$  : Universal gas constant  
 $R_a$  : Reaction rate (1/s)  
 $S_a$  : Source term due to chemical reaction (W/m<sup>3</sup>)  
 $t$  : Time (s)  
 $u_i$  : Velocity component of resin in  $x_i$  direction (m/s)  
 $V_f$  : Fiber volume fraction  
 $W$  : Width (m)  
 $w_f$  : Weight fraction of fiber  
 $w_r$  : Weight fraction of resin respectively  
 $x_g$  : Offset distance of the warp yarn from zero coordinate (m)  
 $z_o$  : Center line of fill yarn (m)  
 $z_u$  : Upper boundary of the fill yarn (m)  
 $z_l$  : Lower boundary of the fill yarn (m)  
 $a$  : Wavelength of a yarn (m)  
 $z_t$  : Boundary of elliptical shape of warp yarn (m)  
 $\varepsilon_{air}$  : Volume fraction of air

- $\varepsilon_{resin}$  : Volume fraction of resin
- $\rho_{air}$  : Density of air (kg/m<sup>3</sup>)
- $\rho_{resin}$  : Density of resin (kg/m<sup>3</sup>)
- $\mu_{air}$  : Viscosity of air (Pa s)
- $\mu_{resin}$  : Viscosity of resin (Pa s)
- $\Psi$  : Degree of cure
- $\Delta H$  : Heat of reaction (J/kg)
- $\rho$  : Density (kg/m<sup>3</sup>)
- $\rho_f$  : Density of fiber (kg/m<sup>3</sup>)
- $\rho_r$  : Density resin (kg/m<sup>3</sup>)
- $\theta$  : Angle between fiber direction and x-axis
- $\nu_m$  : Poisson's ratio of matrix
- $\nu_f$  : Poisson's ratio of fiber

# CHAPTER 1

## INTRODUCTION

### 1.1 Problem Statement

The Vacuum Assisted Resin Infusion Molding (VARIM) is a manufacturing process for composite structures [1-3]. In this process, the reinforcement, which is usually composed of several layers of woven fiber mats, is placed in an open mold and a plastic vacuum bag is placed on the top of the mold. The mold is connected with a resin source and a vacuum pump. As the vacuum is drawn through the mold, the liquid resin infuses into the reinforcing fiber mats. Curing and de-molding steps to finish the product follow this. In the vacuum assisted resin infusion molding (VARIM) process a highly permeable distribution fabric, known as distribution medium is used in order to accelerate the infusion process and to enhance the liquid resin penetration in the thickness direction [4]. VARIM has become very attractive fabrication technology in recent years because of its low cost tooling and scalability to very large structures. It minimizes the void contents inside the molded composites, reduces VOC emissions, and results in less scrap than other molding techniques [5, 6]. Nevertheless, VARIM has been used primarily with resin systems that cure at room temperature such as vinyl ester. High temperature polymer matrix composites for high performance applications that require cure at high temperature are currently produced by the autoclave/prepreg molding technique. This

process is not cost effective and limited to small size structures. The potentials of VARIM for fabricating high temperature polymer composite structures with properties and quality match those of the autoclave/prepreg molded ones are widely unexplored.

## **1.2 Objectives**

This research focuses on an exploratory development of VARIM process for manufacturing high temperature polymer matrix composites. It addresses material characterization, process verification and identification of transition pathways.

This work aims at developing a science-based technology for VARIM of high temperature polymer matrix composites for the understanding of the process behavior and the effects of various process parameters on the properties and integrity of the produced composites. Some important issues remain to be explored before high temperature VARIM can be widely used for variety of applications. Process-induced damage in the form of voids, and macro-voids (dry spots) developed during processing are reported as the most significant problems in liquid composite molding particularly for materials that cure at high temperature [6-9]. These process-induced defects can cause significant changes in the geometry and serious degradation of the mechanical properties of the molded structure. The absence of a knowledge base involving the processing-material-performance relationship for VARIM of high temperature polymer composites; delays the introduction of such strategic materials to the next generation high speed and light weight transports.

The numerical-experimental investigation will provide the capability for robust process and tooling design, prediction and characterization of process-induced damage and properties of high temperature polymer composites produced by VARIM. The following are the specific objectives of this study:

- Development of a predictive model based on control volume technique in order to characterize the polymer flow behavior in VARIM of composite structures.
- Development of a 3D finite difference model to determine composite thermal and cure histories during the cure cycle
- Determination of cure-dependent mechanical properties for eight-harness carbon /5250-4 resin system.
- Perform parametric tests using the design of experiments method on VARIM of the eight-harness carbon /5250-4 resin system, in order to investigate the effects of process parameters on the quality of the produced structures and to develop an empirical relationship between process parameters and the evolved properties.

## CHAPTER 2

### LITERATURE REVIEW

#### **2.1 Vacuum Assisted Resin Infusion Molding (VARIM) Process**

High temperature matrix composites are needed for high speed civil transport and advanced tactical fighters. Typical airframe materials for such applications must endure 120,000 hours at temperatures approaching 180°C (350°F) [10]. High temperature matrix composites are currently produced by autoclave/prepreg molding technique. This process is not cost effective and limited to small size structures. Uneven distribution of pressure and temperature during consolidation and curing of large parts are typical problems of the autoclave technique. Such problems can cause an uneven cure, warpage, voids, and low fiber volume fraction [7, 11]. Conventional resin transfer molding (RTM) is also used for manufacturing large composite parts using high temperature polymers. The low volume fraction of fibers (maximum value of 40%) that can be used in the process and the high concentration of voids (greater than 1%) in the molded composites limit RTM to the production of secondary structure members and light load applications. [12]. VARIM offers a manufacturing process of composite materials, which are more affordable than those from autoclave techniques. The application of VARIM manufacturing of the Lockheed Martin Joint Air-to-Surface Standoff Missile (JASSM) has showed cost savings over the autoclave process [13]. Also composite materials produced by vacuum



assisted show superior mechanical properties over those produced by RTM due to the high fiber volume fraction (up 60%).

Until recently, VARIM had not been used for high temperature polymer matrix composites because of the limitation of resins availability with low melt viscosity and low melt stability. Fortunately, the Cycom 5250-4-RTM resin system, introduced by Cytec Engineered Materials, satisfies these needs. This resin reaches very low viscosity during transfer and maintains a low viscosity for several hours. Laminates fabricated from this resin are capable of service temperatures up to 204°C (400°F) [14]. Higher processing temperatures are required to obtain composite materials for high temperature use. The high processing temperature in VARIM presents a challenge for bagging and sealing materials. Criss and Koon [15] used phenylethynyl terminated imides (PETI), which is a high temperature polymer, to fabricate composites using VARIM. The quality of the laminates was determined based on voids contents and mechanical properties. In this work, panels with 4% porosity showed mechanical performance suitable for structural applications. More work is needed to be done to refine the process conditions to reduce porosity and to improve properties.

A comprehensive review for the historical development of vacuum assisted resin infusion (VARI) was introduced by Williams et al. [16]. The study reviewed the progress of VARI from its first development by Macro [17] to the Seemann composites resin infusion manufacturing process (SCRIMP) [18]. The review showed that the development of VARI process has been slow (compared to RTM). Generally, there is little information

available about the properties and process-induced defects of high temperature polymer composites structures produced by VARIM processes. A better understanding of evolved mechanical properties and the significance of process-induced damage in these processes are required before the introduction of new composites systems in the design of large structures for high performance applications.

## **2.2 Resin Flow Behavior**

The proper infusion of the reinforcing fibers with the liquid polymer requires proper positioning of the inlets and outlets, close monitoring of mold temperature and vacuum pressure, and selection of optimum resin flow rate into the mold. Proper positioning of the filling port helps in eliminating the formation of voids and hence in generating composites parts with good quality. Trochu and Gauvin [19] employed a boundary-fitted finite difference method to model a two-dimensional RTM process. Their model is capable of obtaining the resin front and pressure distribution within the mold. They also discussed the limitations of finite difference method in modeling this process. They performed experiments and compared the experimental and numerical results. These investigators noticed the difference between numerical simulations and experimental observations of the resin front positions. They suggested that this difference is due to edge effects. However, they claimed that these edge effects could not be easily modeled numerically.

Later on, A. Hammami [20], and S.G. Advani [7] presented an analysis to describe the race-tracking (edge effect) using appropriate flow equation in an open channel (mold

edge) and Darcy's law in the porous medium. Then an equivalent permeability can be computed for the channel. Pillai and Advani [21] simulated the unsaturated flow encountered in woven fiber mats used in RTM, using a finite element method. The resin flow inside the mold is modeled as a flow through porous media. They presented results on simple flow at constant injection pressure in 1-D flow and constant flow rate radial injection flow. Diallo et al [22] developed a similar model. They addressed the effects of variation in the through thickness and in-plane porosity and permeability. Colestenian and El-Gizawy [23] performed both physical and numerical modeling using a finite element technique on the RTM process. The effects of injection pressure, resin viscosity, type of reinforcement, and mold geometry on mold filling times were investigated. Comparison between the experimental and numerical results of the resin front position indicated the importance of edge effects (race-tracking) in resin flow behavior in small cavities with larger boundary areas. Increasing the permeability at the edge region in the numerical model allowed for reasonable agreement between the numerical and the physical observations of the resin flow front position and mold filling time.

El-Gizawy and Kuan [24] used a control volume technique based on the finite difference method to characterize the polymer flow behavior in resin transfer molding of woven fiber composite structures. In their model, transient terms are considered in order to accurately describe the behavior of the polymer front during the injection stage. An analytical model [25] was introduced in order to investigate the role of vacuum pressure and port locations on flow front control for liquid molding processes. The parametric studies used in this investigation resulted in a relationship that captures the important

physics. This relationship can be used for flow front control and hence avoiding incomplete filling problems. In another study [26], a model was developed to analyze resin flow through a deformable fiber preform in VARIM process. The force balance between the resin and the fiber preform is used to account for the swelling of the preform inside the flexible vacuum bag. The application of the developed model was demonstrated using a large panel with complex geometry.

A recent study [27] introduced a new approach to get an optimum arrangement of gates and vents locations for RTM process design based on the mesh distance concept. In order to reduce the computational time for mold filling simulation, the proposed process used a genetic algorithm, instead of numerical simulation, to determine the gate and vent locations. The model was tested on several cases obtained from literature. The model was found effective, but further work needs to be done to include important process parameters, such as permeability and part thickness. Another study was conducted by B. Kim et al. [28], to determine the optimum gate location based on numerical simulation and optimization process using a genetic algorithm. The results were compared to experiments for several cases with different permeability and different part thickness. The results showed a good agreement between the algorithm and the experimental work. A. Gokce et al. [29] used branch and bound search to find the optimum gate locations in liquid composite molding process. The study is conducted in a virtual optimization and a control environment created by the integration of simulation software and math software. The method was compared with exhaustive search and genetic algorithms. The results were very promising for the case studies conducted for single gate optimization in RTM.

More research is needed to be conducted for multiple gate optimization problems. B. Minaie et al. [30] presented an inverse methodology that directly calculates the optimum inlet conditions in order to achieve a desired filling pattern such that the last point to fill (LPF) location coincides with the preset exit vent location that is specified during RTM process design. The proposed inverse algorithm was successfully applied to a rectangular mold with two inlet gates in order to determine the location of vent. The algorithm needs to be validated with different mold shapes, especially more complex shapes.

Choi and Dharan [31], addressed a novel process to overcome the decay in the pressure with distance from the inlet port in RTM. They proposed a process named articulated RTM in which the mold is designed to be articulated such that the mechanical action of the articulated segments create high local pressure that facilitate the fluid flow and hence reduce the mold filling time with less void generation. Smaller segments and a large number of segments result in shorter mold fill times [32]. However, this approach is very limited to small parts due to the tooling complexity and the high cost. P. Luca et al. [33] gave an overview of the liquid composite molding (LCM) process modeling issues with a review of preforming simulation in RTM. This study emphasized that the critical material parameter that drives the resin flow in the RTM simulation is the permeability.

Joubaud and Trochu [34] presented an approach to simulate vacuum assisted resin infusion based on an equivalent flexible mold permeability using an existing RTM software. The study showed that the porosity of the reinforcement and hence the permeability depend on the vacuum level under the flexible plastic bag. Then the

permeability measured in a stiff mold cannot be used to simulate the VARIM process. A modified value of permeability, called flexible mold permeability, was either measured experimentally or derived from the compressibility and permeability of the fabric. The comparison between an experimental case study and the simulation results showed a fairly good agreement. The simulation did not take into consideration the influence of the flow-enhancing layer, the infusion mesh, or the peel ply, which need to be investigated. Another experimental study was conducted by A. Hammami [35], to investigate the main factor affecting the permeability measurement in the VARIM process. The study investigated experimentally the effect of a flow enhancement layer and the infusion mesh. However, the use of the infusion mesh helped to reduce the filling time. The findings showed the need for additional experimental work, and also, for a simulation model covering the whole parameters which will help in reducing the experimental work needed.

### **2.3 Resin Cure**

A series of analysis on modeling the effect of cure on residual stress development in laminate composites was performed by White and Hahn [36-38]. Their two-dimensional model [36] was developed to predict cure and residual stress in an automotive process. They used cure dependent mechanical properties in their model. In a subsequent work, White and Hann [37, 38] presented experimental results on residual stress formation in an autoclave or hot press processing. Golestanian and El-Gizawy [39] presented results on cure-dependent properties of resin transfer molded thin composites with woven fiber mats. In this study, resin properties are assumed to change from viscoelastic liquid to

properties of the solid as the part cures. Osswald et al. [40] performed analysis on shrinking and warpage of compression-molded fiber reinforced composite parts. Their research concentrated on numerical simulation and experimental investigation of shrinkage and warpage in thin compression molded parts. Their numerical model incorporated cure-dependent mechanical properties of the composite. They considered the composite at a macroscopic scale and did not differentiate between the fiber and resin rich regions.

Bogetti and Gillespie [41] investigated thickness and autoclave temperature effects on formation of residual stresses in laminate composites. Their results indicated complex thermal and cure gradients in thick composite laminates. The effects of these gradients on process induced residual stresses were shown to be important. Tseng and Osswald [42] performed analysis on thermo-mechanical behavior of compression molded composite parts. They used a coupled temperature and stress simulation program to determine residual stress build up during curing of the part. They studied the effect of fiber content, part thickness, unsymmetrical curing and flow-induced fiber orientation on the shrinkage and warpage of the molded parts. Their results indicated a significant effect of warpage on fiber orientation. Their analysis was on compression molding of random fiber composites, since they considered thin composite parts, their thermal analysis was one-dimensional. They also neglected coupling between stretching and bending of the composite laminate. In an effort to simulate the entire VARIM process, a three-dimensional model was developed [43]. It constitutes modules for describing the resin flow, heat transfer, preform compaction, cure kinetics, and residual stresses during

infiltration and cure. The published work shows only the experimental verification of the resin flow module. They addressed VARIM process for resins that cure at room temperature (vinyl ester). Y. Kim and I. Daniel [44], conducted an experimental study to investigate the cure cycle effects on residual stress, and residual strain on new material fabricated by RTM process. Three different cure cycles with different peak temperature and different heat rates were used. The study showed that the residual stress developed at high cure temperature was lower than that developed at a lower cure temperature due to the constraint induced strain. The effect of different heat up rates was not that clear.

The literature review shows that a large portion of the published work on process modeling for woven fiber/high temperature polymer composites deals primarily with the conventional RTM process. Nevertheless, these findings and results could also help in the development of the science-based technology for VARIM processes using high temperature polymers. This work will address the gaps in the current literature and develop a more generic model to simulate the VARIM process. This comprehensive research covers both the infusion (polymer flow) stage and the cure stage. The numerical-experimental investigation will provide a capability for robust process and tooling design, prediction, and characterization of process-induced properties of high temperature polymer composites produced by VARIM.



## **CHAPTER 3**

### **Investigation Approach**

#### **3.1 Process Modeling**

To build a comprehensive process model, a series of simulation modules were developed. These modules cover resin infusion stage, resin cure stage, and cure dependant mechanical properties.

##### **3.1.1 Virtual Flow Module**

The first module deals with characterization of the resin flow behavior during the infusion stage. This model provides guidance for tooling design for efficient and defects free infusion of the resin. It helps in selecting the number and location of inlet and outlet ports in order to prevent the formation of dry spots and to allow for speedy infusion of the resin.

##### **3.1.2 Thermal and Cure Analysis Module**

Thermal and resin cure analysis are performed to model the cure stage of the VARIM process. The three-dimensional transient energy and species equations are solved within the composite part to determine the temperature and cure variations with time. The exothermic chemical reaction in the resin releases heat and thereby acts as a source term

in the energy equation. Thus the energy and species equations become coupled and need to be solved simultaneously. The degree of cure as a function of time and temperature are determined.

### **3.1.3 Cure Dependant Mechanical Properties Module**

Once the composite degree of cure is known with time, the stiffness matrices could be determined as functions of degree of cure and time. Classical Laminate Theory (CLT) is assumed to be applicable to the infinitesimal regions of the composite unit cell. Cure dependent mechanical properties of composite parts with eight-harness fiber mats are determined. Resin properties are assumed to change from that of a liquid to properties of a solid as the part cures. This module takes into account the fiber continuity and undulation. Resin rich areas between fiber bundles and the fraction of resin within the fiber bundles are taken into account too. The components of the stiffness, coupling stiffness, and bending stiffness matrices are modeled for the investigated systems. For the fill and warp yarns, the changes in fiber orientation due to fiber undulation are taken into account.

## **3.2 Experimental Evaluation of VARIM Process**

### **3.2.1 Materials**

The high temperature resin used is CYCOM 5250-4-RTM produced by CYTEC Engineered Materials in California. It is a one-part homogenous Bismaleimide (BMI) resin with some additives to improve toughness [45]. This polymer was developed for use in high performance structural composites requiring high temperature use up to 204 °C

(400 °F). Eight harness carbon woven satin fabrics, made of AS4 carbon fiber, are used in the present composite system to provide the needed reinforcing component.

### **3.2.2 Fabrication Process**

Composite panels with two different thicknesses are manufactured by VARIM using single vacuum port and single injection port system. The volume fraction of the fiber in the composite is maintained at about 58% value. The carbon fiber woven preform is placed on the top of an open mold, then covered and sealed with a vacuum bag. The mold is then connected with a resin source and a vacuum pump. The resin is drawn into the mold by the vacuum. The system is then be heated up to the predetermined maximum cure temperature at specific rate. Once the cure temperature is reached, the system is left to cure for 4 hours and then brought down to the room temperature immediately or after a post cure time at higher temperature.

### **3.2.3 Evaluation of Process-induced Properties**

Several samples of the produced panels are inspected for void contents using electron microscopy and image analysis technique. Tensile properties at room temperature are determined according to the ASTM D3039. Compressive properties are also determined according to the ASTM Standard D6641 using the combined loading compression (CLC) test fixture. Because the composite is being manufactured for use in aerospace applications, the material needs to be tested in such environments, which are high temperature and high humidity. Compression tests are conducted at room temperature and at elevated temperature of 177°C (350°F) dry and wet with 100% relative humidity,

to determine the response of these molded composite materials when stressed in these environments.

### **3.2.4 Experimental Design**

An experimental plan has been designed to study the effects of process variables. A partial factorial design of experiments involves three major parameters is conducted on VARIM for high temperature resin composites. The process variables in the design include: maximum curing temperature, heating rate during the cure stage, and post cure time at higher temperature after curing. In order to obtain generality and precision for the developed experimental database for the process, the experiments needed to generate the required data must be conducted in a systematic and organized way. The unifying feature of statistically designed experiments is that all factors of interest are varied simultaneously. In this way, the maximum amount of information can be extracted with a minimum number of experiments. The response surface methodology (RMS) [46] is useful for cases where the responses of interest are influenced by several process factors and where the main objective is to optimize these responses.

## **CHAPTER 4**

### **MODELING OF VARIM PROCESS**

#### **4.1 Virtual Flow Module**

A virtual flow model for process design in vacuum assisted resin infusion operations is developed. It uses a control volume technique based on finite difference method to characterize flow behavior during resin infusion in molding woven fiber composite structures. In order to enhance the visual capability of the developed virtual model, a geometric reconstruction scheme is used to present the resin flow front at fixed time increment. The Graphic Interchange Format (GIF) is used to combine images into a single file to create animation. This model provides capabilities for prediction of flow pattern and evolved defects. Several case studies were conducted to evaluate the effectiveness of the developed model.

Numerical simulation of the resin during the hot infusion stage in the newly developed VARIM is not yet fully developed or verified. The design of the process and tooling in VARIM is currently conducted following the tedious trial and error approach. The present work aims at investigating the applicability of the model originally developed by [23, 24] from RTM to the infusion stage in VARIM process involving stiff lower half mold and flexible upper half mold. Necessary boundary conditions will be modified for the new process (VARIM). Moreover a post process phase will be added to the

established numerical simulation enabling the model to create animation of the flow behavior in VARIM and therefore make it truly virtual.

#### **4.1.1 Numerical Modeling**

The developed model deals with characterization of the resin flow behavior during the infusion stage. This model provides guidance for tooling design for efficient and defects free infusion of the resin. It also helps in selecting the number and location of inlet gates and evacuation ports in order to prevent the formation of dry spots and allow for speedy infusion of the resin. In order to simulate the flow behavior in VARIM, the following assumptions are considered:

- (1) The properties of resin do not vary and no curing takes place during the isothermal infusion process.
- (2) Capillary and inertia effects are neglected.
- (3) The surface tension is neglected compared to the dominant viscous force.

Resin flow through fiber mats, are modeled as a two-phase fluid flow through porous media. The fractional volume of fluid (VOF) technique is used to characterize the behavior of the free boundary at the interface between the two fluids involved in the process (air and resin). Just before the application of the vacuum pressure and the introduction of the resin, the volume fraction of resin is zero for the whole region, and the volume fraction of air is equal to one and the volume fraction of resin is equal to zero. In the VOF model, the location of the interface between two phases, resin and air, is

accomplished by the solution of a continuity equation for the volume fraction of resin phase as follows:

$$\frac{\partial \varepsilon_{resin}}{\partial t} + \frac{\partial u_i \varepsilon_{resin}}{\partial x_i} = 0 \quad (1)$$

The air phase volume fraction will be computed based on the constraint:

$$\varepsilon_{air} = 1 - \varepsilon_{resin} \quad (2)$$

A single momentum equation is solved throughout the domain, and the resulting velocity field is shared between the two phases. The momentum equation, assuming no gravity and external body force, takes the following form:

$$\frac{\partial}{\partial t}(\rho u_j) + \frac{\partial}{\partial x_i}(\rho u_i u_j) = -\frac{\partial P}{\partial x_j} + \frac{\partial}{\partial x_i} \mu \left( \frac{\partial u_i}{\partial x_j} + \frac{\partial u_j}{\partial x_i} \right) - \sum_{i=1}^3 \frac{\mu}{k_{ji}} u_i \quad (3)$$

Where  $(-\sum_{i=1}^3 \frac{\mu}{k_{ji}} u_i)$  is the viscous loss term (Darcy) when fluid flows through porous media, and  $(k_{ji})$  is the permeability tensor of fiber mats (when high permeability layers are used over the fiber preform an effective permeability tensor is used [26]).

Modeling of resin flow under vacuum bagging in VARIM process requires the knowledge of the fiber mat permeability. The porosity of the reinforcement and other

porous media used in VARIM and hence the permeability depends on the vacuum level under the flexible plastic bag [47]. Since high permeable layers are used over the fiber mat, a proper value of permeability, representing the flow resistance called “effective permeability”, is to be measured experimentally using the empirical Darcy’s law:

$$K_{eff} = \frac{u\mu_{resin}}{dP / dx} \quad (4)$$

The experimental set up, shown in Figure 4-1, was used to measure the effective permeability of the model process. A digital video camera was used to record the resin flow front through the transparent vacuum bagging. Procedures and recommendations reported earlier [7, 23] were followed in the measurements.

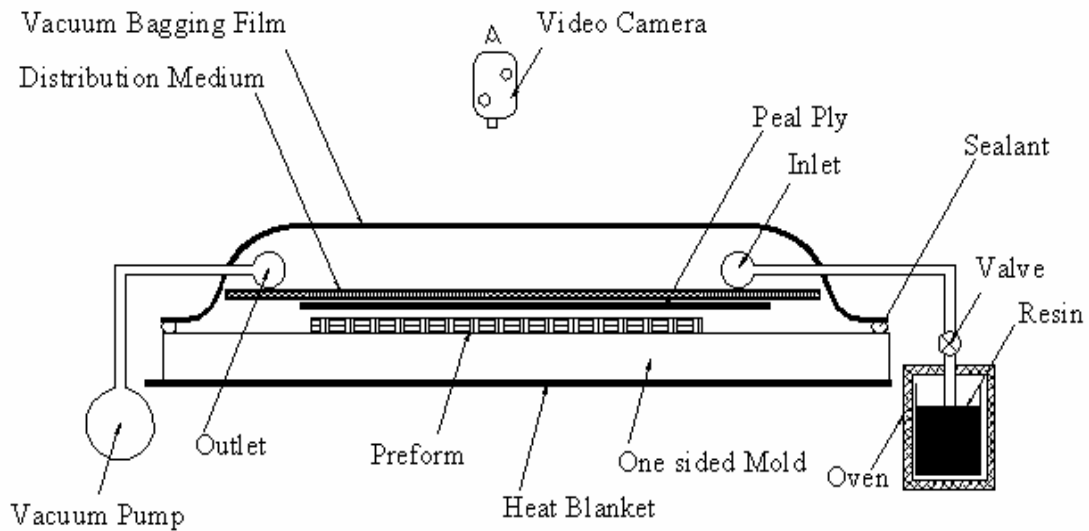


Figure 4-1. Schematic diagram of the experimental setup.



For each control volume,

$$\rho = \varepsilon_{resin} \rho_{resin} + \varepsilon_{air} \rho_{air} \quad (5)$$

and

$$\mu = \varepsilon_{resin} \mu_{resin} + \varepsilon_{air} \mu_{air} \quad (6)$$

Where in equations (1) through (6),

$\varepsilon_{air}$  : volume fraction of air

$\varepsilon_{resin}$  : volume fraction of resin

$\rho_{air}$  : the density of air (kg/m<sup>3</sup>)

$\rho_{resin}$  : the density of resin (kg/m<sup>3</sup>)

$\mu_{air}$  : the viscosity of air (poise)

$\mu_{resin}$  : the viscosity of resin (poise)

t: time (s)

$u_i$ : the velocity component of resin in  $x_i$  direction

P: pressure (N/m<sup>2</sup>)

$K_{eff}$  : effective permeability (m<sup>2</sup>).

One of the common problem with RTM and VARIM is the race tracking, which can lead to macro-voids. Race tracking is caused by the presence of high permeability areas near the mold edges. These high permeable areas are created by the unraveling of fiber bundles during the cutting of the preform or by improper preform placement inside the

mold. This phenomenon could not be completely prevented but it may be reduced. Modeling race tracking can help in mold design and deciding the location of mold vents. S.G. Advani [7] presented an analysis to model the race tracking using the Navier-Stokes equation for flow inside a duct, considering the flow at the mold edge as a flow in a four-edge channel. Then an equivalent permeability can be computed for the channel by equating the channel flow rate to Darcian flow rate.

$$K_{race} = \frac{h^2}{12} \left[ 1 - \frac{192h}{\Pi^5 w} - \sum_{i=1,3,5,\dots}^{\infty} \frac{\tanh(i\Pi w / 2h)}{i^5} \right] \quad (7)$$

Where:

$K_{race}$ : equivalent race tracking permeability ( $m^2$ )

$h$ : race tracking channel height (m)

$w$ : race tracking channel width (m).

In this case the flow inside the mold will be modeled as a flow through porous media with different permeability at the edges.

The mathematical model is solved using a control volume based finite difference technique. Applying the boundary conditions to the governing equations solves the pressure field. The characterization of the free boundary (the resin flow front) is handled using the concept of fractional volume of fluid (VOF). The orientation of the resin flow front is determined by the direction of the gradient of the volume fraction of the resin or air phase within the cell, and that of the neighbor cell which shares the face in question. When the cell is near the interface between two phases, the geometric reconstruction

scheme is used. The geometric reconstruction scheme represents the interface between fluids using a piecewise-linear approach.

#### **4.1.2 Visual Presentation and Animation of the Results**

In order to enhance the visual capability of the developed numerical model, the geometric reconstruction scheme introduced by D. L. Youngs [48] is used in the presentation of the numerical results. This scheme can visually present the profile of the infused resin flow front profile using the flow through cells that exist around the interface between the two fluids (resin and air). This interface is presented in the geometric reconstruction scheme using a piecewise-linear approach. It assumes that the interface has a linear slope within each cell, and uses it for prediction of the advection of the resin through the cell faces. This scheme shows more accurate flow behavior than the donor acceptor scheme used before by [24].

Furthermore, the Graphic Interchange Format (GIF) is used in order to combine images generated by the geometric reconstruction scheme into a single file to create animation. The combined techniques of the geometric reconstruction and GIF provide an effective virtual way of illustrating the effects of process variables and tooling design on the flow behavior and the potential formation of dry spots during the infusion stage in VARIM.

#### **4.1.3 Case Studies**

Several case studies using the developed model are conducted in order to characterize the flow behavior inside the mold. The FLUENT control volume based finite difference

technique is used to solve the mathematical model. This is a general purpose finite difference analysis program that has the capability of simulating a wide range of physical phenomena, including steady state or transient flow, laminar or turbulent flow, multiphase flow. The model is solved based on the following assumptions:

- 1- The effective permeability measured under the flexible vacuum bagging in the x-direction is equal to the one in the y-direction.
- 2- The part thickness is relatively small compared to its length and width.
- 3- The infusion process is assumed to be conducted under isothermal conditions at 121 °C (250 °F).

The reinforcement used in these case studies consisted of six layers of eight-harness carbon fiber mats. Cycom 5250-4-RTM BMI resin was used in this study. Figure 4-2 shows the model capability to predict the flow front and the resin-air interface. The model can predict the void location and the percentage of resin-air in zones that contain a mixture of both phases.

The flow of resin, through a preform of carbon fiber mats, was investigated and, some of the results were compared with experimental observations. During one of these experiments, as shown in Figure 4-3, the resin infusion was stopped before filling the whole mold cavity and the part was cured at this filling stage, to be as an example for the actual flow front. The thick white line in Figure 4-3 represents the actual resin flow front. As shown in Figure 4-4, the model is able to predict the same shape of the flow front of the resin, as in Figure 4-3, and also the interface zone between the two phases.

Race tracking represents a major problem for all resin molding processes. In race tracking the movement of the fluid at both mold sides, or at one side only, with higher permeability regions, is faster than the bulk of the fluid. Race tracking can lead to the formation of macro-voids (dry spots) in the molded composite part during manufacturing. Figure 4-5-(a) shows the effect of race tracking at one side of the mold, on the resin flow front during infusion. Figure 4-5-(b) shows that, due to race tracking, the resin flow front almost closed the venting port before filling the whole mold. This behavior leads to macro-void by trapping air inside the mold. Figure 4-6-(b) shows another case study with damage in the form of area of macro-void. Figure 4-6-(a) shows how precise the model to predict that damage, which is almost the same size and almost the same location as in the molded (defected) part. Changing the mold design by introducing an additional vent close to the location of the dry spot, eliminated the damage and led to sound structure. Figure 4-7 displays the experimental observation of the flow front during infusion (Fig. 4-7-a) and the simulation results (Fig.4-7-b). There is a good agreement between the actual experimental results and the virtual (simulated) ones. Figure 4-7-c shows the actual flow front near the end of the infusion stage. It is evident that mold design modification has resulted in eliminating all potential dry spots.

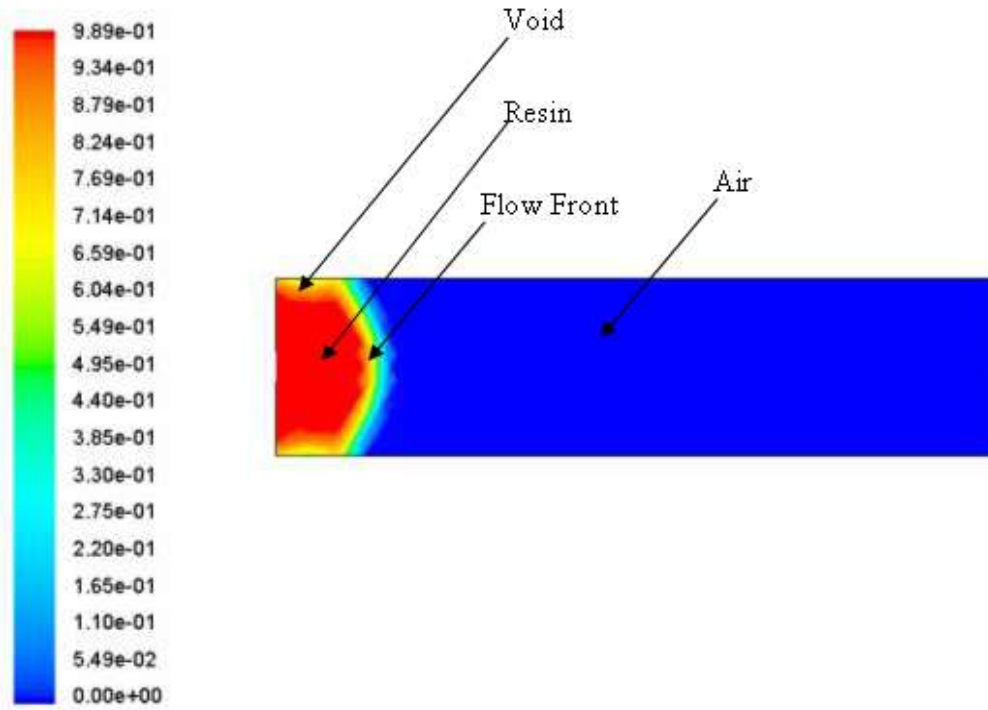


Figure 4-2. Resin flow front during infusion stage.

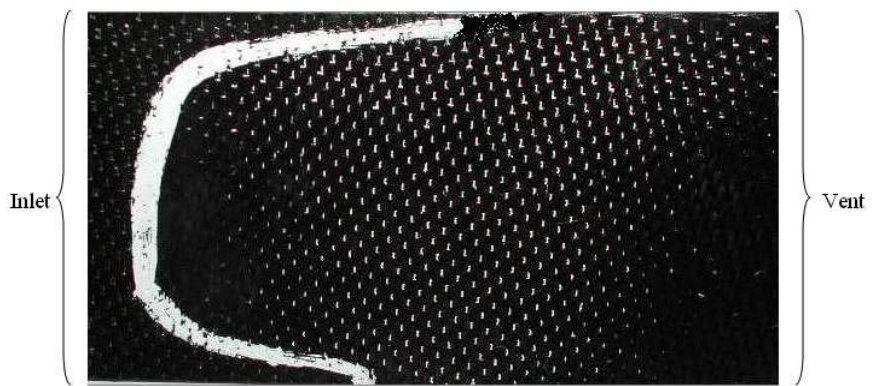


Figure 4-3. The thick white line represents the actual resin flow front.

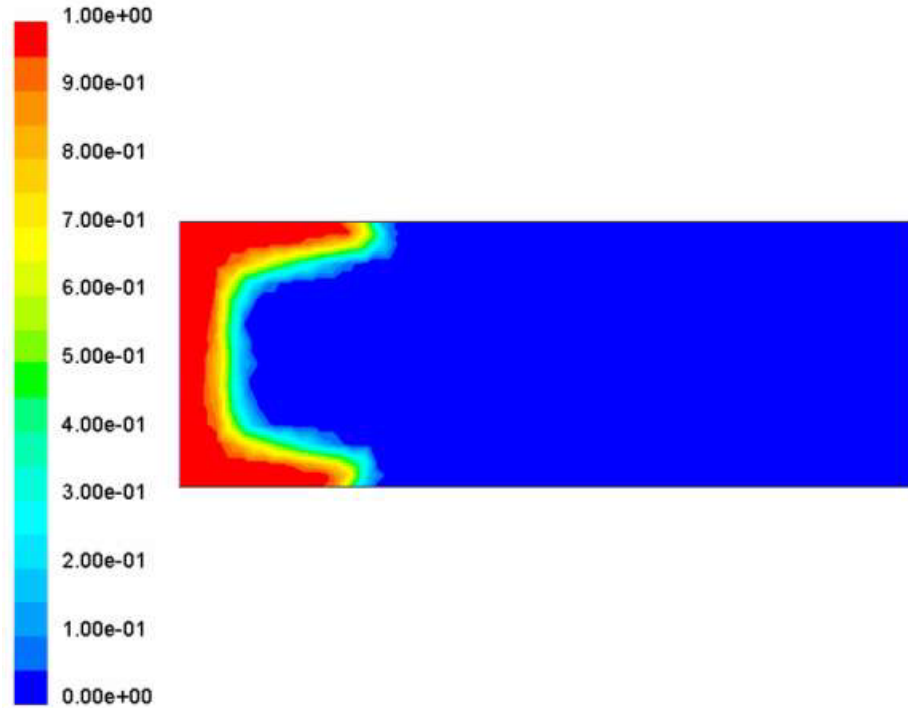


Figure 4-4. Resin flow front with the effect of race-tracking during resin infusion.

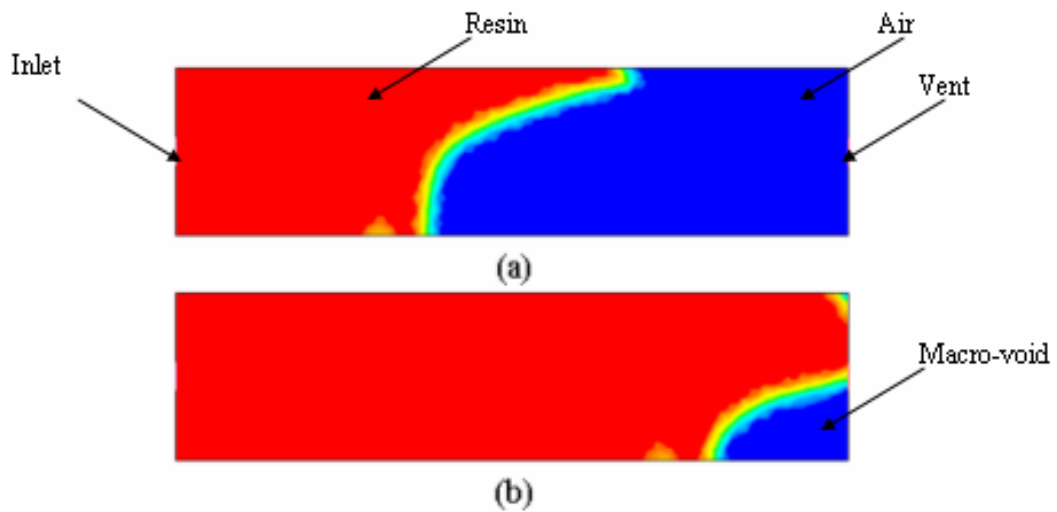


Figure 4-5. Race-tracking effect, (a) the flow front during infusion and (b) macro-void due to race-tracking effect at the end of mold filling.

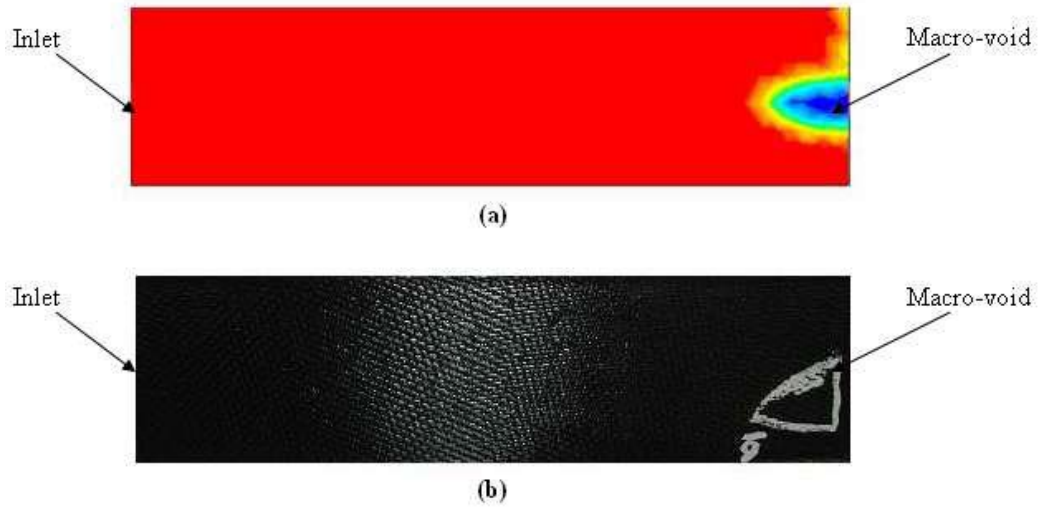


Figure 4-6. Macro-void due to race-tracking effect, (a) the simulation result and (b) the actual part (the thick white line surrounds an air void).

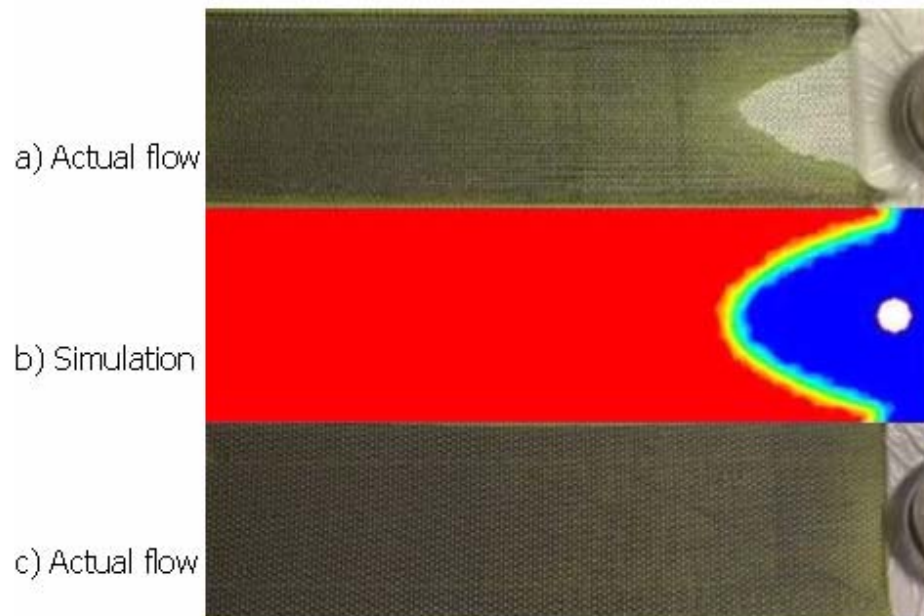


Figure 4-7. Resin flow front during infusion stage, a) experimental, b) simulation results, c) actual flow front near the end of infusion stage.



## 4.2 Thermal and Resin Cure Analysis

Thermal and resin cure analysis is performed to model the cure stage of the VARIM process. The three-dimensional transient energy and species equations are solved within the composite part to determine the temperature and cure variations with time. The exothermic chemical reaction in the resin releases heat and thereby acts as a source term in the energy equation. Thus the energy and species equations become coupled and need to be solved simultaneously.

To determine the degree of cure as a function of the temperature and the time during the cure cycle, the energy and species equations are solved as follows:

The energy equation is given by:

$$\rho C_p \frac{DT}{Dt} = \nabla \cdot (k \nabla T) + S_a \quad (8)$$

In the species equation, the degree of cure is defined by:

$$\Psi = \frac{C_I - C_A}{C_I} \quad (9)$$

Where  $C_A$  is the local concentration of the uncured resin, and  $C_I$  is the initial concentration of uncured resin at any time. The three-dimensional species equation is based on the model:

$$\frac{D\Psi}{Dt} = R_a \quad (10)$$

Where  $\frac{D\Psi}{Dt}$  and  $\frac{DT}{Dt}$  are the material derivatives of the degree of cure and temperature respectively.  $C_p$  is the specific heat and  $k$  is the thermal conductivity of the resin saturated.  $S_a$  is, the source term due to chemical reaction, given by:

$$S_a = C_l (\Delta H) R_a \quad (11)$$

Where  $\Delta H$  is the heat of reaction and  $R_a$ , the reaction rate term, is given by the autocatalytic kinetic model presented by [49] as follows:

$$\frac{D\Psi}{Dt} = (K_1 + K_2 \Psi) (1 - \Psi)^n \quad (12)$$

$$K_1 = A_1 \exp(-E_{k1}/RT) \quad (13)$$

$$K_2 = A_2 \exp(-E_{k2}/RT) \quad (14)$$

Where  $K_1$  and  $K_2$  are the reaction rate constants,  $A_1$  and  $A_2$  are the Arrhenius constants,  $E_k$  is the activation energy,  $R$  is the universal gas constant, and  $n$  is the order of the reaction.

Lumped properties based on weight average thermo-physical properties were used in the energy and species equations. The properties were determined as follows [39]:

$$\rho = \frac{\rho_r \rho_f}{\rho_r w_r + \rho_f w_f} \quad (15)$$

$$k = \frac{k_r k_f}{k_r w_r + k_f w_f} \quad (16)$$

$$c_p = w_r c_{pr} + w_f c_{pf} \quad (17)$$

$$w_f = \frac{V_f}{V_f + \frac{\rho_r}{\rho_f} (1 - V_f)} \quad (18)$$

$$w_r = 1 - w_f \quad (19)$$

Where  $\rho$ ,  $\rho_f$ , and  $\rho_r$  are the densities of the composite, the fiber, and the resin, respectively;  $k$ ,  $k_f$ , and  $k_r$  are the thermal conductivities;  $c_p$ ,  $c_{pf}$ , and  $c_{pr}$  are the specific heats of the composite, the fiber, and the resin, respectively; where  $w_f$ , and  $w_r$  are the weight fractions of the fiber mat and the resin respectively;  $V_f$  is the fiber volume fraction.

## **4.3 Cure Dependant Mechanical Properties**

### **4.3.1 Fiber Mat Structure**

To model the mechanical properties of carbon fiber mat composites, the geometry of the mat was analyzed at microscopic level. Figure 4-8 shows a schematic of a top view of eight-harness (8H) weave. This number (8H) refers to the number of yarns that are passed over by one yarn. In an eight harness satin weave, yarns are weaved by passing over seven and under one yarn before the pattern repeats itself. The fiber yarns which run in x-direction are called the fill yarns, and those running in the y-direction are called the warp yarns, with the same fibers count in both directions.

The cross section of some samples produced by VARIM were prepared, polished, and analyzed under optical microscope. Figure 4-9-(b) shows the shape of a cross section through the thickness of the molded sample. All the dimensions of the fill and warp yarn were obtained from the observation under the microscope and this shape was redrawn in CAD system as shown in Figure 4-9-(a). These observations showed that the warp yarn, which crosses over the fill yarn, looks like an ellipse. Due to the high compression in VARIM process, the following seven yarns, which cross under the fill yarn, regroup together to act as a one bundle.

The analysis is performed on a unit cell which represents the entire mat. The geometry of eight-harness mat repeats itself every eight yarns in both x- and y-directions. The unit cell chosen for the analysis should contain all the patterns present in the mat. The complete unit cell for eight-harness mat consists of eight rows. Figure 4-10 shows the geometry of

eight-harness carbon fiber mat as was seen under the microscope. Each section represents a cross section of the mat along the y-direction, as shown in Figure 4-8. These sections were used in modeling the composite mechanical properties and sitting up the stiffness matrices.

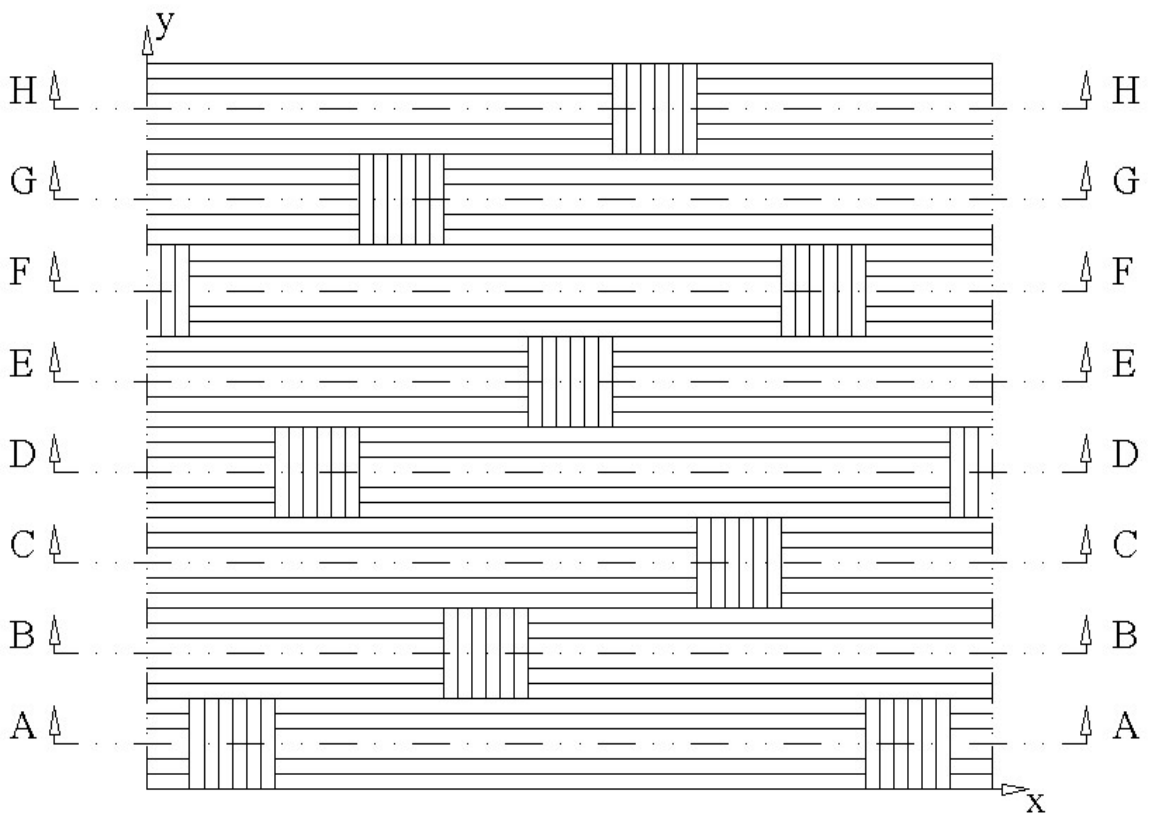


Figure 4-8. Schematic of a top view of eight-harness carbon fiber mat.

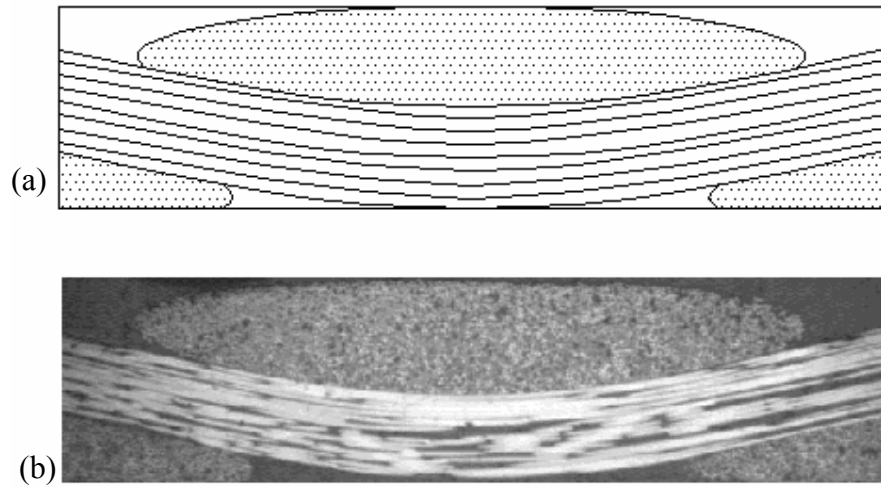


Figure 4-9. Geometry of a cross section of eight-harness carbon fiber mat, (a) a CAD drawing (b) a picture obtained by optical microscope for sample produced by VARIM.

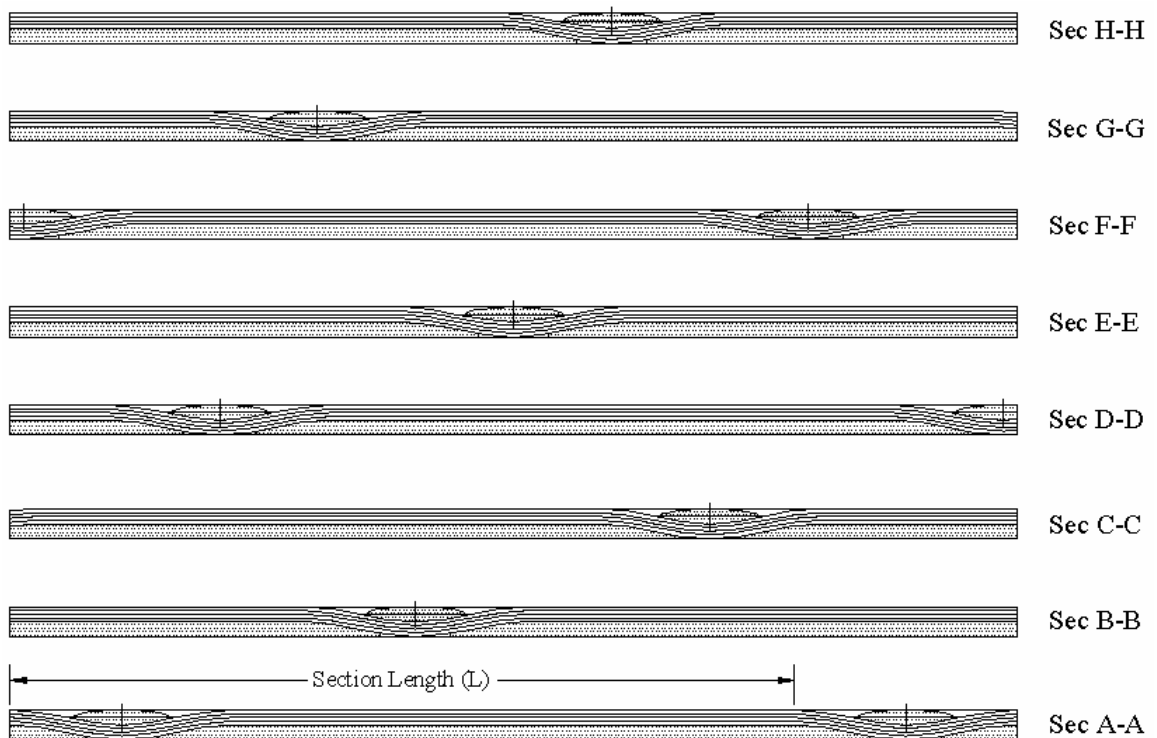


Figure 4-10. Geometry of eight-harness carbon fiber mat. Each section represents a cross section of the mat along the y-direction.

### 4.3.2 Shape Function Formulation

The shape function was formulated based on the observation of the cross section of molded samples by VARIM under the microscope. The fill yarn was modeled as a sin wave, Figure 4-11 shows the CAD drawing for one layer of the fiber mat, with the fill yarn as a sin wave. The figure shows also a picture obtained by optical microscope for a sample produced by VARIM.

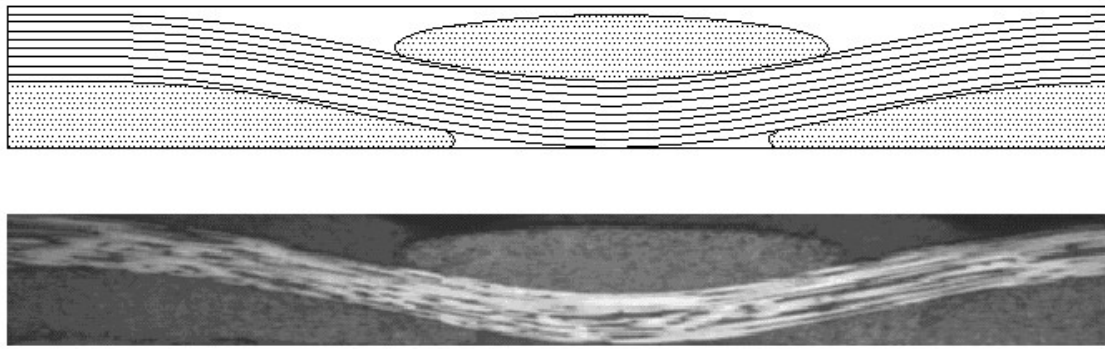


Figure 4-11. Geometry of a cross section of eight-harness carbon fiber mat, (a) a CAD drawing (b) a picture obtained by optical microscope for sample produced by VARIM.

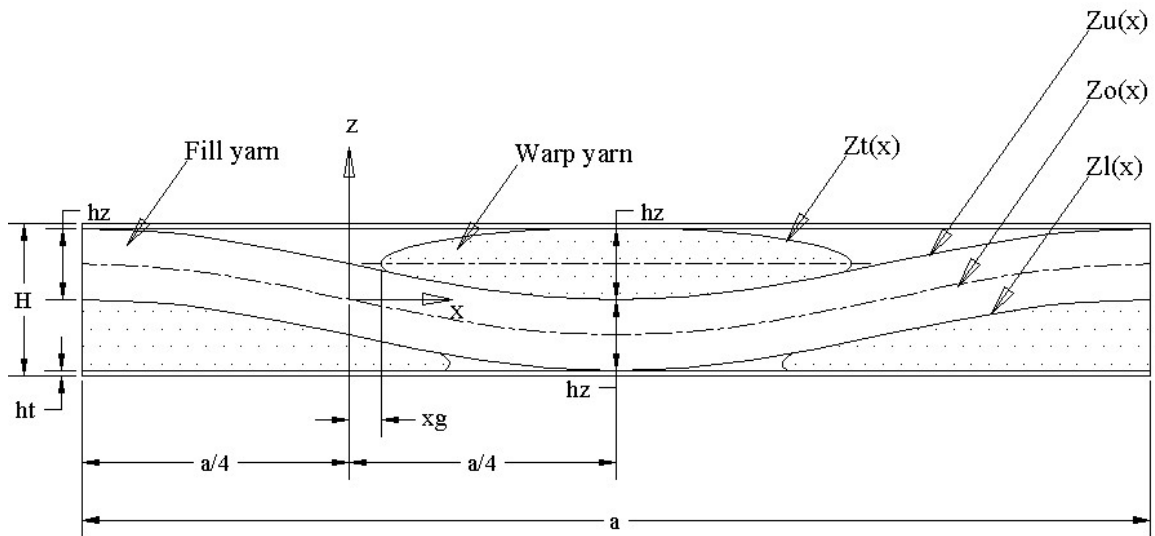


Figure 4-12. Geometrical relation between the fill yarn and the warp yarn of 8H fiber mat.

The geometrical relation between the fill yarn and the warp yarn of eight-harness fiber mat, as shown in Figure 4-12, was used to define the shape function based on the shape characterization performed by Ito and Chou [50].

The center line of the fill yarn  $z_o$  is defined as:

$$z_o(x) = -\frac{h_z}{2} \sin\left(\frac{2\pi}{a}x\right) \quad \text{where} \quad \left(-\frac{a}{4} \leq x \leq \frac{3a}{4}\right) \quad (20)$$

The fill yarn thickness,  $h_z$ , is assumed to be constant. The upper boundary of the fill yarn is defined as:

$$z_u(x) = z_o(x) + \frac{h_z}{2} \quad (21)$$

And the lower boundary of the fill yarn is defined as:

$$z_l(x) = z_o(x) - \frac{h_z}{2} \quad (22)$$

The shape of the warp yarn cross section, based on the observation under the microscope, is assumed to be elliptical and given as:

$$z_t(x) = \frac{2h_2}{a - 4x_g} \sqrt{(2x - 2x_g)(a - 2x_g - 2x)} + h_z - h_c \quad \text{where} \quad \left(x_g \leq x \leq \left(\frac{a}{2} - x_g\right)\right) \quad (23)$$

Based on the geometrical shape the variable,  $h_c$  in the previous equation is defined as:

$$h_c = \frac{h_z}{2} \left(\sin\left(\frac{2x_g\pi}{a}\right) + 1\right) \quad (24)$$

The local angle between fiber direction and x-axis is:

$$\theta(x) = \tan^{-1}\left(\frac{dz_o(x)}{dx}\right) \quad (25)$$



Where, in the previous equations:

$z_o$  : center line of fill yarn

$z_u$  : upper boundary of the fill yarn

$z_l$  : lower boundary of the fill yarn

$h_z$  : yarn thickness

$a$  : wavelength of a yarn

$z_t$  : boundary of elliptical shape of warp yarn

$x_g$  : offset distance of the warp yarn from zero coordinate

$\theta$  : angle between fiber direction and x-axis

Some samples of the molded composite material, produced by VARIM, were polished and observed using an optical microscope. Measurements were made, under the microscope, for wavelength of a yarn, yarn thickness, elliptical shape of the warp yarn, and some other necessary dimensions to draw the cross section in CAD system. The area of the elliptical shape of the warp yarn, and the total fiber bundle cross section area were used to calculate the bundle fiber volume fraction.

### 4.3.3 Stiffness Matrix Formulation

Classical Laminate Theory (CLT) is assumed to be applicable to the infinitesimal regions of the composite unit cell. The in-plane stiffness constants for each infinitesimal length (dx) are given as follows:

$$A_{ij}(x, y), B_{ij}(x, y), D_{ij}(x, y) = \int_0^H (1, z, z^2) Q_{ij} dz \quad (26)$$

$$Q_{ij} = \begin{bmatrix} \frac{E_x}{D_v} & \nu_{yx} \frac{E_x}{D_v} & 0 \\ \nu_{yx} \frac{E_x}{D_v} & \frac{E_y}{D_v} & 0 \\ 0 & 0 & G_{xy} \end{bmatrix} \quad (27)$$

Where:

$A_{ij}$ : extensional stiffnesses

$B_{ij}$ : bending-extension coupling stiffnesses

$D_{ij}$ : bending stiffnesses

$Q_{ij}$ : reduced stiffnesses

$$D_v = 1 - \nu_{xy}\nu_{yx}$$

The stiffnesses of the fill, warp, and the matrix are evaluated based on the properties of each constituent. The fiber volume fraction of the fill and warp was calculated based on the dimension obtained under the microscope for the shape of the yarn and the total cross section area of the fiber in the bundle. The bundle fiber volume fraction was found to be

62%. The properties of the fill and warp yarn are determined based on the rule of mixtures as follows:

The longitudinal Young's modulus of the yarn is given by:

$$E_1 = V_f E_f + (1 - V_f) E_m \quad (28)$$

The transverse Young's modulus of the yarn, using Halphin and Tsi semi-empirical models [51], is given by:

$$E_2 = E_m \left( \frac{1 + \xi \eta V_f}{1 - \eta V_f} \right) \quad (29)$$

$$\eta = \frac{(E_f / E_m) - 1}{(E_f / E_m) + \xi} \quad (30)$$

The reinforcing factor “ $\xi$ ” is given by the empirical formula [52]:

$$\xi = 1 + 40V_f^{10} \quad (31)$$

The shear modulus is given by:

$$G_{12} = G_m \left( \frac{1 + \xi \eta V_f}{1 - \eta V_f} \right) \quad (32)$$

$$\eta = \frac{(G_f / G_m) - 1}{(G_f / G_m) + \xi} \quad (33)$$

$$G_{23} = G_m / (1 - V_f^{1/2} (1 - G_m / G_{23f})) \quad (34)$$

The Poisson's ratios is given by:

$$\nu_{12} = \nu_{13} = V_f \nu_f + (1 - V_f) \nu_m \quad (35)$$

$$\nu_{21} = \nu_{12} E_2 / E_{11} \quad (36)$$

$$\nu_{23} = V_f \nu_{23f} + V_m (2\nu_m - \nu_{21}) \quad (37)$$

Where  $E_m$  and  $E_f$  are the tensile moduli for the matrix and the fiber respectively.  $V_f$  is the fiber volume fraction.  $G_m$  and  $G_f$  are the shear moduli for the matrix and the fiber respectively.  $\nu_m$  is the Poisson's ratio for the matrix and  $\nu_f$  for the fiber.

The changes in fiber orientation due to yarn undulation must be taken into account. The effective elastic constants for the fill and warp yarns are given as follows:

$$\frac{1}{E_x} = \frac{\cos^4 \theta}{E_1} + \frac{\sin^4 \theta}{E_1} + \left( \frac{1}{G_{12}} - \frac{2\nu_{12}}{E_1} \right) \sin^2 \theta \cos^2 \theta \quad (38)$$

$$E_y = E_2 \quad (39)$$

$$\nu_{xy} = E_x \left[ \frac{\nu_{12}}{E_1} (\sin^4 \theta + \cos^4 \theta) - \left( \frac{1}{E_1} + \frac{1}{E_2} - \frac{1}{G_{12}} \right) \sin^2 \theta \cos^2 \theta \right] \quad (40)$$

$$\frac{1}{G_{xy}} = 2 \left( \frac{2}{E_1} + \frac{2}{E_2} + \frac{4\nu_{12}}{E_1} - \frac{1}{G_{12}} \right) \sin^2 \theta \cos^2 \theta + \frac{1}{G_{12}} (\sin^4 \theta + \cos^4 \theta) \quad (41)$$

While the molded composite material using the eight-harness fiber mat is considered to be orthotropic, the matrix (resin) is considered to be isotropic. At the early stages of curing, before gelation, resin acts as a liquid. As the degree of cure increases, more cross linking occurs, and the resin acts as a solid media. The mechanical properties of resin change as a function of degree of cure. Figure 4-13 shows a linear relation between the degree of cure and the mechanical properties of the resin. This model was presented in early ninety and used after that successfully in different studies [39]. This model was used to determine resin mechanical properties as a function of degree of cure. These properties are then used to determine the stiffness matrix for the matrix (resin).

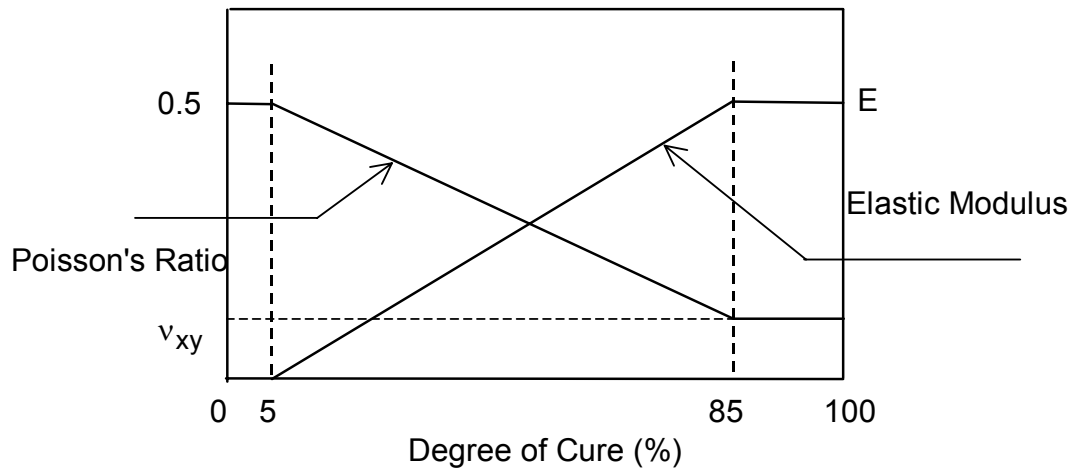


Figure 4-13. Variation of resin elastic modulus and Poisson's ratio with cure [39].

The modulus,  $E_x$ , for each section of the fiber mat, Figure 4-10 shows these different sections, is determined by integration of the modulus of each constituent through the thickness for each infinitesimal length ( $dx$ ). Thus in the region where  $(0 \leq x \leq x_g)$  for section A-A, shown in Figure 4-10, is given as follows:

$$E_x(x) = \frac{1}{H} \left[ \int_0^{h1} E_x^m dz + \int_{h1}^{h2} E_x^w dz + \int_{h2}^{h3} E_x^f dz + \int_{h3}^{h4} E_x^m dz \right] \quad (42)$$

Where  $E_x^m$ ,  $E_x^w$ , and  $E_x^f$  are the moduli in x-direction for the matrix, the warp, and the fill yarn respectively. H is the total thickness of the laminate. From 0 to h1 is the thickness of the matrix bottom layer, from h1 to h2 is warp yarn thickness, from h2 to h3 is the thickness of the fill yarn, and from h3 to h4 is the thickness of the matrix top layer. Similar relations apply to other region within section A-A of the unit cell. Then the effective modulus for this section is obtained by integration of  $E_x(x)$  along the length of the section.

$$E_x = \frac{1}{L_x} \int_0^{L_x} E_x(x) dx \quad (43)$$

Similar steps apply to the other sections, from section B-B to section H-H, to find the  $E_x(x)$  along the length of each section. The effective Young's modulus,  $\bar{E}_x$ , for the whole laminate is obtained by taking the average of  $E_x$  for all of the sections.

All other properties (e.g.  $\nu_{xy}$  and  $G_{xy}$ ) and the stiffness constants ( $A_{ij}$ ,  $B_{ij}$ , and  $D_{ij}$ ) are obtained in similar manner.

## 4.4 Discussion of Cure Modeling Results

### 4.4.1 Thermal and Cure Analysis Results

The three dimensional transient energy and kinetic equations are nonlinear and coupled through the source term. These equations were solved using a control volume based finite difference technique [53]. The exothermic chemical reaction in the 5250-4 RTM resin releases heat and acts as a heat source. Therefore the energy and the species equations, equations 8 and 9, were solved together simultaneously. A MATLAB code was written, using a control volume based finite difference, to solve for the thermal and cure histories in the cure cycle. Temperature field is determined in the part at each time step. Then, the degree of cure is determined by integration of equation 10 with time.

The reaction kinetics, for 5250-4-RTM resin, was determined by using a differential scanning calorimeter (DSC) [49]. The DSC measured the reaction exthotherm as a function of time as shown in equations from 12 to 14. Table 4-1 summarizes the parameters of the kinetic model, obtained from reference [49]. Heat of reaction,  $\Delta H$  in Table 4-1, was obtained from, the resin manufacturer, CYTEC Engineered Materials Company [14].

Table 4-1. Kinetic parameters for 5250-4-RTM resin

Arrhenius constant, $A_1$ (1/s)	Arrhenius constant, $A_2$ (1/s)	Activation Energy, $E_{k1}$ (kJ/mole)	Activation Energy, $E_{k2}$ (kJ/mole)	Heat of Reaction, $\Delta H$ (kJ/kg)	Order of Reaction, $n$
0.815	40.2	29.3	37.3	249.8	2

The developed model was used to get a complete temperature and cure histories of the molded composites. Several case studies were investigated by the model; Table 4-2 shows some of these cases. In each case, the mold temperature was raised to 120°C (250°F), and kept at this temperature during the resin infusion. Then the mold was heated up to the maximum cure temperature, and kept for four hours, with a certain heating rate, as shown in Table 4-2. After that, the mold was kept at 227°C (440°F) for two hours as a post cure stage.

Table 4-2. Some case studies used to produce composite panel by VARIM

Case No.	Maximum Cure Temp. (°C)	Heating Rate (°C/min.)	Post Cure Time at 227°C (h)
Case 1	194	1.39	2
Case 2	194	0.56	2
Case 3	183	1.39	2
Case 4	205	1.39	2

Figure 4-14 shows a complete temperature and cure histories for case 1, with 194°C (380°F) maximum cure temperature, 1.39 °C/min heating rate, and 2 hours post cure time at 227°C (440°F). The figure shows that the rate of degree of cure sharply increases until the degree of cure reaches about 80 %. Then the curve is leveled off with a very low rate of increase till the end of the cure cycle with a degree of cure very close to 100 %. As shown in the figure, at the end of the cure stage, the degree of cure is 97.5%, and after 2 hours of post cure time it increased to 98.8%.



Figure 4-15 shows the distribution of degree of cure through the thickness and along the length of the composite panel for case 1 during curing stage, after one hour from the beginning of the cure cycle. Figure 4-16 shows the same distribution through the thickness and along the width of the panel. These two sections were taken at the middle of the panel. A section at the middle is a good representative for the panel, based on the observation of several sections taken along the length and the width with almost no difference. The two figures show that the distribution of degree of cure for any layer along the length or the width is almost constant except at the edges. But the main change occurs across the panel thickness, where the degree of cure decreases gradually from the bottom to the top within a range of 1.8%, from 81.3 to 79.5%. Figure 4-17 shows the temperature distribution through the thickness and along the length of the composite panel for case 1 at the of the cure cycle. The temperature distribution shows a trend similar to the distribution of degree of cure. At the end of the cure cycle, the degree of cure is almost the same across the part as shown in Figure 4-18.

Another case was studied, case 2, with a low heating rate  $0.56^{\circ}\text{C}/\text{min}$ , but with the same cure temperature and post cure time as in case 1. The complete temperature and cure histories for case 1 are shown in Figure 4-19. Figure 4-20 shows a comparison for the cure histories for these two cases, 3 and 4. In case 1, with a higher heating rate, it took the material 66 minutes to reach about 80% degree of cure, while in case 2, with a lower heating rate, it took about 115 minutes to reach the same degree.

The effect of maximum cure temperature on the trend of degree of cure was studied through the comparison of two cases, 3 and 4, with the same heating rate and post cure time but with different maximum cure temperature. In case 3 the maximum cure temperature was 183°C (360°F), while it was 205°C (400°F) in case 4. Figure 4-21 shows a comparison for the cure histories for these two cases. In the first hour of the cure cycle, the degree of cure for both cases was the same. Then the case with the higher cure temperature reached a higher degree of cure than the case with the lower one. Both cases reached the same degree of cure at the end of the cure stage and right before the post cure stage.

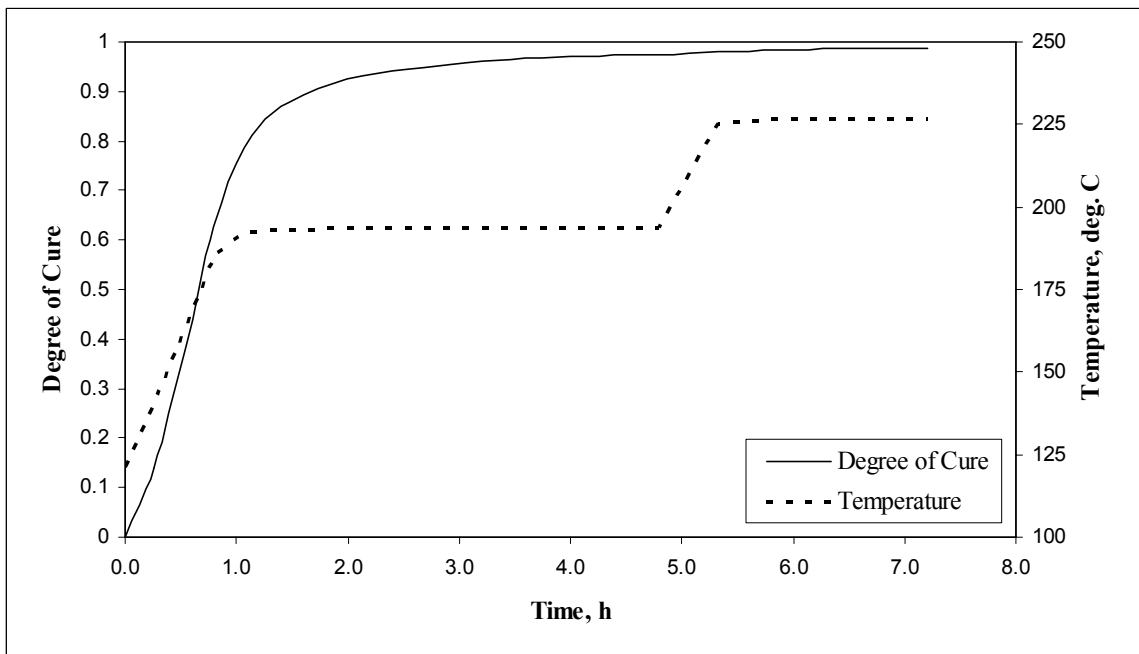


Figure 4-14. Cure and temperature histories for case 1.

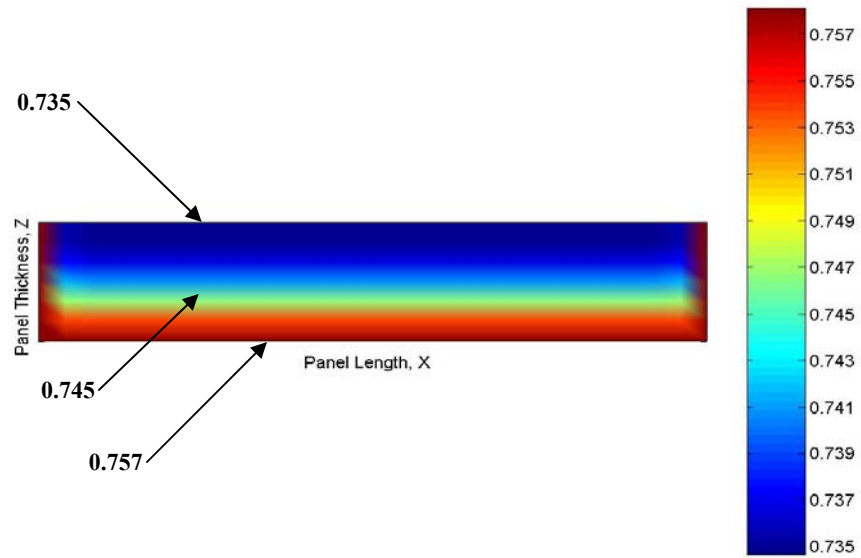


Figure 4-15. Distribution of degree of cure through the panel thickness along the length.

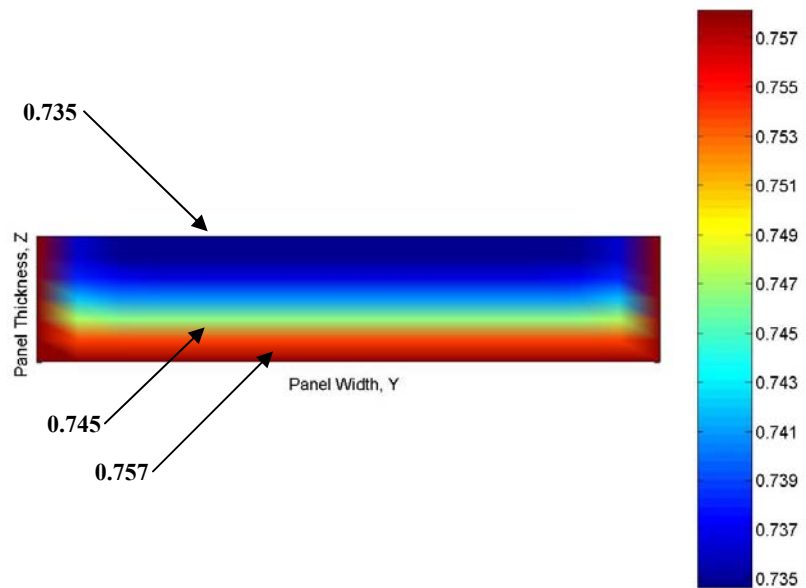


Figure 4-16. Distribution of degree of cure through the panel thickness along the width.

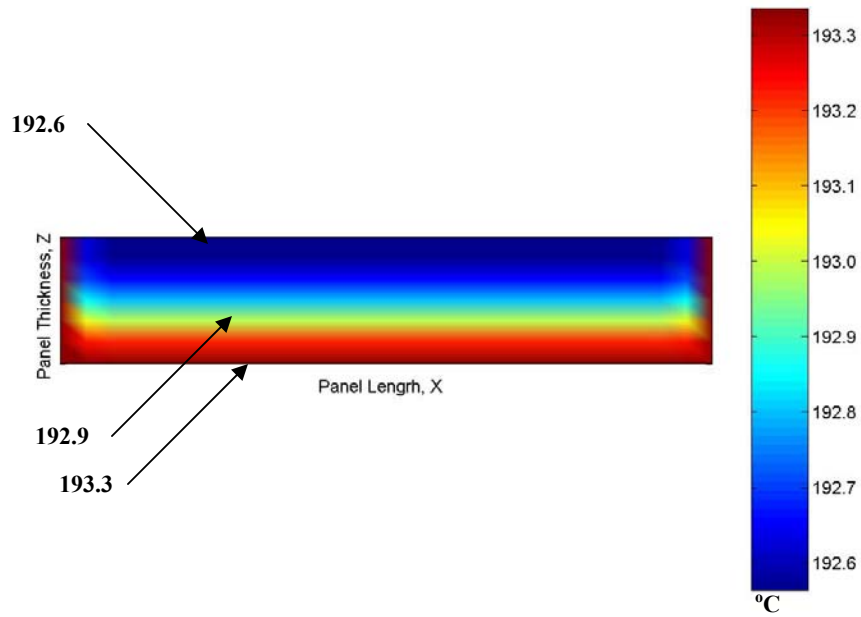


Figure 4-17. Distribution of temperature through the panel thickness along the length.

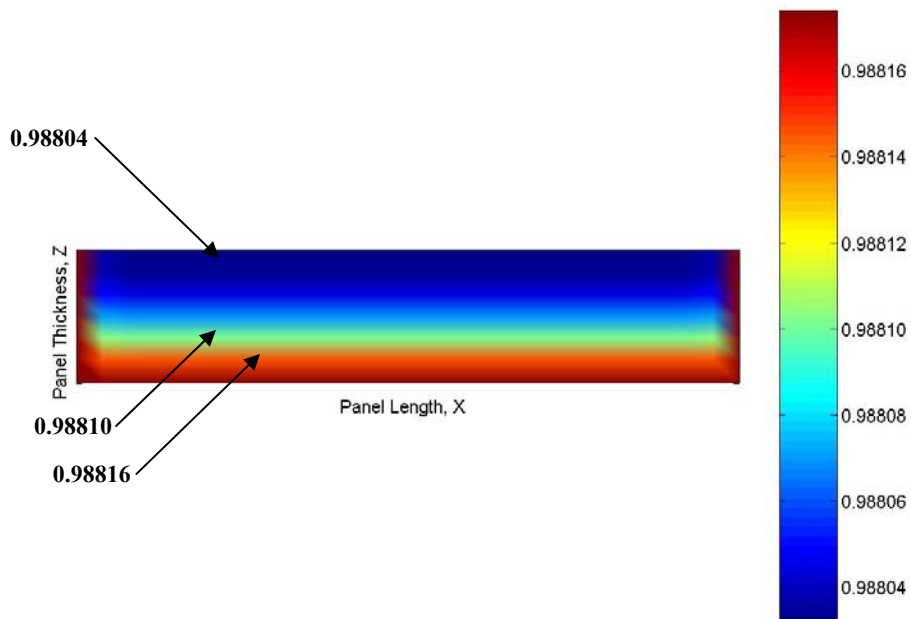


Figure 4-18. Distribution of degree of cure through the panel thickness along the length.

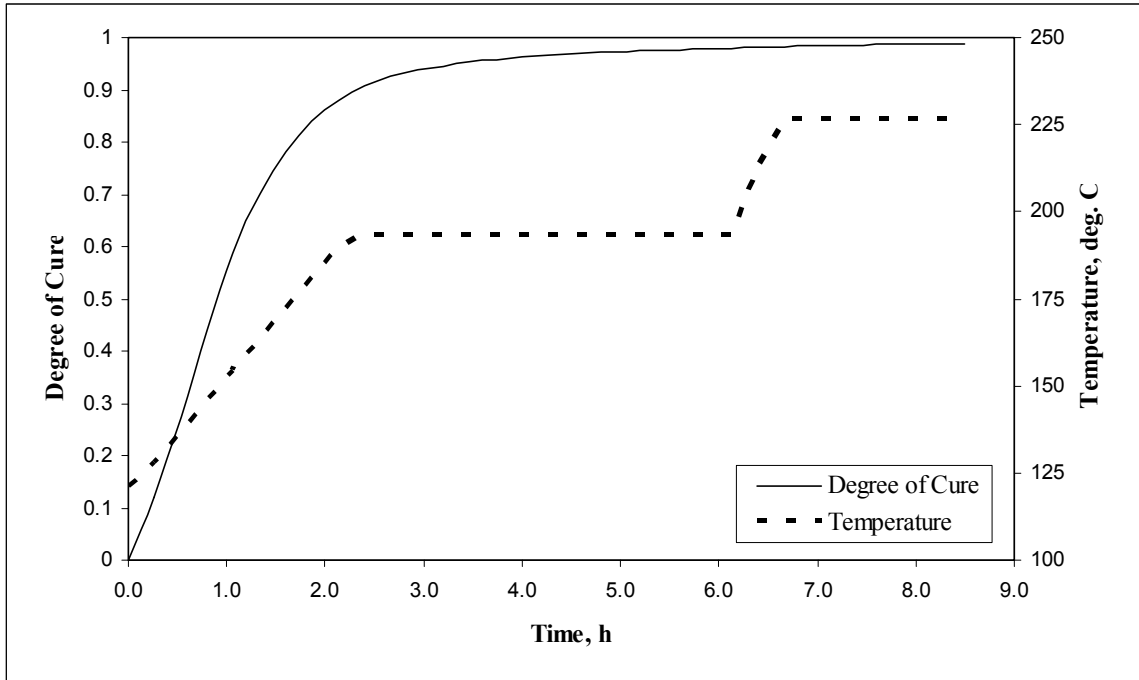


Figure 4-19. Cure and temperature histories for case 2.

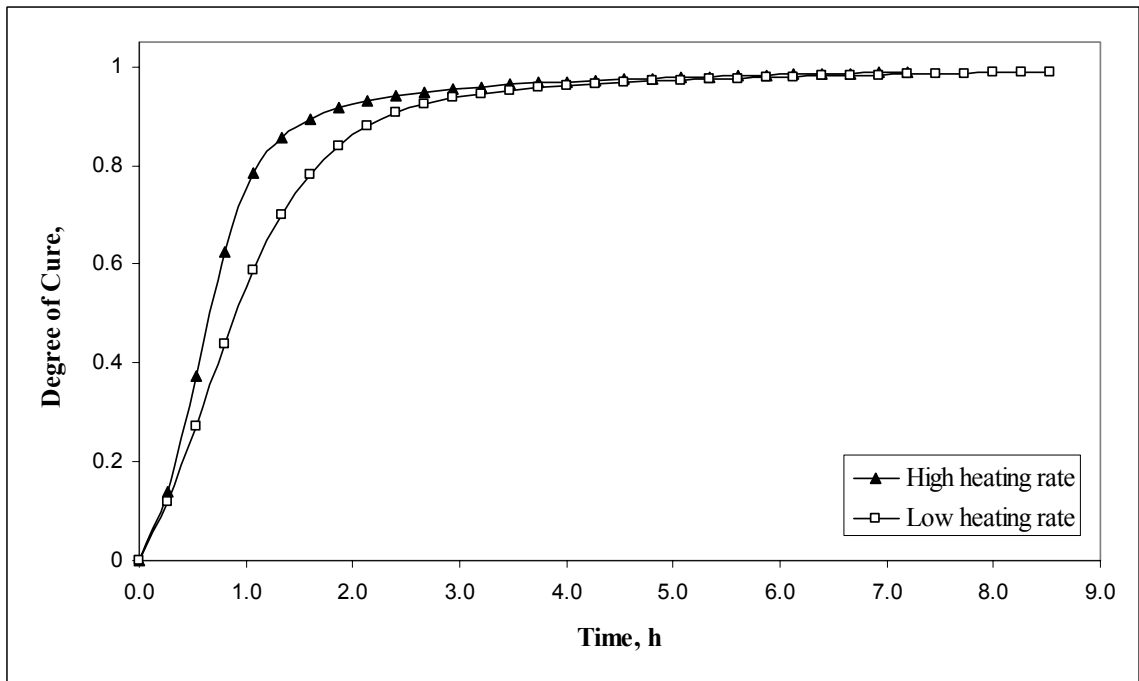


Figure 4-20. Cure history comparison for cases 1 and 2.

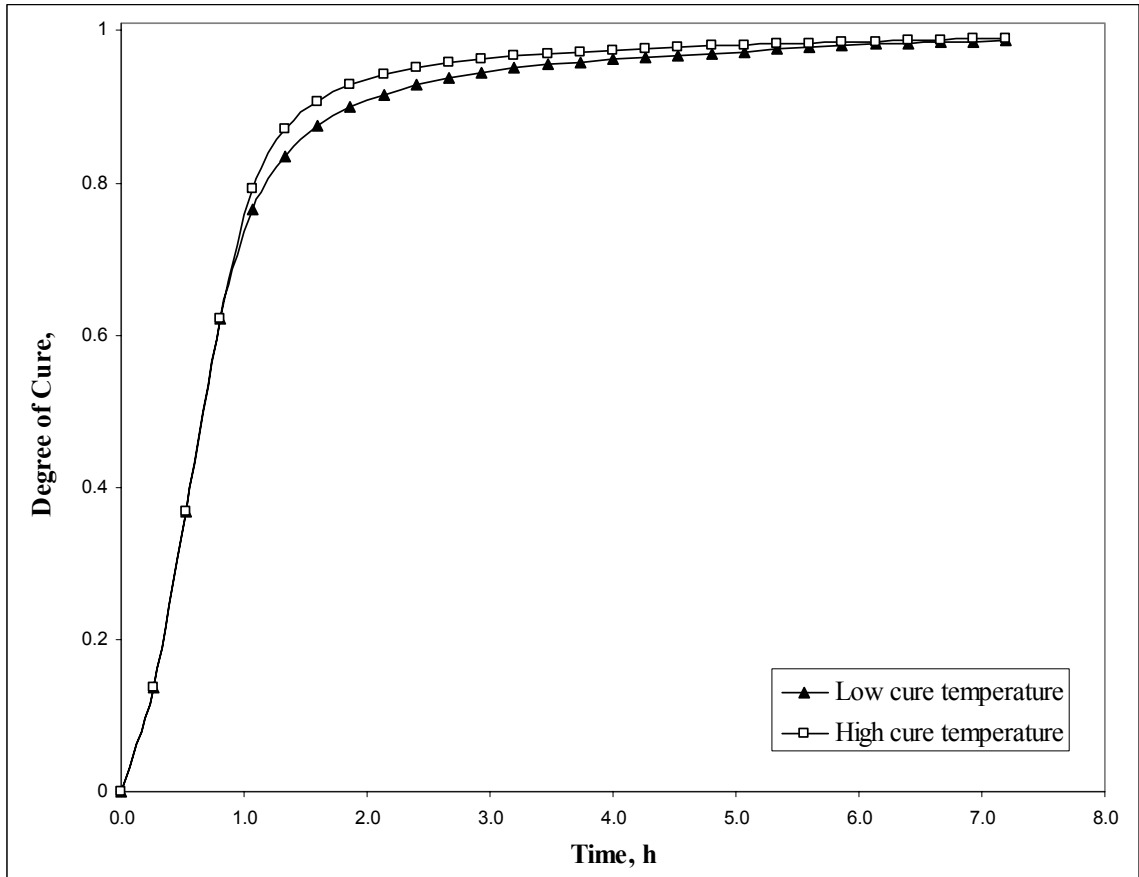


Figure 4-21. Cure history comparison for cases 3 and 4.

#### 4.4.2 Composite Mechanical Properties Results

Once the composite degree of cure is known with time, the stiffness matrices could be determined as functions of degree of cure and time. The mechanical properties and the components of the extensional stiffness, bending-extension coupling stiffness, and bending stiffness matrices were modeled. These properties were determined for every %5 of resin cure and up to the end of the cure cycle. A series of MATLAB codes were written for this model using equations from 20 to 43.

The elastic properties of the fill and warp yarn are calculated by the fiber bundle volume fraction and the elastic properties of fiber and matrix using mechanical properties of each constituent. Table 4-3 shows the elastic mechanical properties of the materials used in this study, which are eight-harness carbon fiber weaved by AS4, and 5250-4-RTM BMI resin. The properties of AS4 carbon fiber were obtained from reference [54], while the properties for 5250-4-RTM were obtained from reference [55],

Table 4-3. Elastic properties of the carbon fiber AS4 and 5250-4-RTM resin

Materials	$E_L$ , GPa	$E_T$ , GPa	$G_{LT}$ , GPa	$G_{TT}$ , GPa	$\nu_{LT}$
Carbon fiber (AS4)	228	40	24	14.3	0.26
Resin 5250-4-RTM	4.6	4.6	1.7	1.7	0.36

First step in the model is to determine the elastic mechanical properties in each infinitesimal region for each section, of the 8 sections, of the unit cell, shown in Figure 4-10. The fiber bundle volume fraction was calculated, based on the dimensions obtained under the microscope for several cross sections of the molded composite, and was found

to be 62%. The cure dependant properties were determined for the resin in the fiber bundle and resin-rich regions. The composite mechanical properties were determined for every 5% of resin degree of cure from zero and up to the end of curing cycle, 100 % for every section of the 8 sections using equation 38 and 39. Figure 4-22 shows the distribution of Young's modulus for section A-A at the end of cure cycle. Figure 4-23 shows the change in the modulus due to fiber undulation for the same section. Then, the average of the modulus through the thickness and along the section length was determined by equation 42 for each section of the unit cell. A curve represents this average is shown in Figure 4-24. Figure 4-25 shows the average for every section of the 8 sections, of the unit cell, along x-direction.

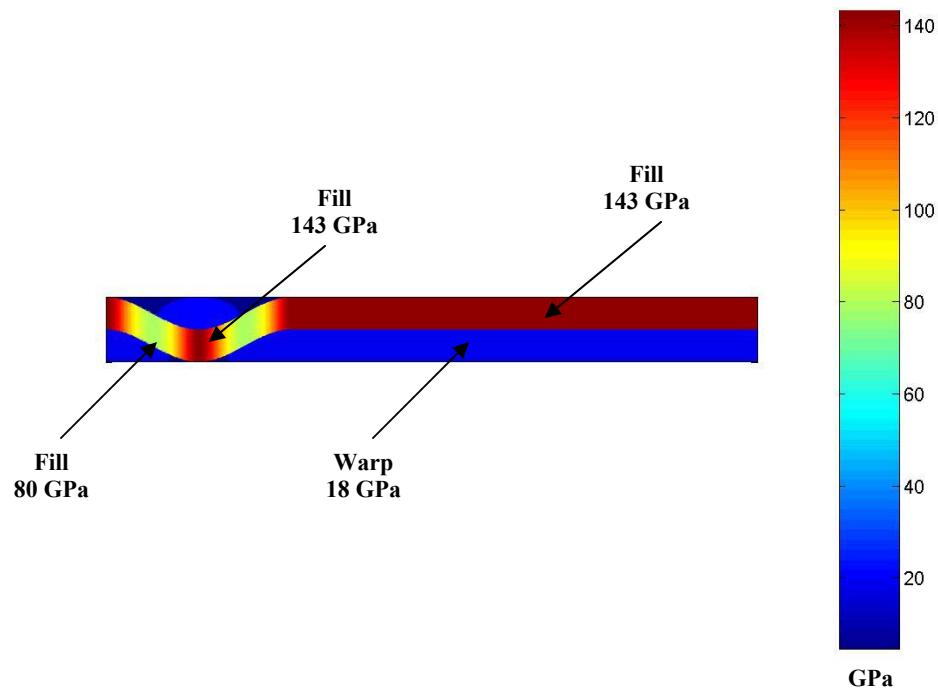


Figure 4-22. Distribution of Young's modulus for section A-A at the end of cure cycle.



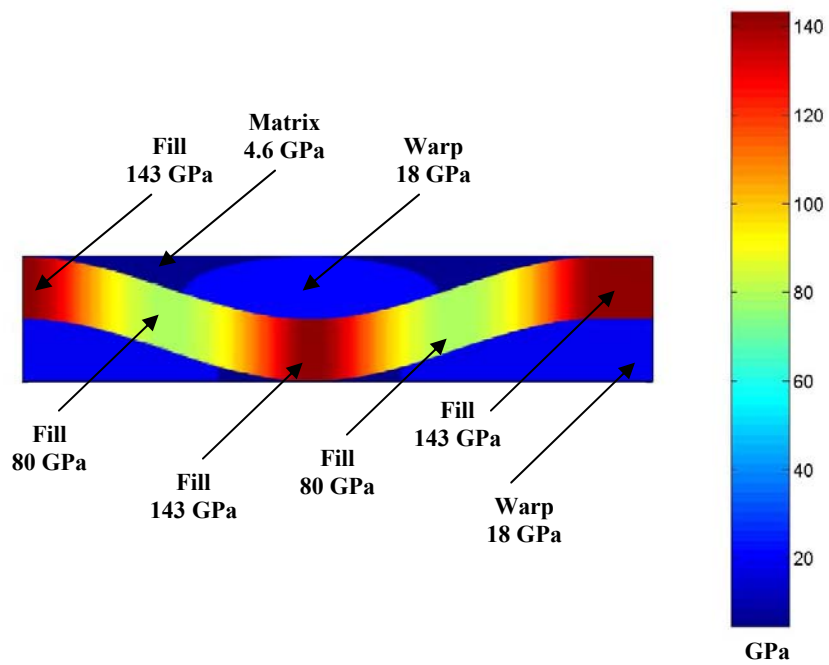


Figure 4-23 Distribution of Young's modulus at an area with fiber undulation.

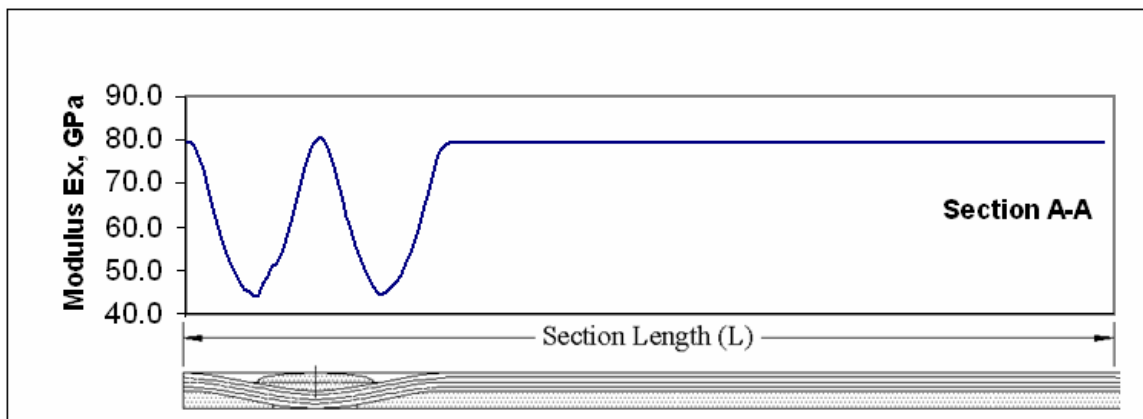


Figure 4-24. Average of Young's modulus through the thickness and along the length.

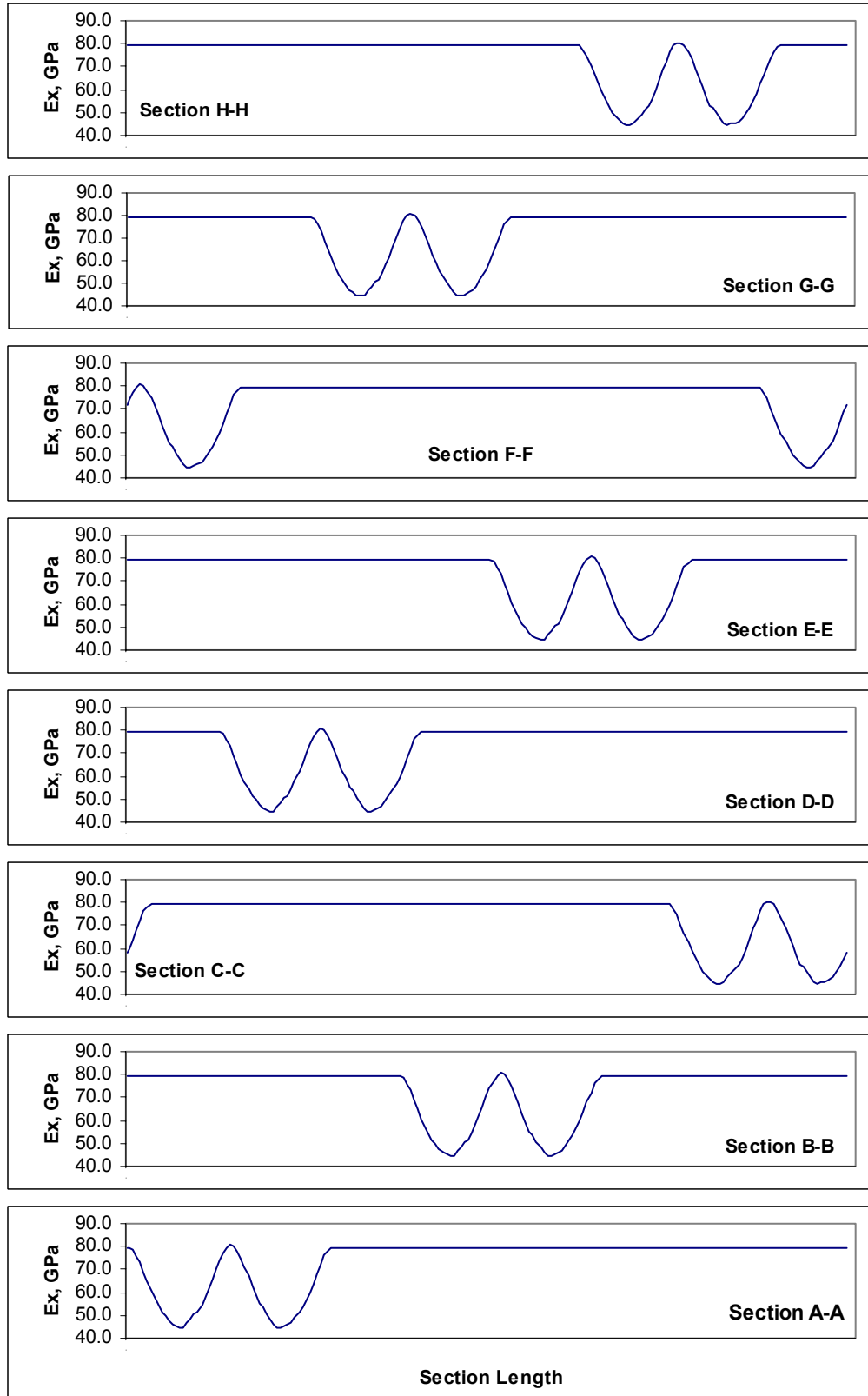


Figure 4-25. Average of Young's modulus through the thickness and along the length.

The distribution of the effective modulus of the unit cell, as shown in Figure 4-26, was determined by taking the average for the 8 sections along the y-direction for a one-layer laminate of carbon fiber mat. A laminate with several layers of carbon fiber randomly distributed, as shown in Figure 4-27, reduced the wavy distribution of the effective modulus. Figure 4-28 shows this distribution for a 6-layer laminate.

The previous steps were repeated to determine the modulus of the laminate at every 5 % of resin degree of cure. The rest of the elastic properties were determined in similar manner. Figure 4-29 shows the variation of Young's modulus with resin degree of cure. The modulus showed an exponential increase with resin degree of cure.

The value of Young's modulus obtained experimentally in this study, as will be presented in section 6.3.2, is 15% less than the value obtained by the mathematical model at 100% degree of cure, shown in Table 4-4. The difference is due to two main reasons; first one is the assumptions of the mathematical model which assumes that there is no interfacial sliding between fiber/matrix or between the layers of the fiber mats. Also, no void in the molded composite was assumed, while the experimental investigation showed a 0.25% average void content. The second reason is due to the difficulties in the experimental investigation, which includes the difficulty to lay up the carbon fiber mats parallel to each other on the top of the mold, and also the difficulty in the machining of the tested specimens with their sides parallel to the direction of the fibers inside the molded panels. These reasons result in a higher value of the mathematical model and in a lower value of the experimentally tested specimens.

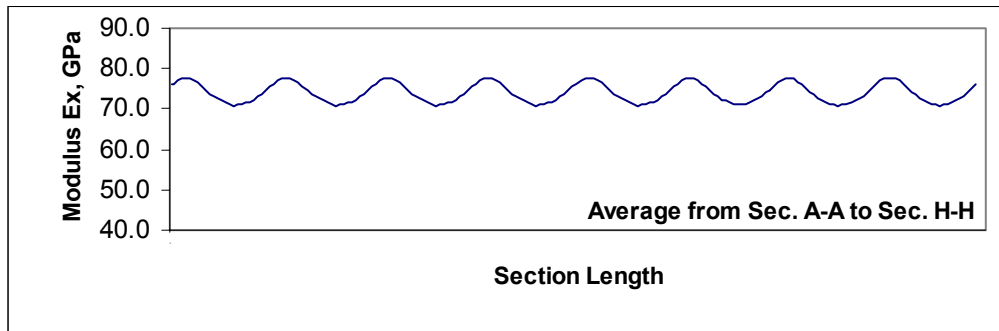


Figure 4-26. Average of Young's modulus through the thickness and along the length for the 8 sections of the unit cell of a one-layer laminate.

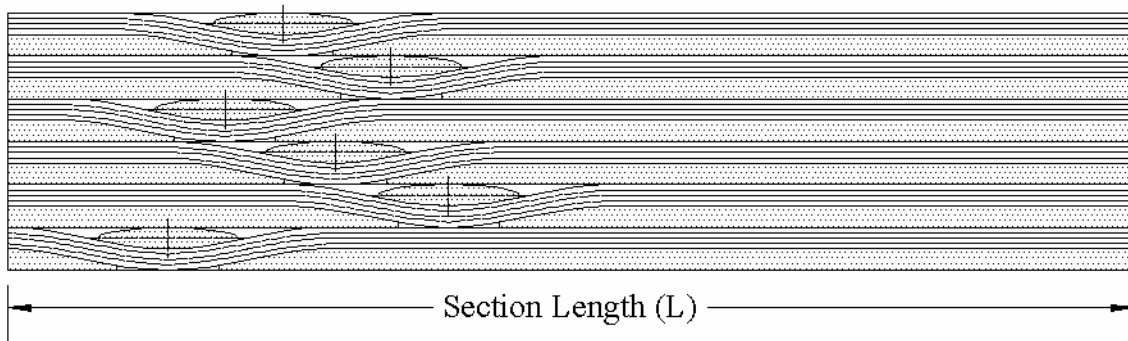


Figure 4-27. A laminate with six layers of carbon fiber randomly distributed.

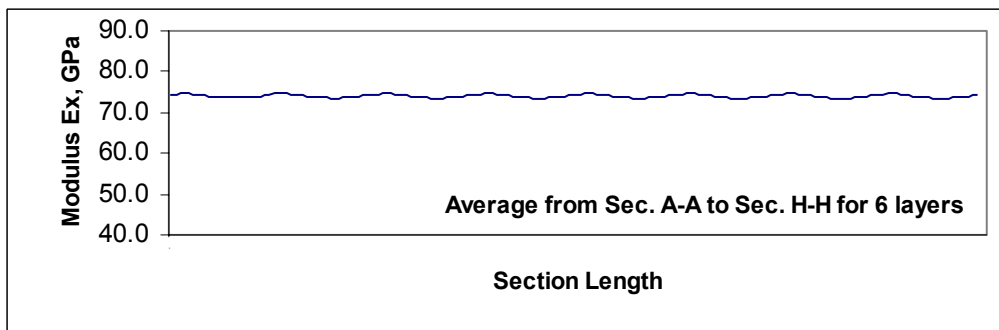


Figure 4-28. Average of Young's modulus through the thickness and along the length for the 8 sections of the unit cell of a six-layer laminate.

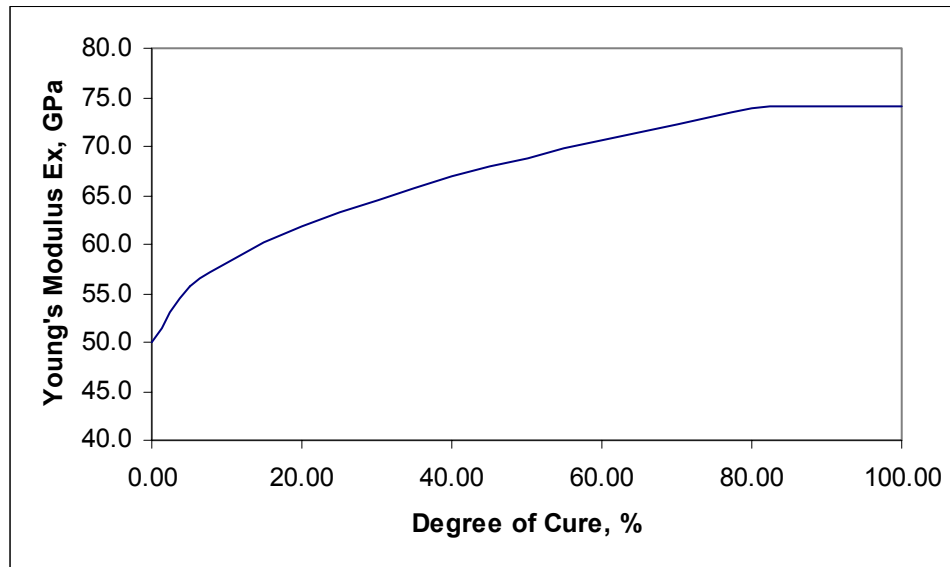


Figure 4-29. Variation of Young's modulus with resin degree of cure.

Table 4-4. Cure dependent properties for carbon fiber/5250-4-RTM resin

Degree of Cure, %	$E_x$ , GPa	$E_y$ , GPa	$G_{xy}$ , GPa	$\nu_{xy}$
20	61.5	61.5	1.4	0.215
40	66.9	66.9	2.7	0.207
60	70.7	70.7	3.8	0.201
80	73.9	73.9	5.0	0.195
100	74.0	74.0	5.1	0.194

Once the effective elastic properties were determined with degree cure, Table 4-4 summarize these properties, the stiffness matrix,  $Q_{ij}$ , and the stiffness constants  $A_{ij}$ ,  $B_{ij}$ , and  $D_{ij}$  were determined by equations 26 and 27. Figure 4-30, 4-31, and 4-32 show the variation of the first component of the extensional stiffness, the bending-extension stiffness, and the bending stiffness, respectively. The extensional stiffness  $A_{11}$  showed an exponential increase with the resin degree of cure. The bending-extension stiffness and the bending stiffness showed a similar trend. The non-zero element of the bending-extension stiffness matrix implies that the normal and shear forces will result in twisting and bending of the composite part.

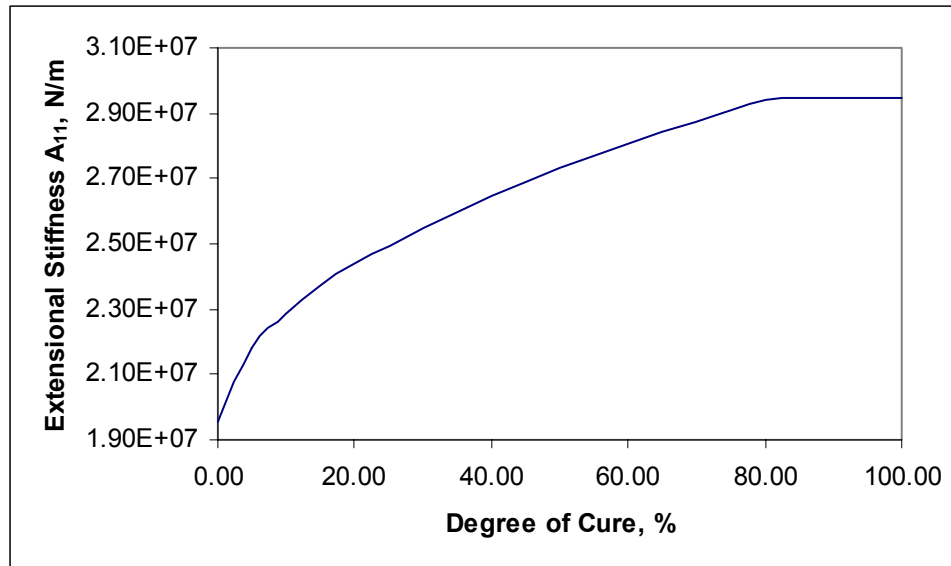


Figure 4-30. Variation of extensional stiffness with resin degree of cure.

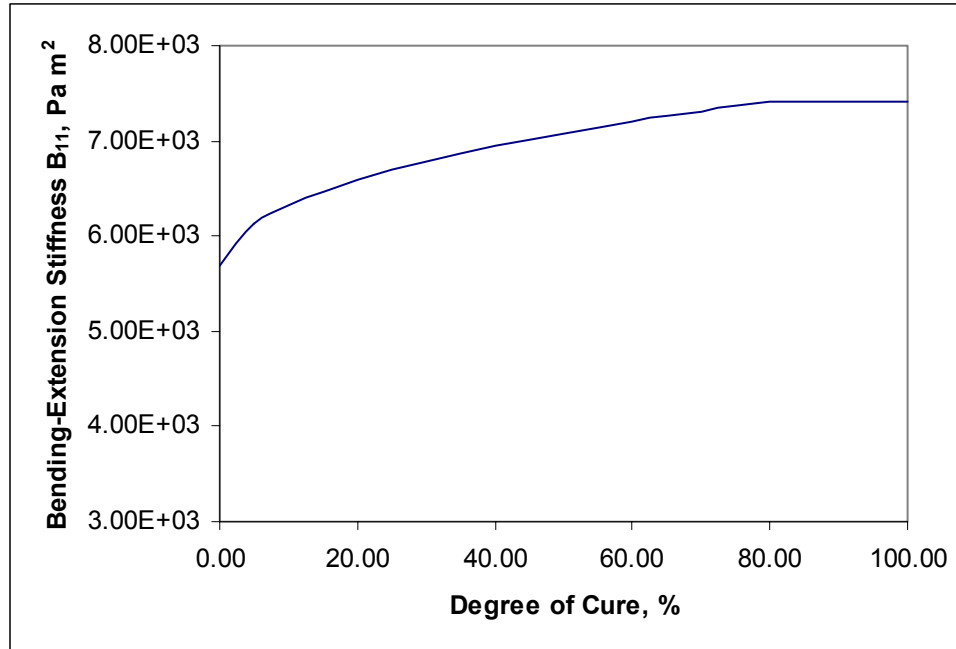


Figure 4-31. Variation of bending-extension stiffness with resin degree of cure.

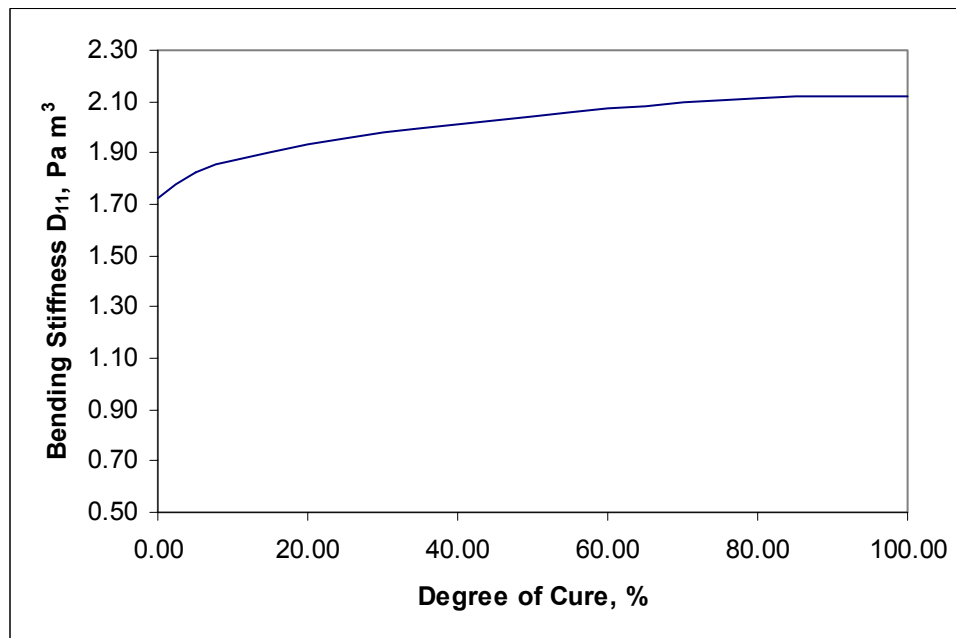


Figure 4-32. Variation of bending stiffness with resin degree of cure.

## **CHAPTER 5**

### **EXPERIMENTAL INVESTIGATION OF VARIM PROCESS**

#### **5.1 Introduction**

In Vacuum Assisted Resin Infusion Molding (VARIM) process, composite panels of 380 mm (15in) length and 175 mm (7in) width with two different thicknesses, 2.1mm (0.084in) and 0.79 mm (0.031in), are molded. Vacuum Assisted Resin Infusion Molding (VARIM) process using single vacuum port and single resin inlet port system is used to evaluate the feasibility of the process to produce a composite structure with properties needed for aerospace application. The volume fraction of the fiber in the composite is maintained at about 58%.

#### **5.2 Materials**

Eight harness carbons woven satin fabrics, made of AS4 carbon fiber, are used in the present composite system to provide the needed reinforcing component and to satisfy the condition of porous media, required by VARIM process.

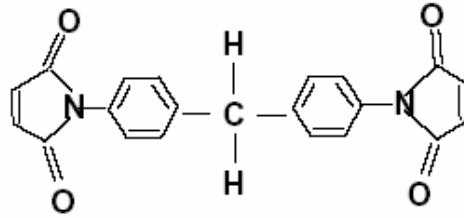
The high temperature resin used is CYCOM 5250-4-RTM produced by CYTEC Engineered Materials in California. It is a one-part homogenous Bismaleimide (BMI) resin with some additives to improve toughness. This polymer was developed for use in



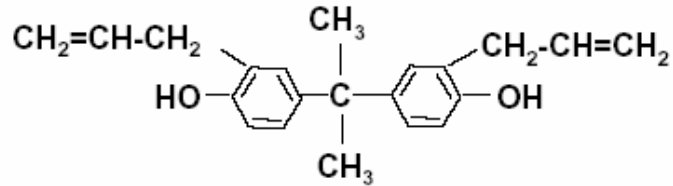
high performance structural composites requiring high temperature up to 204 °C (400 °F) use and increased toughness.

5250-4 RTM is a 3-component modified bisbaleimide (BMI) resin. BMI resins are used for high performance applications due to their high temperature resistance, high glass transition temperature, and excellent chemical corrosion resistance. But the main disadvantage of BMI resins that they are very brittle. 5250-4 RTM resin has three different components to overcome the disadvantage of MBI resin and to improve processing and toughness. These three components are Bismalieimidodiphenylmethane (BMPPM) (44 wt%), Diallyl Bisphenol A (DABPA) (32 wt%), and BMI-1, 3-tolyl (24 wt%) [61]. Figure 5-1 illustrates the chemical structures of the three components. The chemical structure of the combined 3-component 5250-4 RTM resin is shown in Figure 5-2.

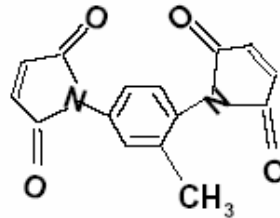
It's known that resins based on BMIs need to be cured at high temperature and postcured at elevated temperature for relatively longer time. The cross linking mechanism during cure and postcure process involves two main steps. First step is the opening of carbon-carbon double bonds (C=C). This step improves the thermal and mechanical properties of the composite. In the second step with more heating time, the cross linking may occur via dehydration of the hydroxyl groups. This step leads to microcracking and hence the deterioration of mechanical properties of composites. This means that longer postcure time may not improve the mechanical properties [62].



4,4' – Bismaleimidodiphenylmethane (BMPM), 44 wt%



O,O'- Diallyl Bisphenol A (DABPA), 32 wt%



BMI-1,3- tolyl, 24 wt%

Figure 5-1. Chemical structures of 5250-4 RTM resin components, taken from.

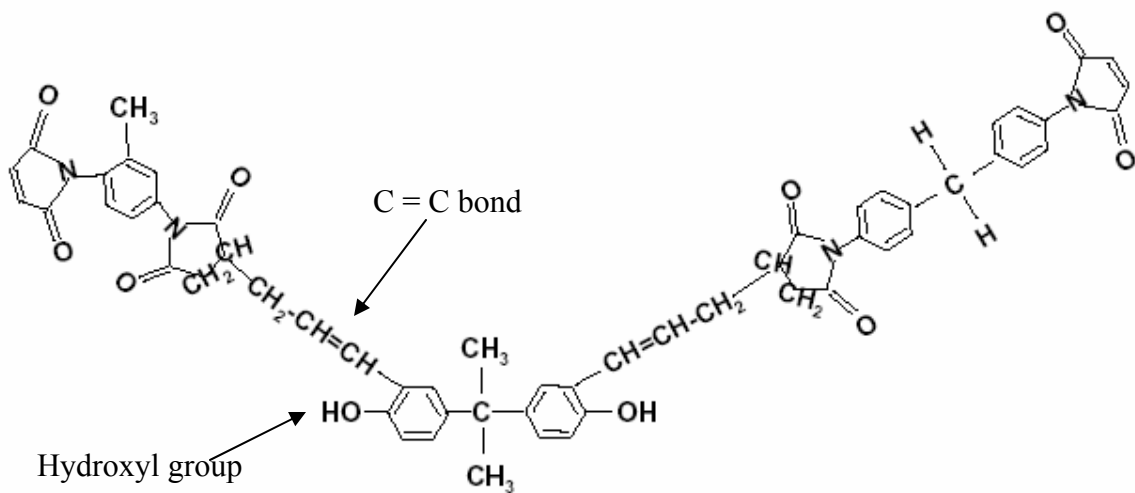


Figure 5-2. Chemical structure of the combined 3-component 5250-4 RTM resin.

### 5.3 Experimental Procedure

The experimental procedure for the vacuum assisted resin infusion molding process can be summarized as follows:

- 1- The surface of a flat Aluminum mold, with a 560mm (22in) length, 255mm (10in) width, and 50mm (2in) thick, is cleaned and sprayed with a release agent dry lubricant (Miller-Stephenson #MS-122AD).
- 2- A release film, with 510mm (20in) length and 200mm (8in) width, which enhances the resin flow, is laid on the top of the mold. The release film is a product of Airtech Int'l, Inc. #A4000.
- 3- A peel ply material (fiberglass coated with a release agent), with 485mm (19in) length and 190mm (7.5in) width, is placed on the top of the release film to prevent the sticking of the preform with the mold. The peel ply material is a high permeable material to allow resin flow to pass through it. The peel ply is a product of Airtech Int'l, Inc. bleeder lease.
- 4- The carbon fiber mat is cut to the required size, which is 380mm (15in) length and 175mm (7in) width, and then stacked one by one on the top of the peel ply. The carbon fiber mat is produced by Hexcel Schwebel #AGP370-8HBA-49.
- 5- Another peel ply sheet is laid on the top layer of the carbon fiber (preform). This sheet prevents the sticking of the preform with the rest of the bagging materials on the top; also it allows resin flow from the top to the preform.
- 6- Highly porous materials of fiberglass cloth and Aluminum screen are laid on the top of the peel ply to accelerate resin flow. The Aluminum screen is 485mm

(19in) length and 190mm (7.5in) width with 0.56mm (0.022in) thick. The size of the screen net is 18-cell in 25mm (1in).

- 7- A high temperature sealant tape, which seals off the vacuum bag, is applied on the edge of the mold all around the sides. The tape is a product of Airtech Int'l, Inc. GS#213-3.
- 8- A high temperature vacuum bag, with 510mm (20in) length and 330mm (13in) width, is used to cover the whole top of the mold including the sealant tape. The vacuum bag is produced by Airtech Int'l, Inc. #WN1500.
- 9- Two vacuum valves are connected to both sides of the mold, one of them is a resin inlet and the other is a resin outlet or a vacuum port. The base of the valve is placed under the vacuum bag and the rest of the valve is attached to the valve base through the vacuum bag. The vacuum valve is a product of Airtech Int'l, Inc. VAC valve 399.
- 10- Vacuum pressure 735mm (29in) of mercury is applied under the bagging to withdraw the air within the mold.
- 11- The resin, which is in a solid state at room temperature, is melted in a vacuum oven at 120°C (250°F) to get all the gases out of it.
- 12- The tool is then heated to 120°C (250°F) using a heat blanket, with 610mm (24in) length, and 305mm (12in) width, to have an isothermal resin injection. The heat blanket, with 120V, 12A, and 1kW, is a product of Briskheat #SRL512012X24.
- 13- The resin is then transferred to an air-circulating oven at 120°C (250°F) and the mold inlet tube is to be dipped to the bottom of the resin can inside the oven.
- 14- The inlet valve is then opened and the resin is allowed to infuse within the fabric.

15- After the whole preform is infused by the resin the vacuum is reduced to 177mm (7in) of mercury and the resin supply is closed off.

16- The mold is covered by glass wools as an insulation, and then is heated to the maximum cure temperature with a certain heating rate and allowed to cure for 4 hours, and then cooled to room temperature immediately or after several hours of post cure time according to the experimental design.

17- Temperature changes during curing are monitored using an imbedded thermocouple inside the mold.

Figure 5-3 shows a schematic diagram of the setup. Figures 5-4, 5-5, and 5-6 show some pictures of the experimental setup of VARIM process.

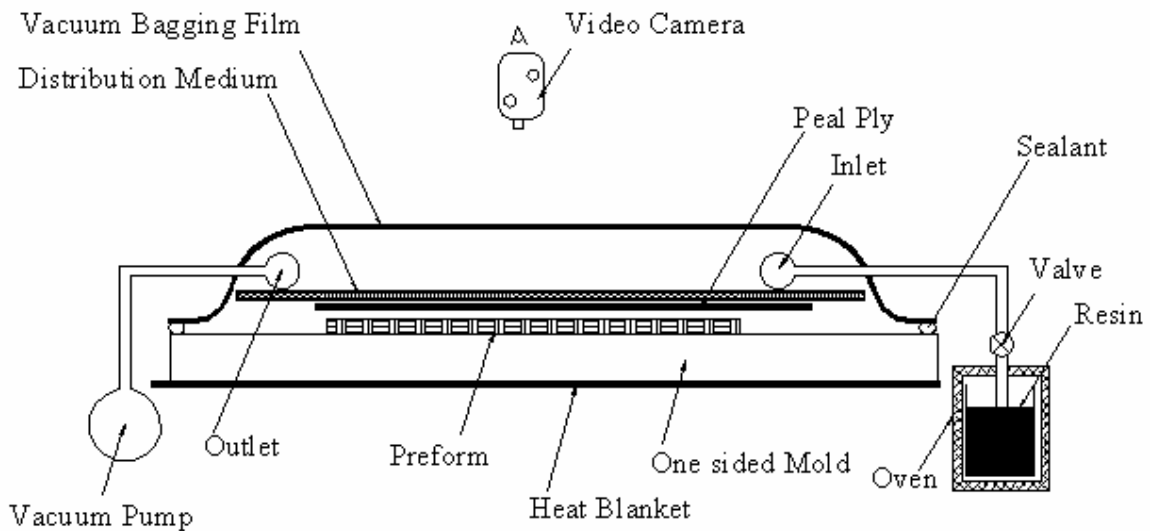


Figure 5-3. Schematic diagram of the experimental setup.

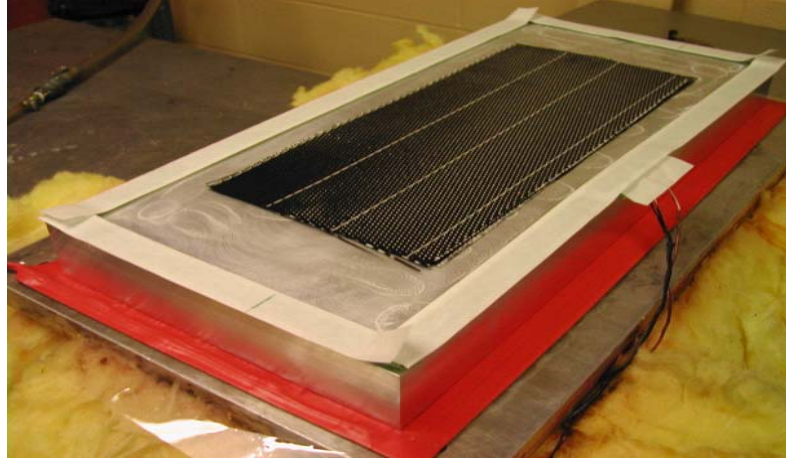


Figure 5-4. VARIM experimental setup-carbon fiber at the top of the mold.

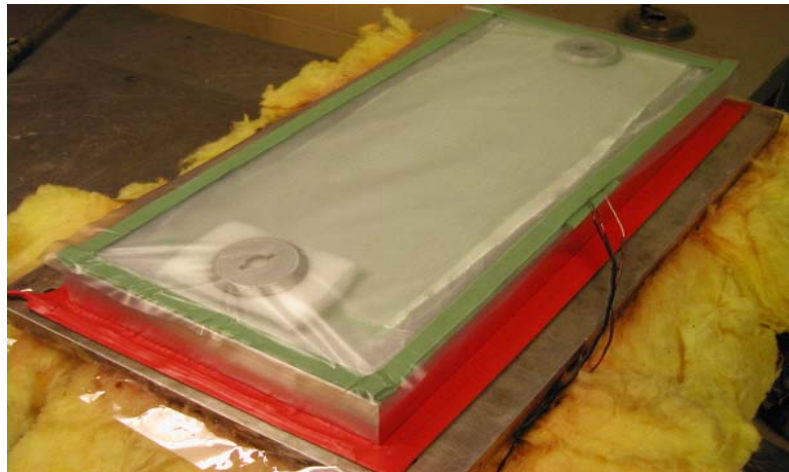


Figure 5-5. VARIM experimental setup-vacuum bag covers the mold.

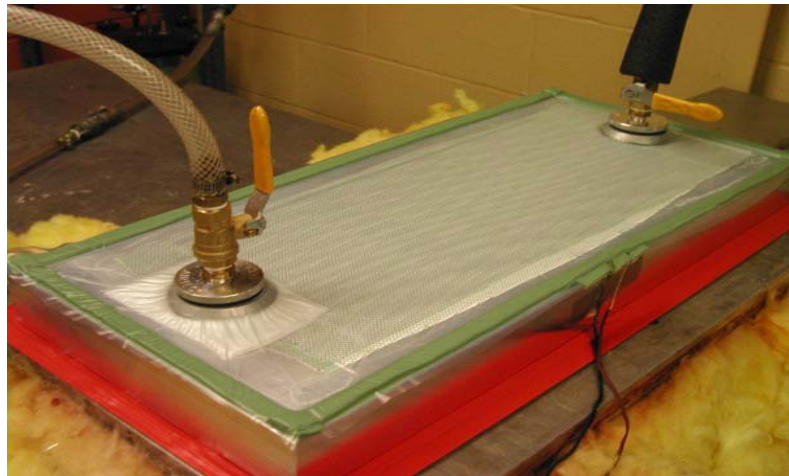


Figure 5-6. VARIM experimental setup.

## 5.4 Experimental Design

A partial factorial design of experiments was conducted on VARIM for high temperature resin composites. The process variables in the design includes: maximum curing temperature, heating rate during the cure stage, and post cure time at higher temperature after curing. Samples from the produced composites were evaluated for mechanical properties and damage assessment in the laboratory in order to establish relationships between process parameters and the properties of VARIM composites.

In order to obtain generality and precision for the developed experimental database for the process, the experiments needed to generate the required data must be conducted in a systematic and organized way. The unifying feature of statistically designed experiments is that all factors of interest are varied simultaneously. In this way, the maximum amount of information can be extracted with a minimum number of experiments. The response surface methodology (RSM) [46] is useful for cases where the responses of interest are influenced by several process factors and where the main objective is to optimize all these responses. In this method, a low order polynomial is fitted between the response parameters of the process. A three parameter RSM with central composite design was adopted. The design involves a fraction of first-order ( $2^n$ ) factorial design, two “star points” on the axis of each design variable, and one center point. The parameters were explored at five levels that cover the wide range of process conditions. The levels are represented by the commonly used codes (-1, +1, 0) on the factorial portion of the design, and values (-2, +2) on the axial portion. Table 5-1 displays the parameters, their corresponding levels and values.

A total of different 15 experiments, as shown in Table 5-2, were conducted. Each experiment will be repeated three times in order to have good estimation of experimental errors.

Table 5-1. Control factor levels corresponding to their coded levels

Level	Maximum Cure Temp. (°C)	Heating Rate (°C/min.)	Post Cure Time at 227°C (h)
-2	183	0.56	0
-1	188	0.83	2
0	194	1.11	4
1	199	1.39	5
2	205	1.67	6

Table 5-2. Three parameter central composite design

Exp No.	Maximum Cure Temp. (°C)	Heating Rate (°C/min.)	Post Cure Time at 227°C (h)
1	188	1.67	0
2	188	1.67	4
3	188	1.12	0
4	188	1.12	4
5	199	1.67	0
6	199	1.67	4
7	199	1.12	0
8	199	1.12	4
9	183	1.39	2
10	205	1.39	2
11	194	0.56	2
12	194	0.84	2
13	194	1.39	6
14	194	1.39	5
15	194	1.39	2



## 5.5 Specimens Preparation

The composite parts were cut first using a solid carbide slitting saw on a milling machine. All precautions were taken to cut the molded panels parallel to fiber direction. A special fixture was designed to be used for that purpose. Figure 5-7 shows the machining and the fixture used. Figure 5-8 shows a panel after being cut. Then a band saw was used to cut all the samples roughly at both edges. Finally the edges of samples were machined on a milling machine using a carbide end mill with diamond coating to achieve the required tolerances according the standards. Figure 5-9 shows the machining process. The same procedure was followed in the preparation of the specimen for tensile test and for compression test as well.

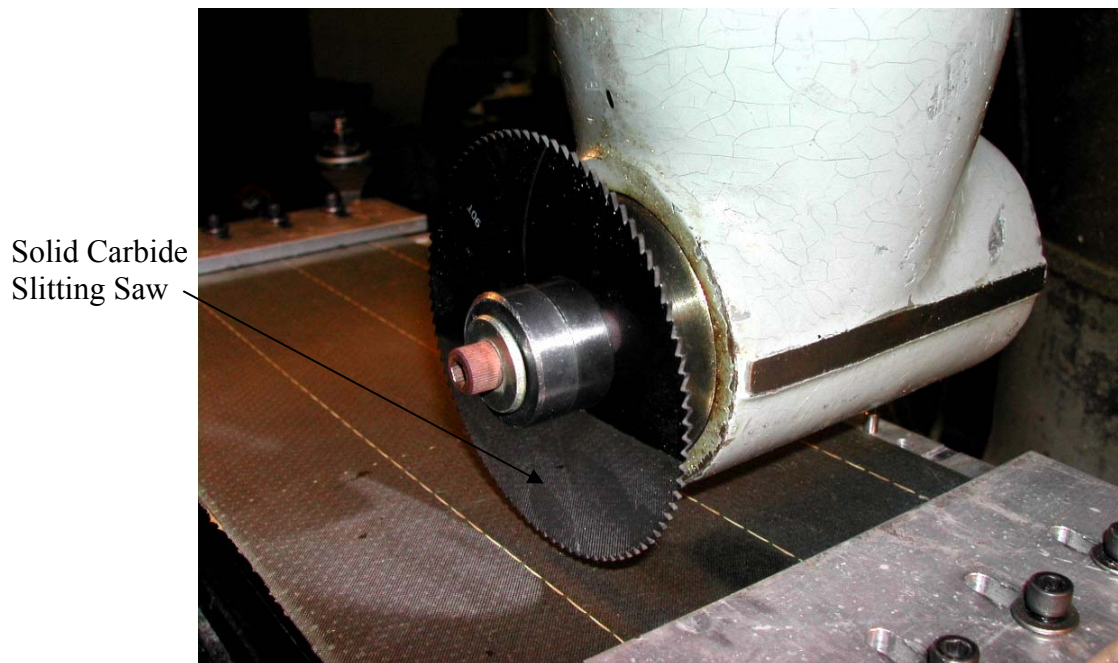


Figure 5-7. Machining of composite specimen using a special fixture.



Figure 5-8. Lateral lines being cut in the composite panel.

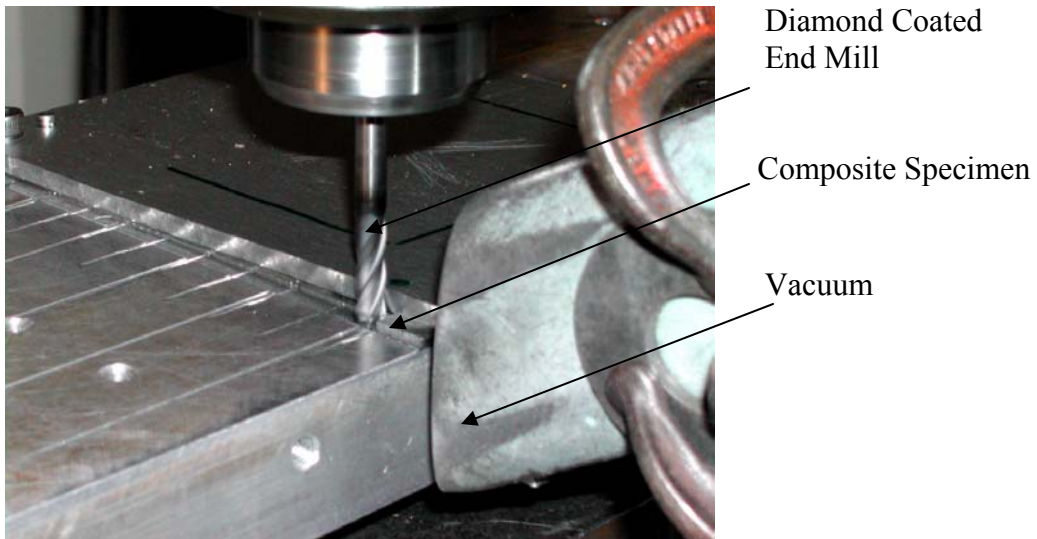


Figure 5-9. Machining of the edges of carbon fiber composite specimen.

## 5.6 Conditioning Chamber

An environmentally controlled conditioning chamber has been designed and built to expose the composite specimens molded by VARIM to an atmosphere with a high humidity as the actual aerospace working condition. The conditioning chamber is shown in Figure 5-10. The chamber consists of a stainless steel base, and a glass jar. The chamber is equipped with an electrical heater, a thermocouple, and a vacuum inlet tube. The setup of the chamber is shown in Figure 5-11. The chamber is connected to a vacuum pump, a distilled water tank. A pressure gage and a drierite are installed between the vacuum pump and the inlet valve. The electrical heater and the thermocouple are connected to a temperature controller.

The specimens were first dried twice in an oven at 160°C (325°F) for two and half hours and then left to cool down to room temperature. The conditioning chamber was loaded by the specimens as shown in Figure 5-12. The specimens were first exposed to a vacuum pressure of 735mm (29in) of mercury for 24 hours. This step was done to take all the gases out of the specimens. The water inlet valve was opened, and the water got into the chamber, until it covered the electrical heater, about 25mm (1in) of water height. Due to that the relative humidity inside the chamber was raised to 100%. The vacuum valve was closed at that time. The specimens were exposed to 100% relative humidity for 3400 hours (140 days) to reach to saturation condition [55-59]. The chamber temperature was kept at 80°C (176°F) to accelerate the process of moisture absorption [60].

After the 3400 hours, the heater of was turn off and the chamber was left to cool down to room temperature. The specimens were removed out of the conditioning chamber and placed in a plastic bag. One by one of the specimens, was taken out of the bag and was wiped by an absorbent lint free towel. Immediately, the specimen was weighed using a digital balance with a precision of +/-0.001 gram. Moisture weight gain of the specimen,  $M$ , was calculated according to ASTM standard (D5229) by the following equation:

$$M = \frac{W - W_d}{W_d} \times 100 \quad (1)$$

Where  $W_d$  is the weight of the dried specimen, and  $W$  is the weight of the specimen final weight after conditioning.

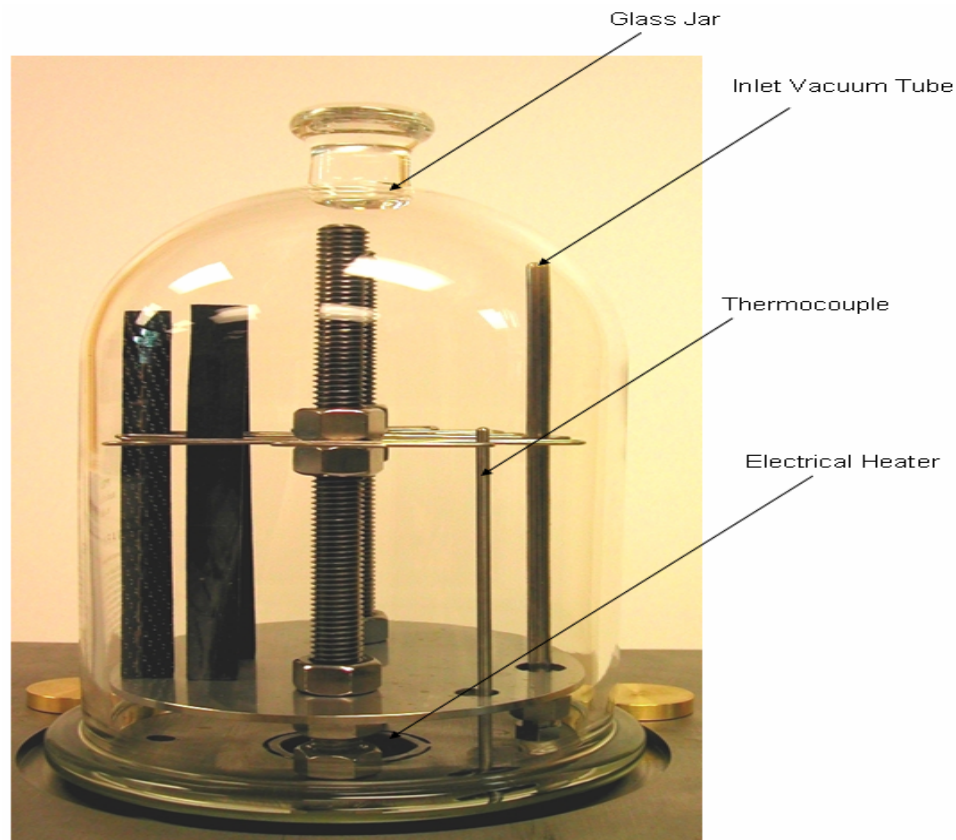


Figure 5-10. Environmentally controlled chamber.

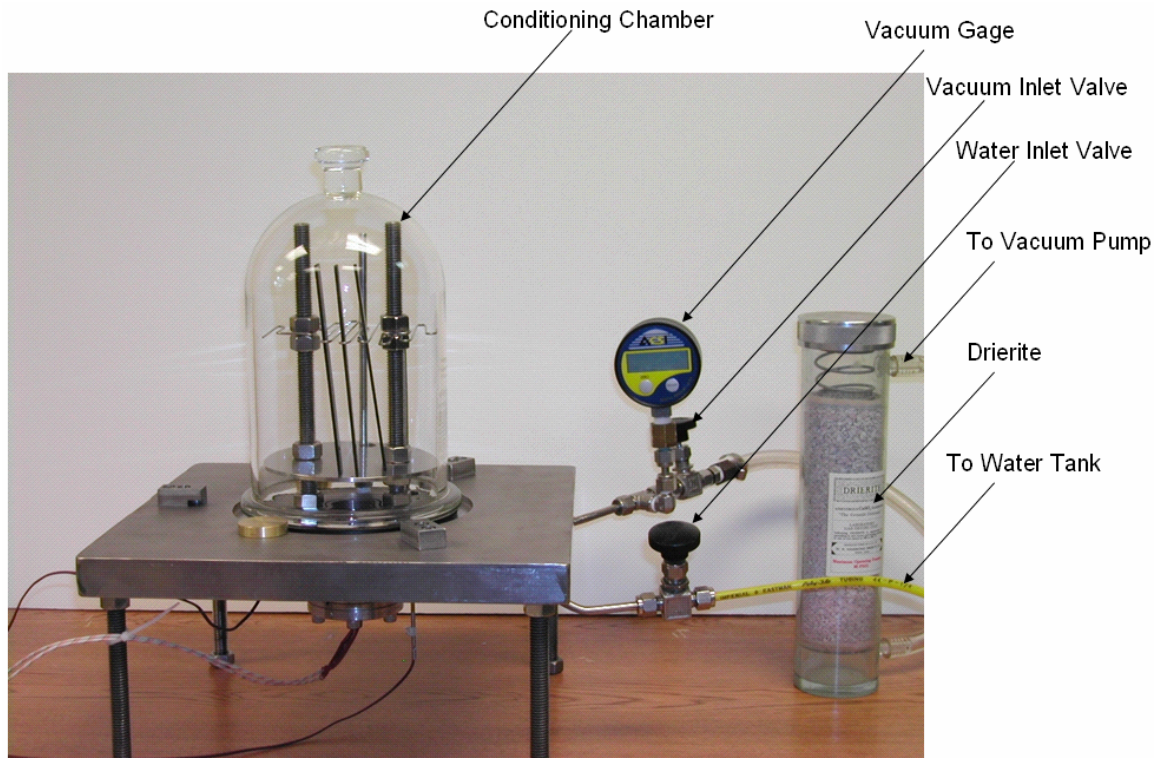


Figure 5-11. Setup of conditioning chamber.



Figure 5-12. Composite specimens loaded in the conditioning chamber.

## CHAPTER 6

# CHARACTERIZATION OF PROPERTIES OF COMPOSITES MOLDED BY VARIM

### 6.1 Introduction

In this chapter the feasibility of VARIM for fabricating high temperature polymer matrix composites was examined. The present study involves the following investigative steps:

1. Physical demonstration of the feasibility of VARIM to produce composite panels with the desired properties.
2. Evaluation of the effects of the new process on properties and process-induced damage evolved during VARIM.
3. Development of an empirical relationship between process parameters and the evolved properties and determination of the optimum process window for the required properties
4. Comparison of properties of VARIM produced composites with properties developed using conventional RTM and autoclave/prepreg molding techniques.

## 6.2 Internal Structure of Molded Panels

Several molded panels were inspected for void contents using scanning electron microscope and image analysis technique. Figure 6-1 displays one of the SEM micrograph of the internal structure of the molded composites. The average voids percentage was found to be 0.25%. This is much lower than what normally found in panels produced by RTM technique (3%). It is also less than what Aerospace industry would accept in this type of structure (1%). Table 6-1 shows percentage of voids obtained by image analysis of sectioned samples produced by VARIM. Figure 6-2 shows a sample report of one of the images analyzed for voids content in the structure.

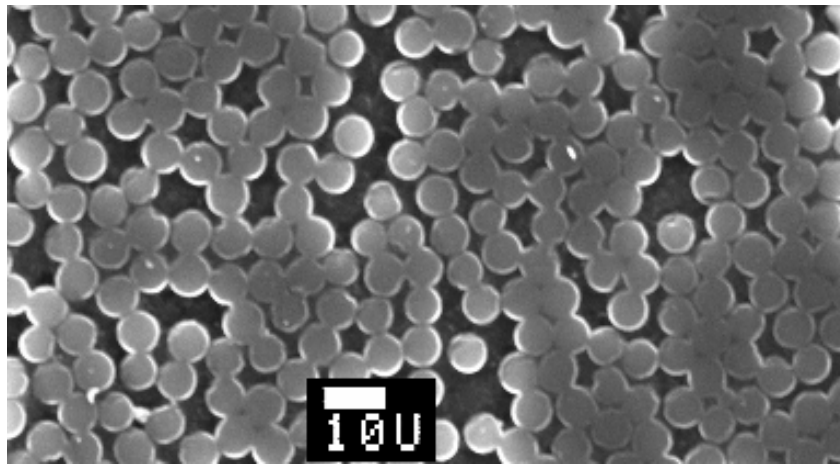


Figure 6-1. Scanning electron micrograph of composite material produced by VARIM.

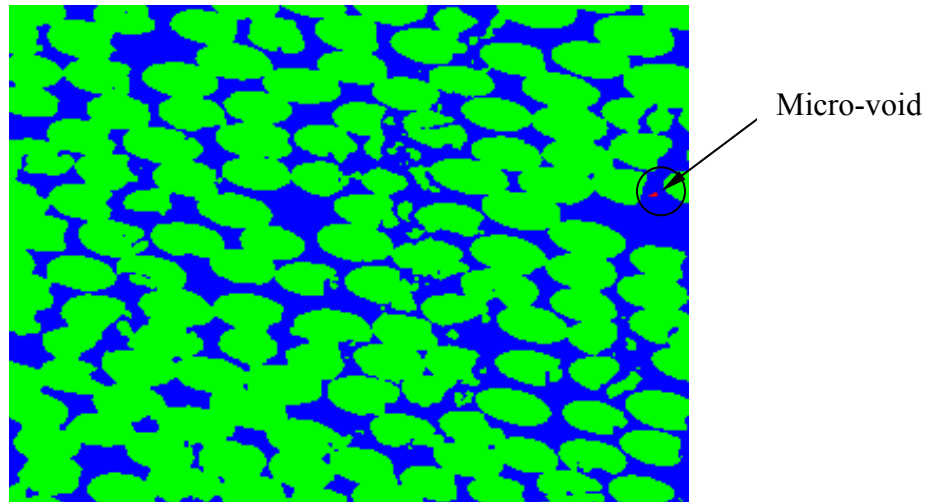


Figure 6-2. Image analysis micrograph report showing the low micro-voids contents (average 0.25%).

Table 6-1. Percentage of voids obtained by image analysis for some samples produced by VARIM

Sample No.	Percentage of Voids Content (%)
1	0.38
2	0.24
3	0.09
4	0.39
5	0.34
6	0.08
Avg	0.25
Stand. Deviation	0.14



### **6.3 Characterization of Room-Temperature Tensile Properties**

Room temperature tensile strength and tensile modulus of panels produced by VARIM were determined. Tension test was performed using ASTM standard test method for tensile properties of polymer matrix composite materials. Designation: D 3039/D 3039M-00. Latest revision: December, 2002.

#### **6.3.1 Test Procedure**

The Specimens used in the test are 200 mm (8.0 in) long, 25 mm (1.0 in) wide, and on average 0.79 mm (0.031 in) thick, to prevent slippage of the specimen inside the hydraulic grips of the MTS machine; strips of emery cloth were glued to the ends of the specimen. As shown in Figure 6-3, 64 mm (2.5 in) long by 25 mm (1 in) wide emery cloth tabs are used on both ends of the specimen. Specimens were placed in the hydraulic grips of the MTS machine leaving 12.5 mm (0.5 in) of emery cloth showing on top and bottom. In Figure 6-4, the emery cloth extends past the grips approximately 12.5 mm (0.5 in.) The coupon is shown again in b); the light colored portion of the emery cloth was the area inside the grips. This practice helps to relieve stress concentrations at the grip edge by distributing the load on the emery cloth down the sides of the coupon. An extensometer was used to record strain. The machine which was used in the test is Series 812 Materials Test System from MTS Systems Corporation. Hydraulic grips were used with a gripping pressure of 10 MPa. The tension test was performed using a constant head speed of 1.27 mm/min (0.05 in/min).

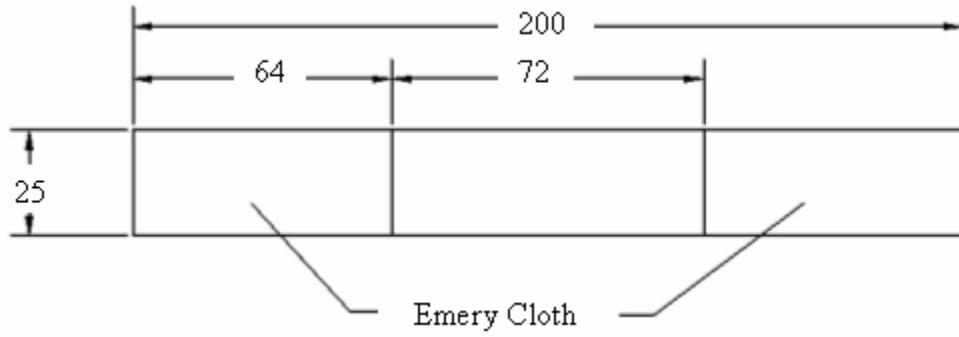


Figure 6-3. Dimensions in millimeter of coupon used in tensile test.



Figure 6-4. Tension test setup for composite sample, note the emery cloth extends past the grips approximately 12.5 (0.5 in). The sample is shown again in b); the light colored portion of the emery cloth was the area inside the grips. A new sample is shown in c).

### 6.3.2 Data Collection

The data was collected and recorded during the test from the extensometer and the MTS by LABVEIW. The data collected was load in the pounds, ram displacement in inches, and strain. The ultimate tensile strength was calculated based on the maximum load recorded and the dimension measured of the gage length of the sample (width and thickness). Since the material has a linear response stress-strain curve, the tensile modulus was calculated as the slope of the linear fit of the stress-strain curve obtained by LABVEIW. Figure 6-5 shows the stress-strain curve for one of the cases, where the maximum cure temperature is 188°C (370°F) and the heating rate is 1.67°C/min (3°F/min) without a post cure time.

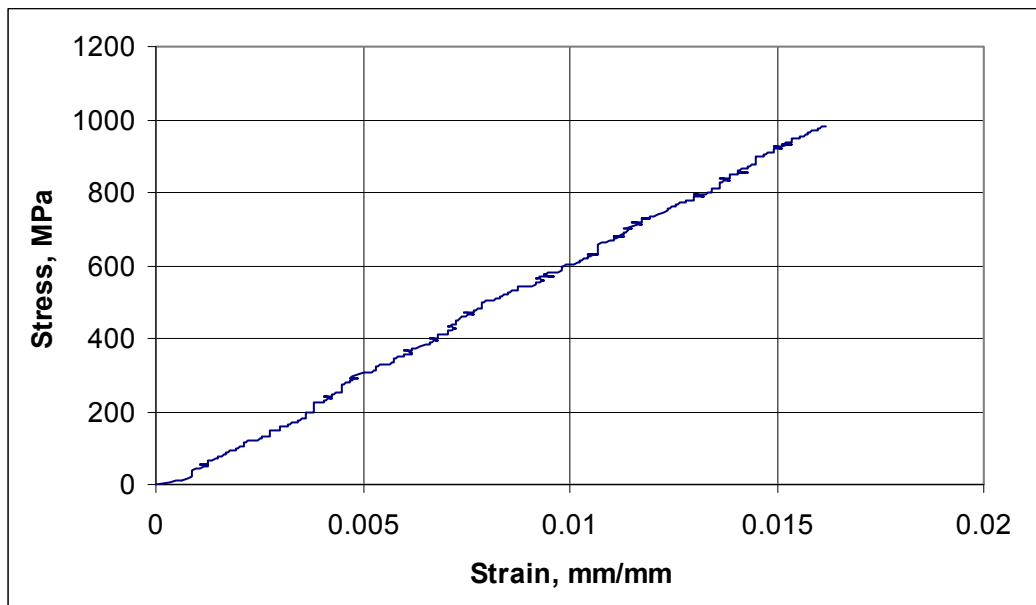


Figure 6-5. Stress-strain curve of tensile test for one of the cases.

According to ASTM standards the percentage of coefficient of variation of the ultimate tensile strength and tensile modulus is calculated as follows:

$$\bar{x} = \left( \sum_{i=1}^n x_i \right) / n \quad (1)$$

$$S_{n-1} = \sqrt{\left( \sum_{i=1}^n x_i^2 - n\bar{x}^2 \right) / (n-1)} \quad (2)$$

$$CV = 100S_{n-1} / \bar{x} \quad (3)$$

where:

$\bar{x}$  : sample mean (average)

$S_{n-1}$  : sample standard deviation

CV : sample coefficient of variation, in percent

n : number of specimens

$x_i$  : measured property.

Table 6-2 shows the effect of process parameters on ultimate tensile strength. Some cases were repeated several times to count for error and mistakes. The tensile test for case No. 1 was performed for 21 samples and it came with a coefficient of variation of 7.1 %.

Cases no. 2 and 6 were performed for 10 times and came with a coefficient of variation of 4 and 8.5 % respectively. The average coefficient of variation for the 15 cases was found

to be 5.2 %. Table 6-2 also shows the standard deviation and the coefficient of variation for each case. Figure 6-6 shows the scatter plot for ultimate tensile strength for each case. The effect of process parameters on the tensile modulus is shown in Table 6-3. The maximum coefficient of variation was found to be 4.8 % for case No. 1. The average coefficient of variation for all cases was found to be 3 %. The scatter plot for tensile modulus for each case is shown in Figure 6-7.

Table 6-2. Process parameters effect on ultimate tensile strength for each case

Case No.	Maximum Cure Temp. (°C)	Heating Rate (°C/min.)	Post Cure Time at 227°C (h)	No of Samples Tested	Tensile Strength		
					Max. Tensile Strength (MPa)	Standard Deviation	Coefficient of Variation %
1	188	1.67	0	21	917	65	7.1
2	188	1.67	4	10	828	33	4.0
3	188	1.12	0	5	892	69	7.8
4	188	1.12	4	5	804	38	4.7
5	199	1.67	0	8	847	62	7.3
6	199	1.67	4	10	786	66	8.5
7	199	1.12	0	5	841	46	5.5
8	199	1.12	4	5	778	26	3.3
9	183	1.39	2	5	884	24	2.7
10	205	1.39	2	5	817	45	5.5
11	194	0.56	2	5	825	21	2.5
12	194	0.84	2	5	828	35	4.3
13	194	1.39	6	5	838	40	4.7
14	194	1.39	5	5	808	54	6.7
15	194	1.39	2	5	856	34	4.0

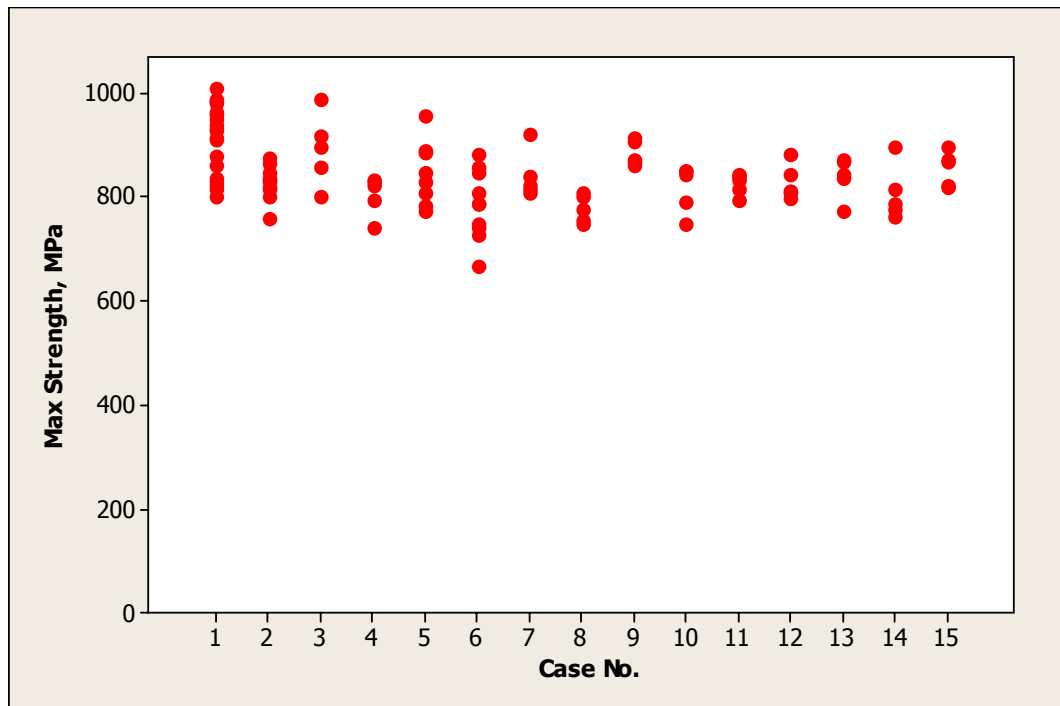


Figure 6-6. Scatter plot of tensile strength for each case shown in table 6-2.

Table 6-3. Process parameters effect on tensile modulus for each case

Case No.	Maximum Cure Temp. (°C)	Heating Rate (°C/min.)	Post Cure Time at 227°C (h)	No of Samples Tested	Tensile Modulus		
					Average Tensile Modulus (GPa)	Standard Deviation	Coefficient of Variation %
1	188	1.67	0	21	63	3	4.8
2	188	1.67	4	10	62	3	4.5
3	188	1.12	0	5	64	1	1.1
4	188	1.12	4	5	59	3	4.2
5	199	1.67	0	8	61	1	2.0
6	199	1.67	4	10	63	2	3.0
7	199	1.12	0	5	61	2	3.1
8	199	1.12	4	5	59	2	3.5
9	183	1.39	2	5	60	1	1.4
10	205	1.39	2	5	61	2	3.5
11	194	0.56	2	5	60	2	4.1
12	194	0.84	2	5	60	2	3.1
13	194	1.39	6	5	61	3	4.5
14	194	1.39	5	5	62	1	1.5
15	194	1.39	2	5	61	1	1.4

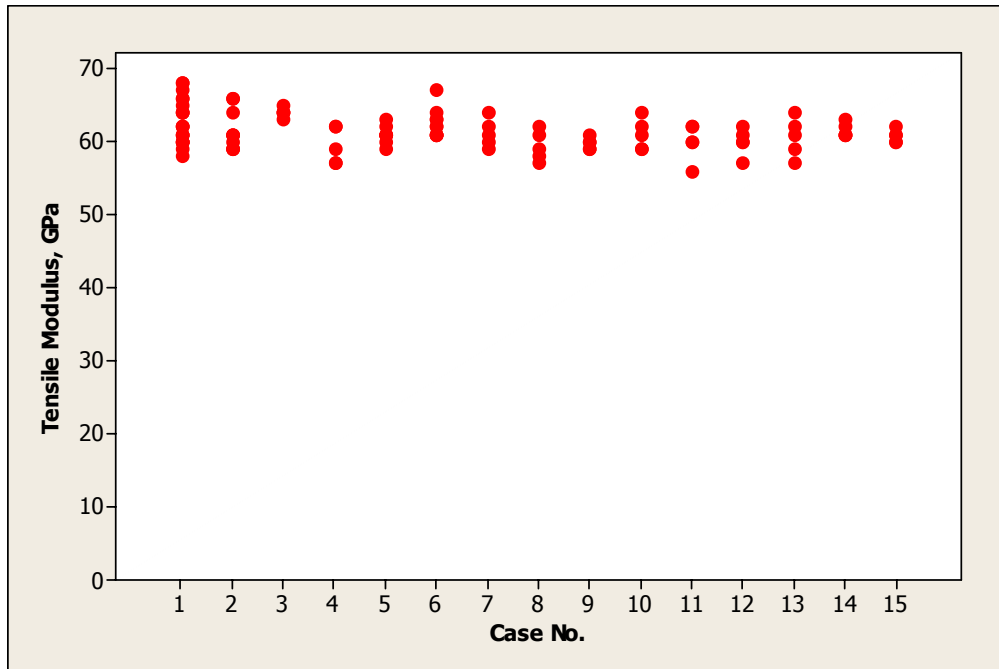


Figure 6-7. Scatter plot of tensile modulus for each case shown in table 6-3.

### 6.3.3 Response Analysis

The responses obtained from the different 15 cases as shown in Tables 6-2 and 6-3, were analyzed using graphical representation of the mean effects of each parameter. The response analysis helps in identifying those parameters that have the greatest impact on the process. Figures 6-8 to 6-10 show the average main effects of process parameters, which are post cure time, maximum cure temperature, and heating rate, on ultimate tensile strength, respectively. These figures show that the trend of the ultimate tensile strength decreases as the post cure time and the maximum cure temperature increase within the range used for both parameters. Figure 6-10 shows that as the heating rate increases from  $0.56^{\circ}\text{C}/\text{min}$  ( $1^{\circ}\text{F}/\text{min}$ ) to  $1.67^{\circ}\text{C}/\text{min}$  ( $3^{\circ}\text{F}/\text{min}$ ) the composite strength increases slightly.

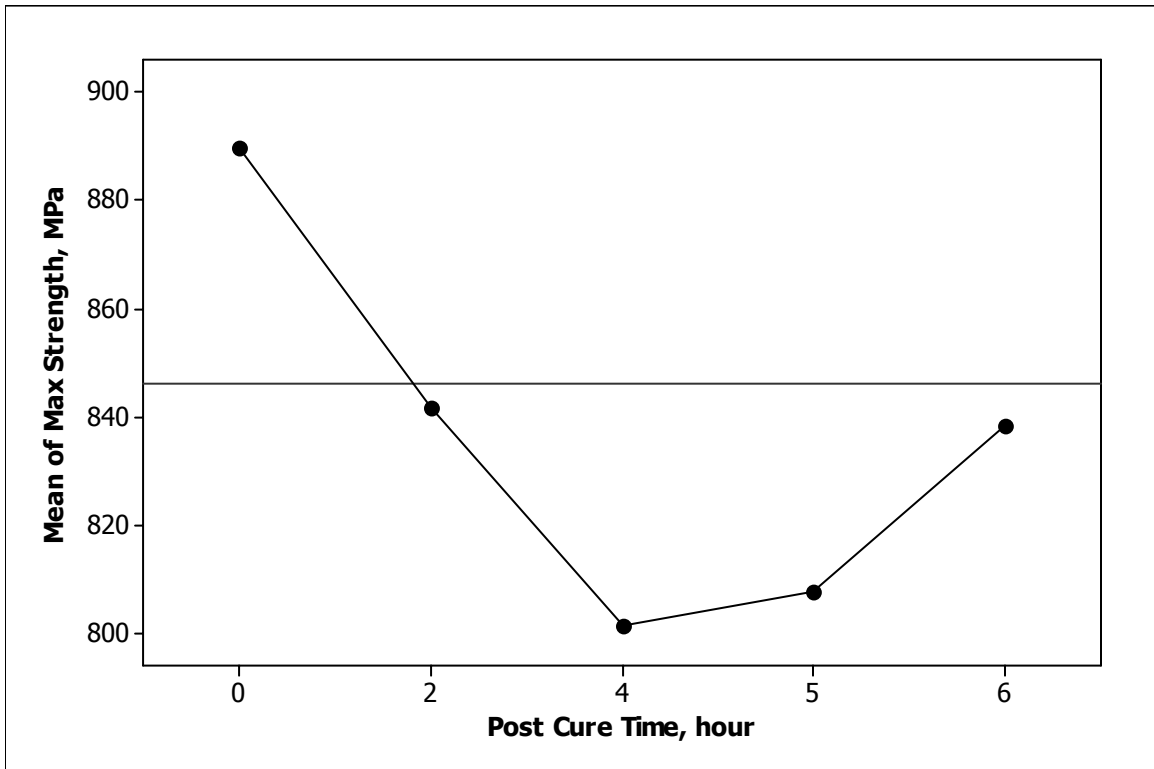


Figure 6-8. Average main effect of post cure time on ultimate tensile strength.



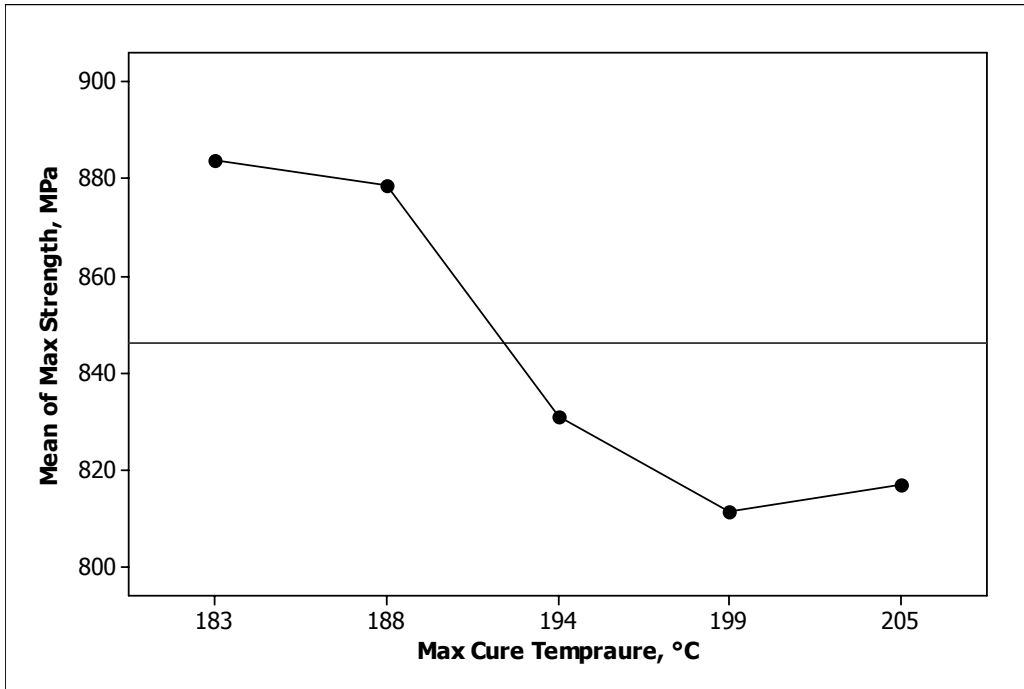


Figure 6-9. Average main effect of max cure temperature on ultimate tensile strength.

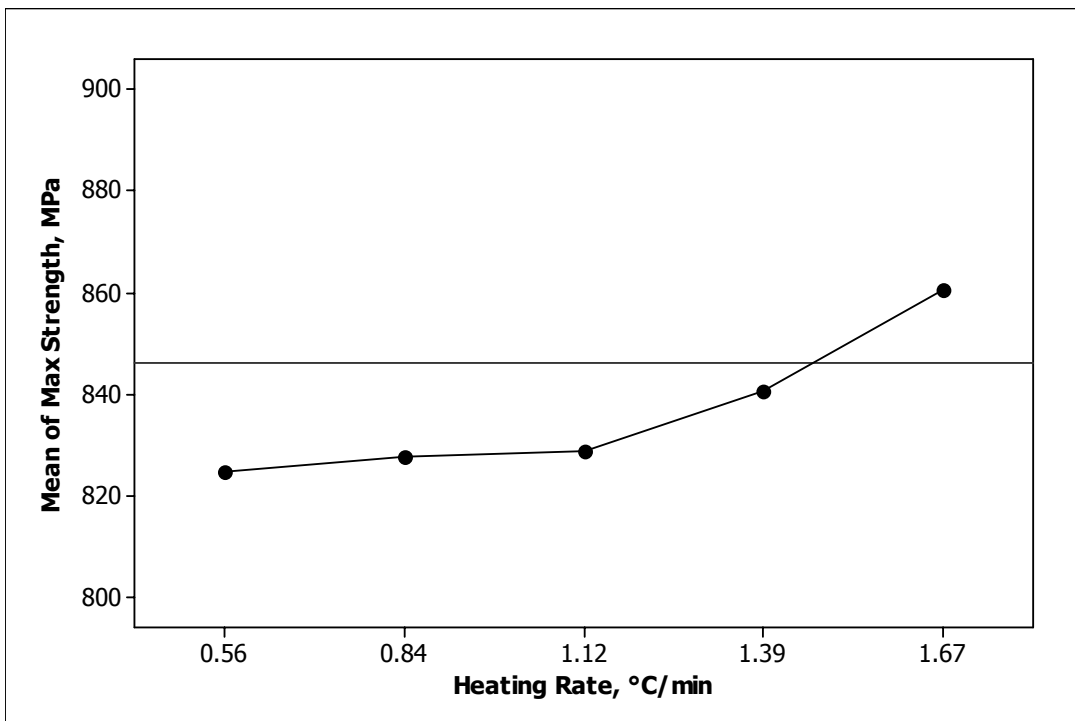


Figure 6-10. Average main effect of heating rate on ultimate tensile strength.

Analysis of variance (ANOVA) was performed to investigate the effect of process parameters on the obtained responses (maximum tensile strength and tensile modulus). Table 6-4 summarizes the analysis of variance. The p-values (P) and F-ratios (F) are used in the analysis to estimate the significance of each parameter on the experimental responses [63, 64]. F-ratio in the analysis is compared to F a 5%, commonly used, upper critical value of the F distribution (F table). If F-ratio is greater than F-table, the parameter is statistically significant. The p-value (P) is compared to level of significance,  $\alpha$ -value. The commonly used value for  $\alpha$  is 5%. If p-value is less than or equal to  $\alpha$ -value, the parameter has a significant effect. As shown in Tables 6-4, the p-values for maximum cure temperature, and post cure time are less than  $\alpha$ -value, which is 0.05. Then, these two parameters within the range used in the experiment are, statistically, significant factors. F-ratios for maximum cure temperature and post cure time are 5.254 and 10.361 respectively as shown in Table 6-4. The F-ratios confirm the same results as before, since they are greater than F-table (2.72). Post cure time is the most significant parameters, as it has the highest F-ratio. The analysis of response, as shown before in Figures 6-8 and 6-9, shows that these two parameters have strong effect on tensile strength. The ANOVA shows also that heating rate, with F-ratio less than F-table and p-value greater than  $\alpha$ -value, is an insignificant parameter.

Table 6-4. Analysis of variance for ultimate tensile strength

Source	Sum Squares	DF	Mean Square	F	P
Max Cure Temp	42124.7	3	14041.6	5.254	0.002
Heating Rate	6217.5	3	2072.5	0.775	0.511
Post Cure Time	83075.8	3	27691.9	10.361	0.000
Error	237872.9	89	2672.73		
Total	449794.9	103			

Where in the ANOVA tables, the DF is the degree of freedom, F is the error variance ratio, and P is the percentage of confidence level of the parameters.

Figures 6-11 to 6-13 show the average main effects of process parameters, which are post cure time, maximum cure temperature, and heating rate, on tensile modulus, respectively. Figure 6-11 shows that as the heating rate increases the modulus slightly increases. As shown in Figures 6-12 and 6-13 the effects of post cure time and maximum cure temperature on tensile modulus are not clear and the data is scattered around the average line. The analysis of variance (ANOVA), summarized in Table 6-5, shows that post cure time is the dominant parameter over the other two parameters, heating rate and maximum cure temperature. The analysis shows that post cure time is slightly significant as its F-ratio, 2.71, is equal to F-table, 2.72. Heating rate and maximum cure temperature are insignificant parameters as their F-ratios are less than the F-table.

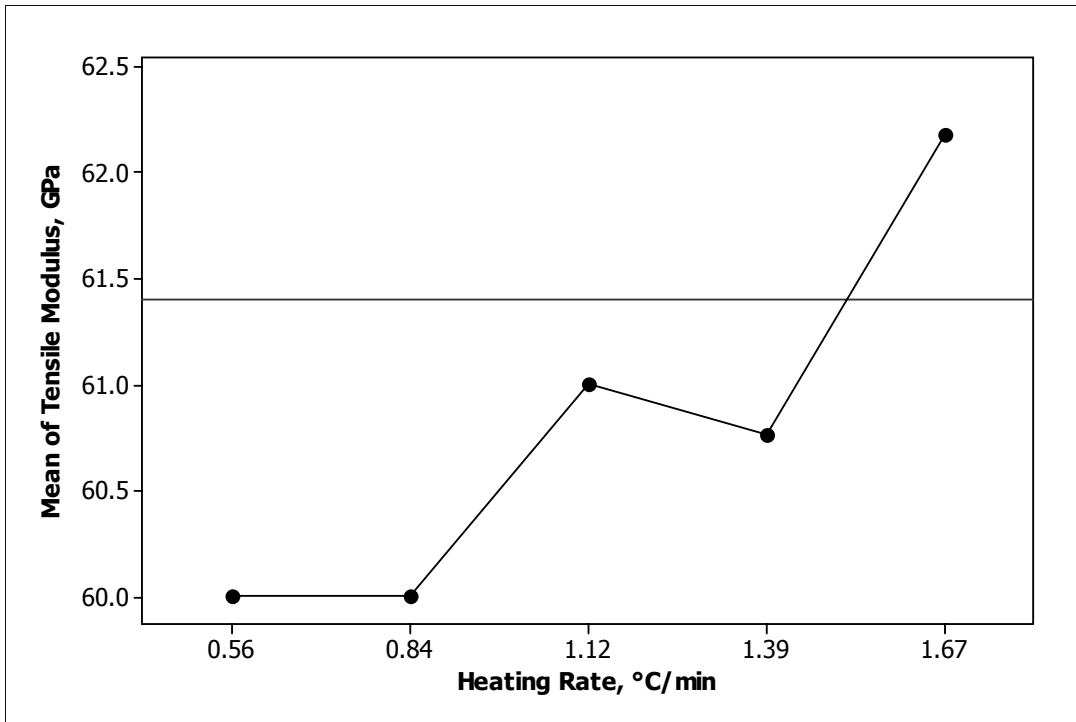


Figure 6-11. Average main effect of heating rate on tensile modulus.

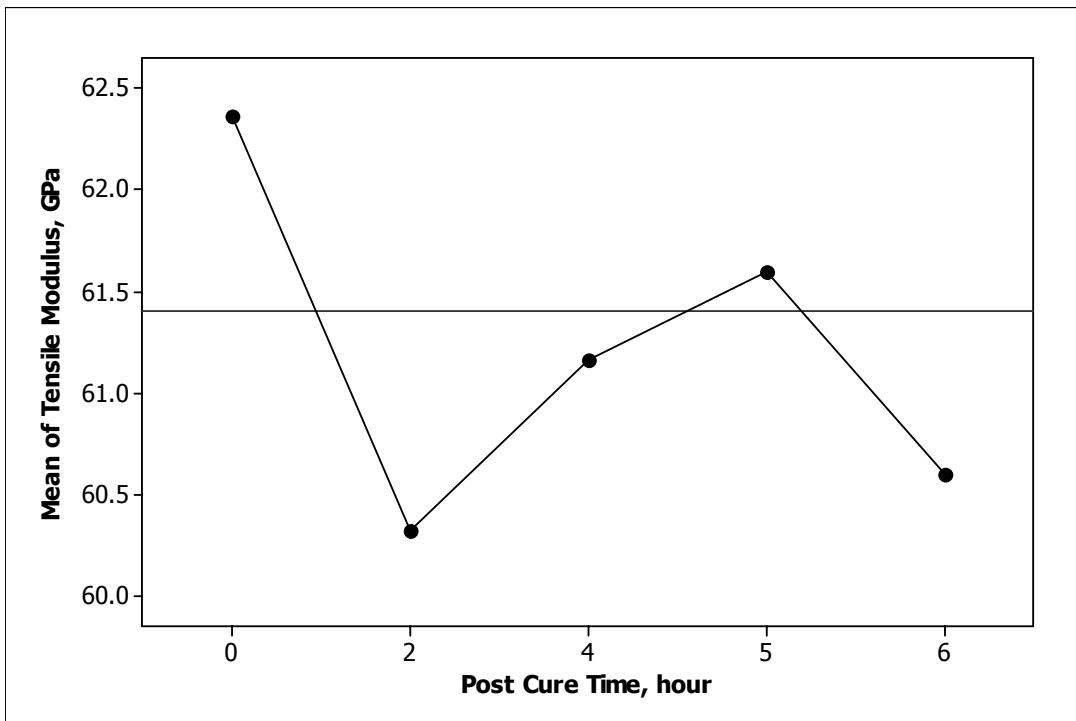


Figure 6-12. Average main effect of post cure time on tensile modulus.

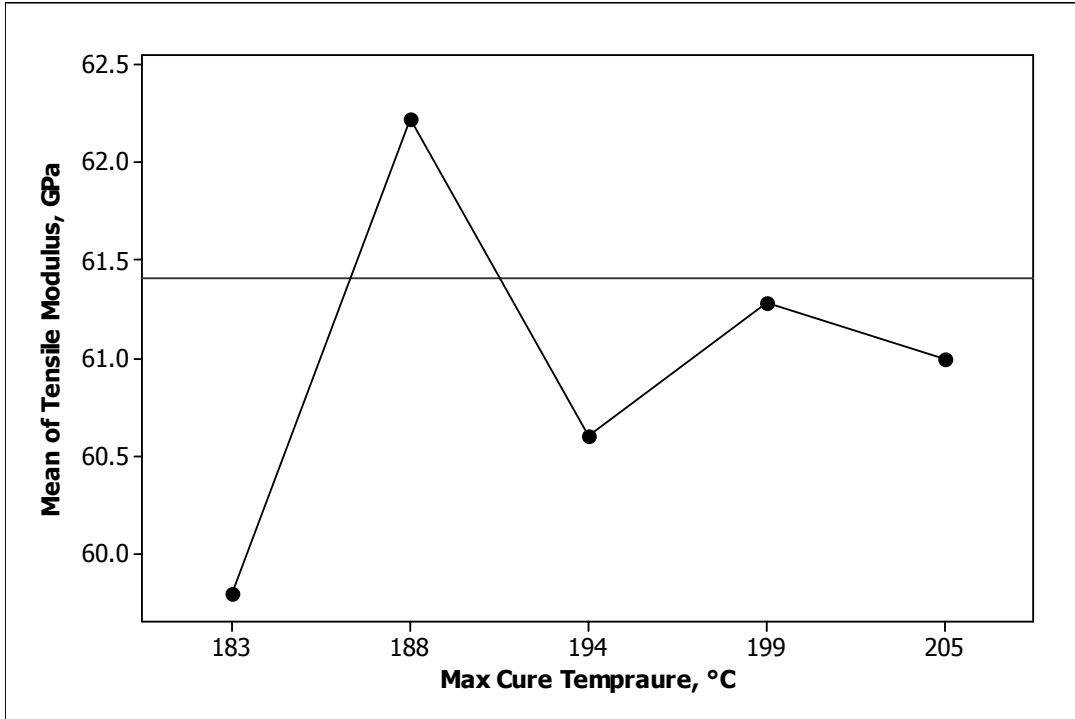


Figure 6-13. Average main effect of max cure temperature on tensile modulus.

Table 6-5. Analysis of variance for tensile modulus at room temperature

Source	Sum Squares	DF	Mean Square	F	P
Max Cure Temp	15.6	3	5.19	1.036	0.381
Heating Rate	14.9	3	4.951	0.988	0.402
Post Cure Time	34.1	3	11.379	2.271	0.086
Error	445.9	89	5.01		
Total	611.0	103			

## **6.4 Characterization of Compressive Properties of the Molded Materials under Different Environmental Conditions**

Compressive properties were also determined according to the ASTM Standard D6641 using the combined loading compression (CLC) test fixture. Since the composite is being manufactured for use in aerospace applications, the material needs to be tested in such similar environments, which are high temperature and high humidity [65]. A series of tests were accomplished at elevated temperatures and 100% relative humidity, to determine the response of the composite when stressed under these conditions. Compression tests were conducted at room temperature and at elevated temperature of 177°C (350°F) wet and dry.

### **6.4.1 Room Temperature Compression Test**

#### **6.4.1.1 Test Procedure**

Room temperature compressive strength of panels produced by VARIM was determined. Compression test was performed according to ASTM standard test method using the Combined-Load Compression (CLC) fixture [66], shown in Figure 6-14. Designation: ASTM standard D-6641. The compressive load is applied to the specimen by combined end and shear loading.

The specimen is un-tabbed rectangular strip of the molded composite. Specimens, used in the test, are 140 mm (5.5 in) long, 12.5 mm (0.5 in) wide, and on average 2.1 mm (0.084 in) thick. The tension test was performed using a constant head speed of 1.27 mm/min (0.05 in/min).

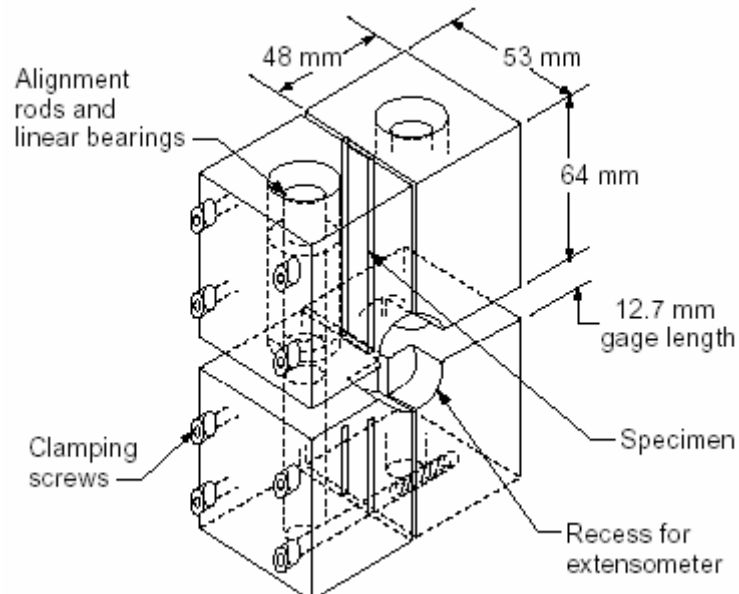


Figure 6-14. Combined loading compressive test fixture, taken from [66].

#### 6.4.1.2 Data Collection

The data was collected and recorded during the test from the MTS by LABVEIW. The data collected was only the load in pounds. The maximum compressive strength was calculated based on maximum load recorded and the dimension measured of the gage length of the sample (width and thickness).

Table 6-6 shows the effect of process parameters on the maximum compressive strength. The maximum and the minimum coefficient of variation were found to be 12.8% and 2% for case No. 2 and case No. 1, respectively. The average coefficient of variation for the 15 cases was found to be 5.7%. Table 6-6 also shows the standard deviation and the coefficient of variation for each case. Figure 6-15 shows the scatter plot for maximum compressive strength for each case.

Table 6-6. Process parameters effect on compressive strength at room temperature

Case No.	Maximum Cure Temp. (°C)	Heating Rate (°C/min.)	Post Cure Time at 227°C (h)	No of Samples Tested	Compressive Strength		
					Average Compressive Strength (MPa)	Standard Deviation	Coefficient of Variation %
1	188	1.67	0	3	620	12	2.0
2	188	1.67	4	3	538	15	2.8
3	188	1.12	0	3	564	26	4.7
4	188	1.12	4	3	476	61	12.8
5	199	1.67	0	3	555	22	3.9
6	199	1.67	4	3	495	13	2.6
7	199	1.12	0	3	557	33	6.0
8	199	1.12	4	3	481	44	9.2
9	183	1.39	2	3	501	46	9.1
10	205	1.39	2	3	477	30	6.2
11	194	0.56	2	3	480	24	5.1
12	194	0.84	2	3	523	28	5.3
13	194	1.39	6	3	498	13	2.6
14	194	1.39	5	3	507	32	6.3
15	194	1.39	2	3	455	33	7.2

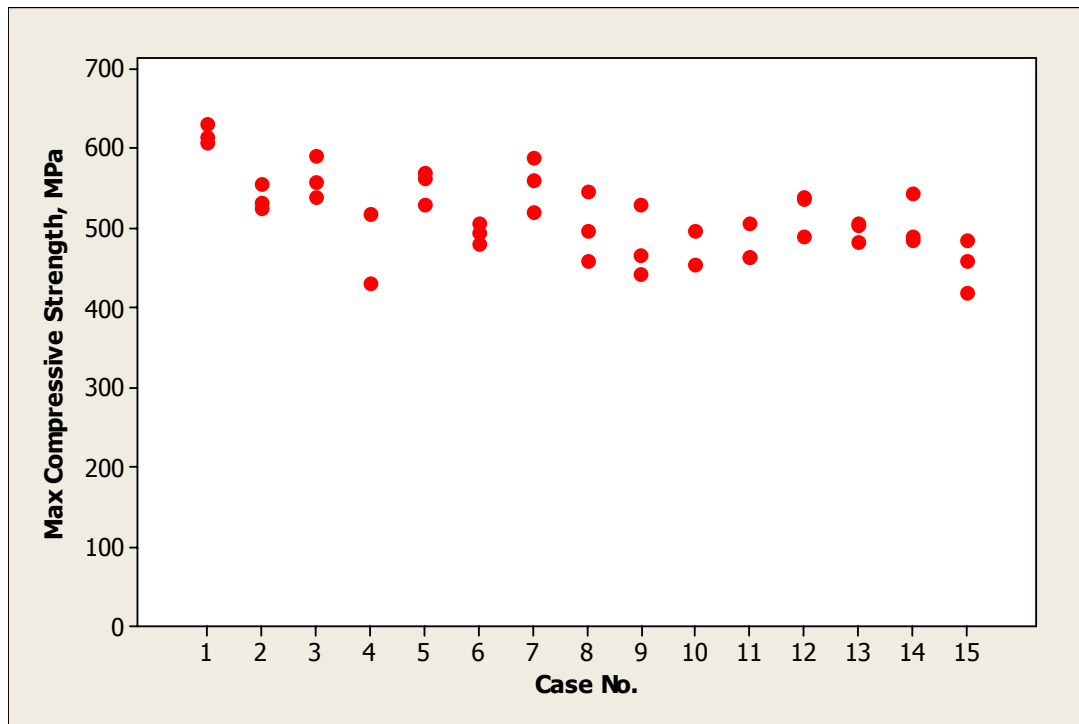


Figure 6-15. Scatter plot of tensile modulus for each case shown in table 6-6.



### 6.4.1.3 Response Analysis

The responses obtained from the different 15 cases as shown in Table 6-6, were analyzed using graphical representation of the mean effects of each parameter. Figures 6-16 to 6-18 show the average main effects of process parameters, which are post cure time, maximum cure temperature, and heating rate, on max compressive strength. Figure 6-16 shows that the max compressive strength decreases as the post cure time increases within the range used in the experiments, from zero to 2 hours and then almost stays within the same range. Figure 6-17 shows that the max compressive strength increases as the heating rate increases from  $0.56^{\circ}\text{C}/\text{min}$  ( $1^{\circ}\text{F}/\text{min}$ ) to  $1.67^{\circ}\text{C}/\text{min}$  ( $3^{\circ}\text{F}/\text{min}$ ). Except at heating rate  $1.39^{\circ}\text{C}/\text{min}$  ( $2.5^{\circ}\text{F}/\text{min}$ ) it showed a drop in the compressive strength. The effect of maximum cure temperature is not clear and the data is scattered around the average line as shown in Figure 6-18.

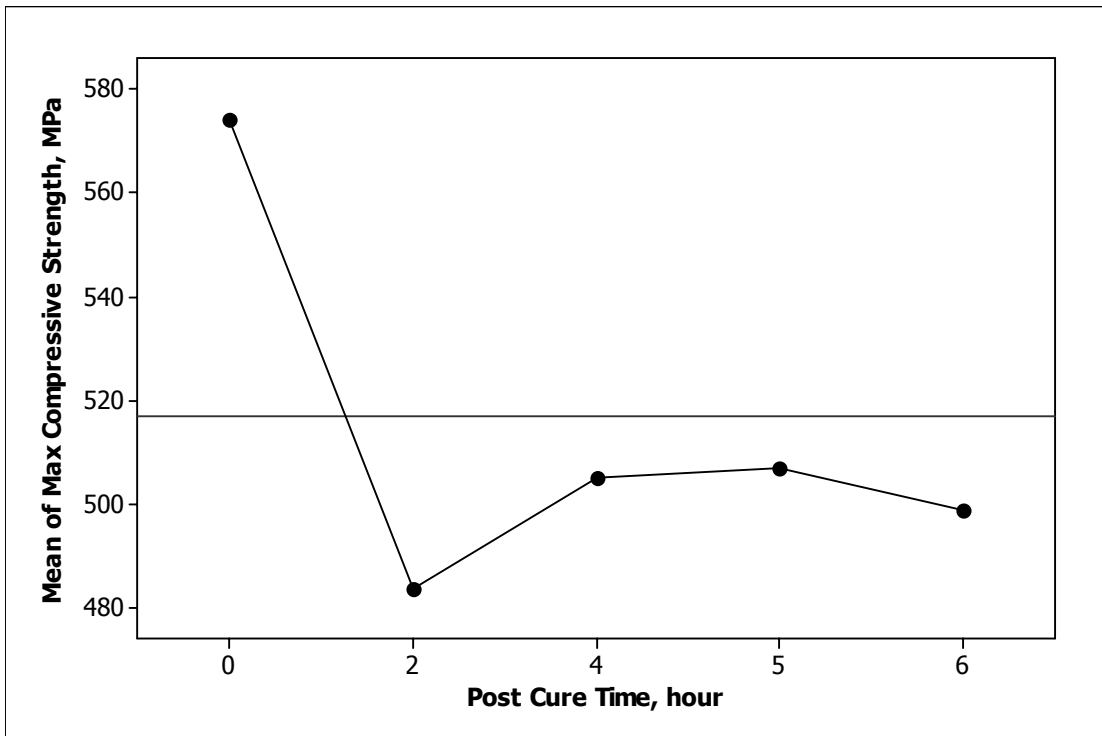


Figure 6-16. Average main effect of post cure time on compressive strength.

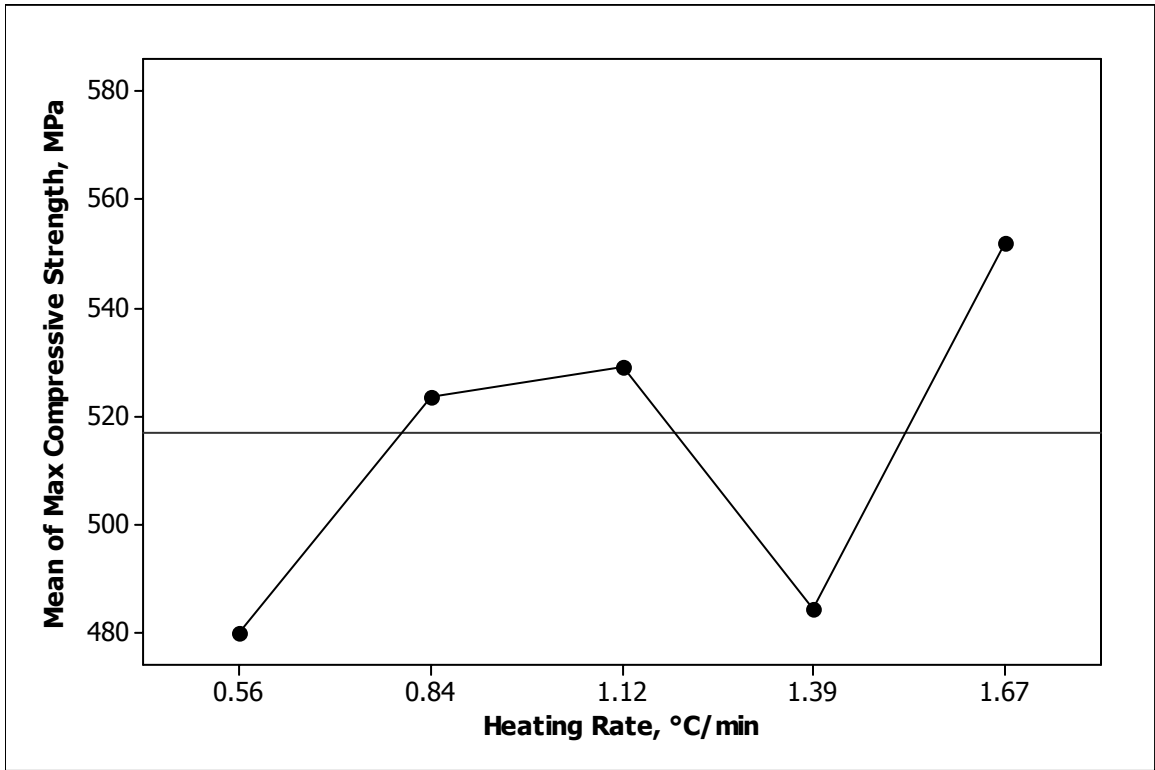


Figure 6-17. Average main effect of heating rate on compressive strength.

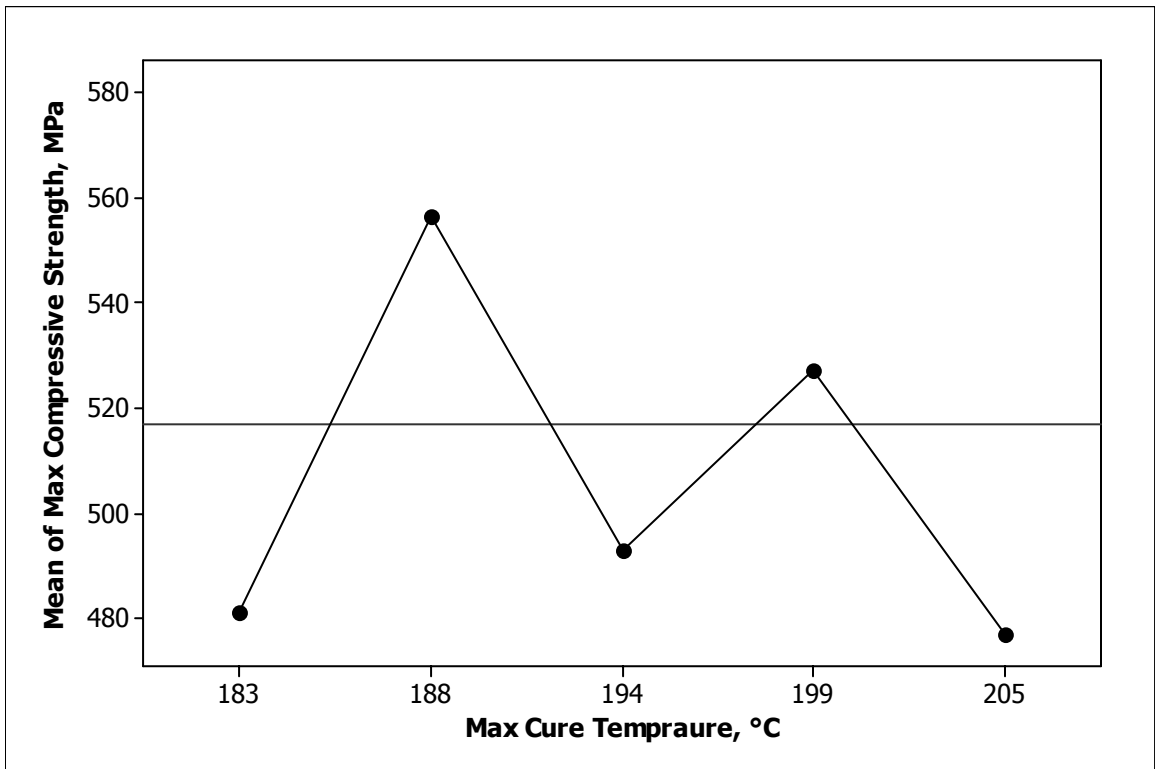


Figure 6-18. Average main effect of max cure temperature on compressive strength.

The analysis of variance (ANOVA) shows that post cure time in the range used in the experiments is the most significant parameter followed by heating rate. As shown in the ANOVA Table 6-7 p-values for these two parameters are less than the percentage of confidence,  $\alpha$ -value, which is 0.05. F-ratios for these two parameters, heating rate and post cure time, are 4.166 and 12.196 respectively as shown in Table 6-7. Their F-ratios confirm the same results as before, since they are greater than F-table (2.83). Also, the analysis shows that maximum cure temperature is statistically insignificant. The p-value for maximum cure temperature, 0.243, is greater than the  $\alpha$ -value, 0.05.

Table 6-7. Analysis of variance for max compressive strength at room temperature

Source	Sum Squares	DF	Mean Square	F	P
Max Cure Temp	4036.8	3	1345.61	1.473	0.243
Heating Rate	11414.6	3	3804.86	4.166	0.015
Post Cure Time	33415.0	3	11138.3	12.196	0.000
Error	25572.0	28	913.286		
Total	104222.8	42			

## 6.4.2 High Temperature-Dry Compression Test

### 6.4.2.1 Test Procedure

The effect of elevated temperature on compressive strength and modulus of panels produced by VARIM were determined. Compression test was performed according to ASTM standard test method using the Combined-Load Compression (CLC) fixture. Designation: ASTM standard D-6641. The compressive load is applied to the specimen by combined end and shear loading. The CLC fixture was modified to be equipped with a heating coil and a thermocouple. Figure 6-19 shows a picture of the modified fixture. The thermocouple is connected to a temperature controller to control the heating rate. The heating coil and the thermocouple are shown in Figure 6-20.

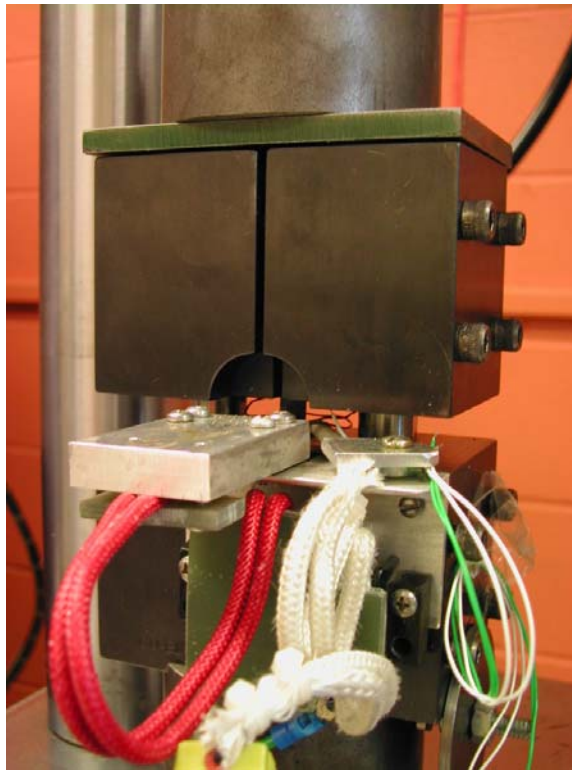


Figure 6-19. Combined load compression (CLC) modified fixture.

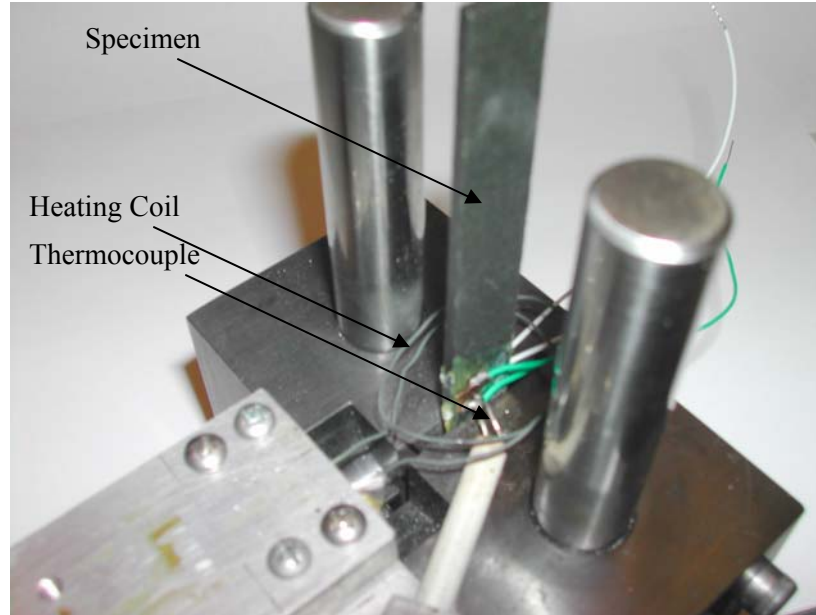


Figure 6-20. One half of the CLC modified fixture showing the heating system.

The specimen is un-tabbed rectangular strip of the molded composite. Specimens, used in the test, are 140 mm (5.5 in) long, 12.5 mm (0.5 in) wide, and on average 2.1 mm (0.084 in) thick. The tension test was performed using a constant head speed of 1.27 mm/min (0.05 in/min). The specimen was heated inside the CLC modified fixture with a high heating rate, 15°C/min. The high heating rate was used as a similar condition to the actual working condition [67]. The specimen was heated from room temperature up to 177°C (350°F) and kept at this level for 10 minutes to reach to a homogeneous temperature distribution before applying the load.

A strain gage was used to measure the strain during the test. Special glue for high temperature application was used to attach the strain gage to the specimen. This glue needs to be cured at elevated temperature, so the specimen with the glued strain gage was

heated at an air circulating oven to 163°C (325°F) for two hours and half with a heating rate of 15°C/min, as recommended by the manufacturer. Figure 6-21 shows the specimen used in the test.



Figure 6-21. The specimen with the strain gage used in the compression test.

#### **6.4.2.2 Data Collection**

The data was collected and recorded during the test from the MTS by LABVEIW. The data collected was the compressive load, the corresponding strain, and the specimen temperature. The maximum compressive strength was calculated based on maximum load recorded and the dimension measured of the gage length of the sample (width and thickness). The compressive modulus was calculated as the slope of the linear fit of the stress-strain curve obtained. Figure 6-22 shows the stress-strain curve for one of the cases, where the maximum cure temperature is 199°C (390°F) and the heating rate is 1.11°C/min (2°F/min) without post cure time.

Table 6-8 shows the effect of process parameters on the ultimate compressive strength. The average coefficient of variation for the 15 cases, every case repeated 3 times, was found to be 7.7 %. Table 6-8 also shows the standard deviation and the coefficient of variation for each case. Figure 6-23 shows the scatter plot for ultimate compressive strength for each case.

The effect of process parameters on the compressive modulus is shown in Table 6-9. The maximum coefficient of variation was found to be 11.3 % for case No. 3. Case numbers 2 and 15 have the lowest coefficient of variation, 0.2 %. The average coefficient of variation for all cases was found to be 3.7 %. The scatter plot for compressive modulus for each case is shown in Figure 6-24.

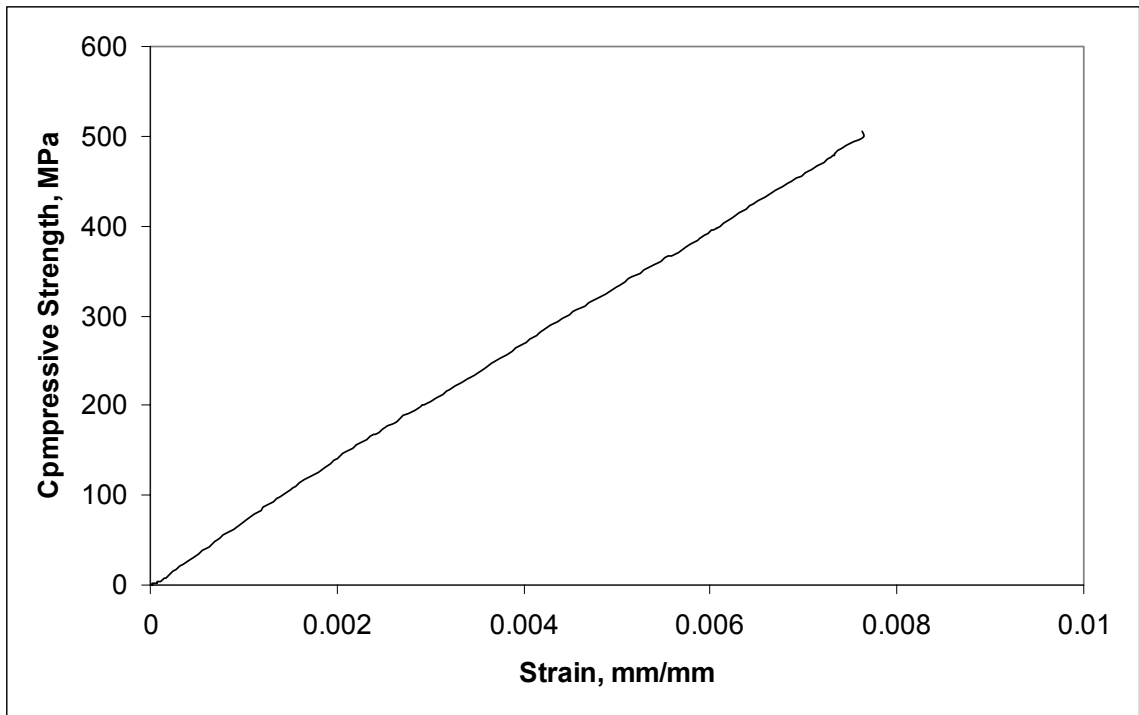


Figure 6-22. Stress-strain curve for compression test of one of the cases.

Table 6-8. Process parameters effect on the compressive strength for high temp-dry

Case No.	Maximum Cure Temp. (°C)	Heating Rate (°C/min.)	Post Cure Time at 227°C (h)	No. of Samples Tested	Compressive Strength		
					Compressive Strength (MPa)	Standard Deviation	Coefficient of Variation %
1	188	1.67	0	3	533	35	6.5
2	188	1.67	4	3	327	34	10.4
3	188	1.12	0	3	466	47	10.2
4	188	1.12	4	3	358	18	5.0
5	199	1.67	0	3	438	42	9.6
6	199	1.67	4	3	404	33	8.1
7	199	1.12	0	3	391	48	12.2
8	199	1.12	4	3	463	5	1.1
9	183	1.39	2	3	480	46	9.5
10	205	1.39	2	3	396	20	5.0
11	194	0.56	2	3	433	46	10.6
12	194	0.84	2	3	435	45	10.4
13	194	1.39	6	3	444	12	2.7
14	194	1.39	5	3	515	47	9.2
15	194	1.39	2	3	436	23	5.2

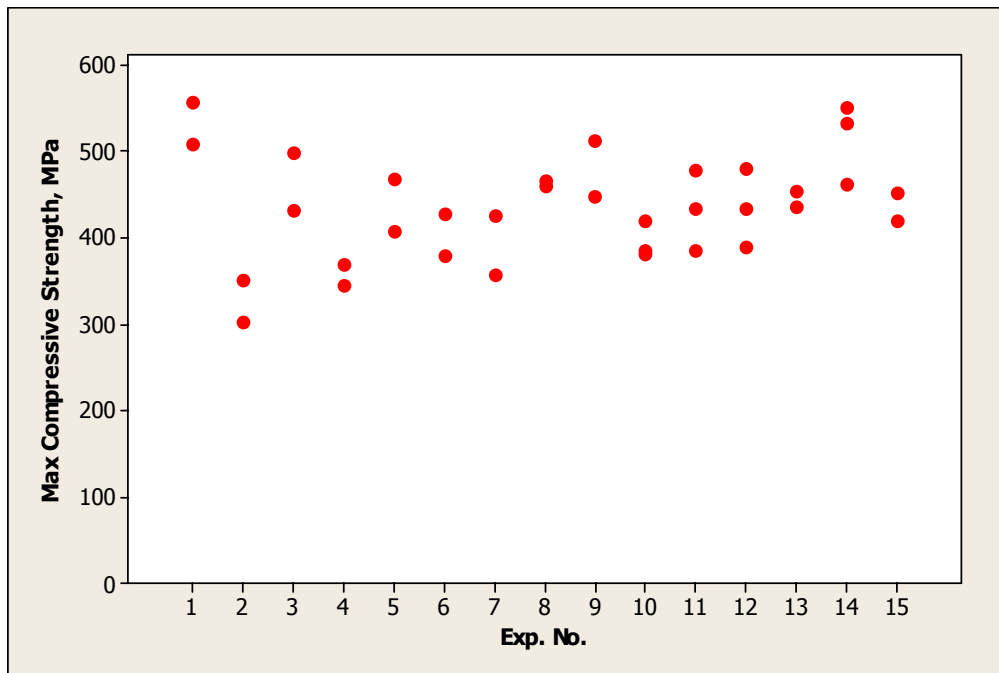


Figure 6-23. Scatter plot of compressive modulus for each case shown in table 6-8.



Table 6-9. Process parameters effect on the compressive modulus for each case

Case No.	Maximum Cure Temp. (°C)	Heating Rate (°C/min.)	Post Cure Time at 227°C (h)	No. of Samples Tested	Compressive Modulus		
					Compressive Modulus (GPa)	Standard Deviation	Coefficient of Variation %
1	188	1.67	0	3	61	3	4.7
2	188	1.67	4	3	63	1	1.1
3	188	1.12	0	3	58	7	11.3
4	188	1.12	4	3	63	3	4.1
5	199	1.67	0	3	59	1	1.9
6	199	1.67	4	3	63	3	4.3
7	199	1.12	0	3	65	2	3.1
8	199	1.12	4	3	62	0	0.2
9	183	1.39	2	3	61	1	2.4
10	205	1.39	2	3	64	4	6.7
11	194	0.56	2	3	60	2	4.1
12	194	0.84	2	3	65	0	0.0
13	194	1.39	6	3	62	4	7.0
14	194	1.39	5	3	62	3	4.4
15	194	1.39	2	3	59	0	0.2

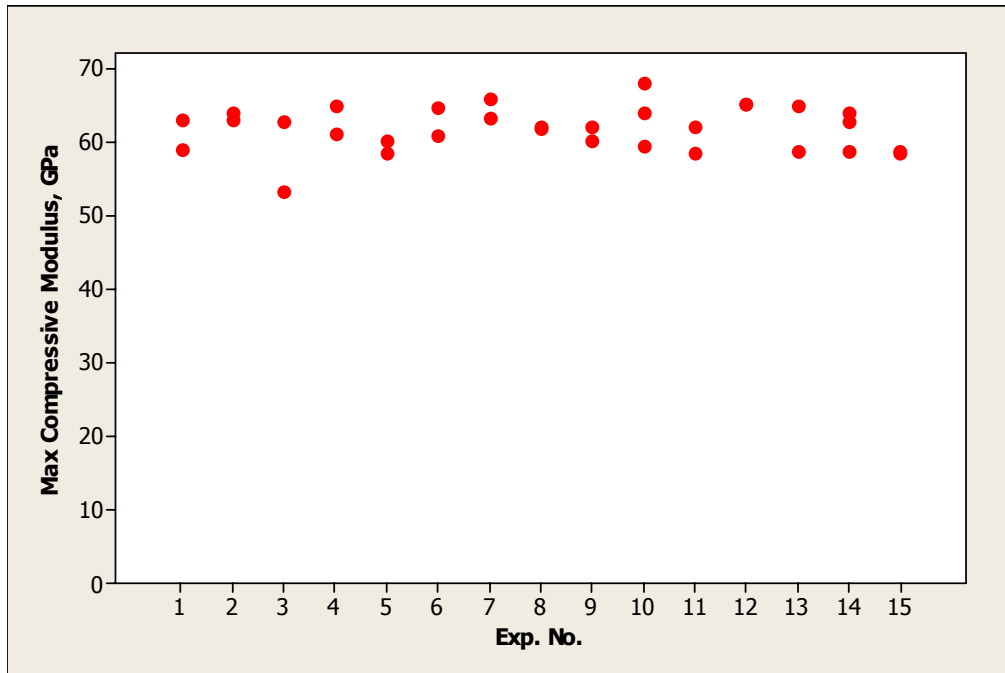


Figure 6-24. Scatter plot of compressive modulus for each case shown in table 6-9.

### 6.4.2.3 Response Analysis

The responses obtained from the 15 different cases as shown in Tables 6-8 and 6-9, were analyzed using graphical representation of the mean effects of each parameter. Figures 6-25 to 6-27 show the average main effects of process parameters, which are post cure time, maximum cure temperature, and heating rate, on compressive strength, respectively. Figure 6-25 shows that the compressive strength decreases as the post cure time increases from zero to 4 hours, and then it increases at post cure time of 5 hours. After that the strength decreases at post cure time of 6 hours. Figure 6-26 shows that the trend of compressive strength decreases as the maximum cure temperature increases except at cure temperature of 194°C (380°F) the strength shows a slight increase. The heating rate, as shown in Figure 6-27, does not show a clear effect on compressive strength, since the data is scattered around and close to the average line.

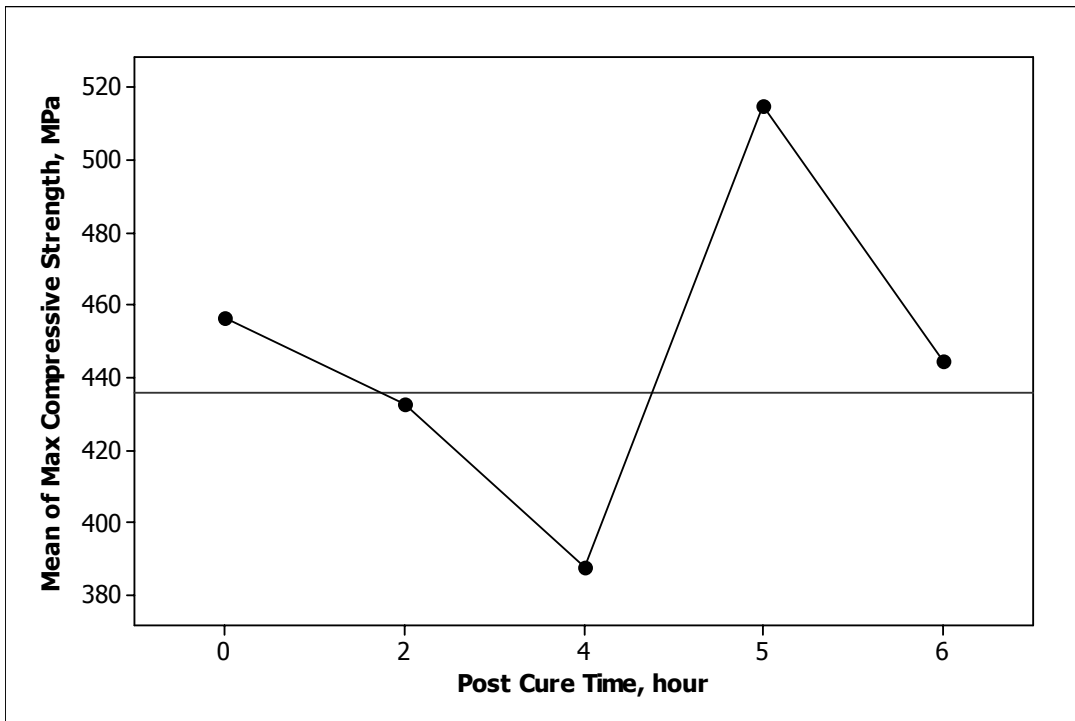


Figure 6-25. Average main effect of post cure time on compressive strength.

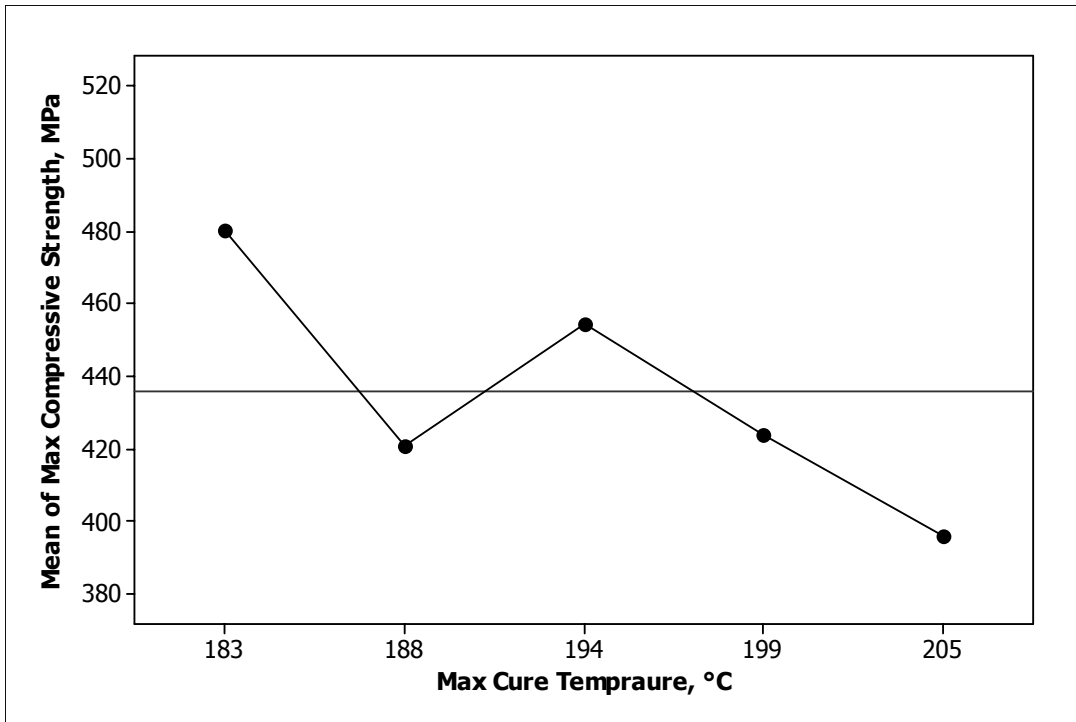


Figure 6-26. Average main effect of max cure temperature on compressive strength.

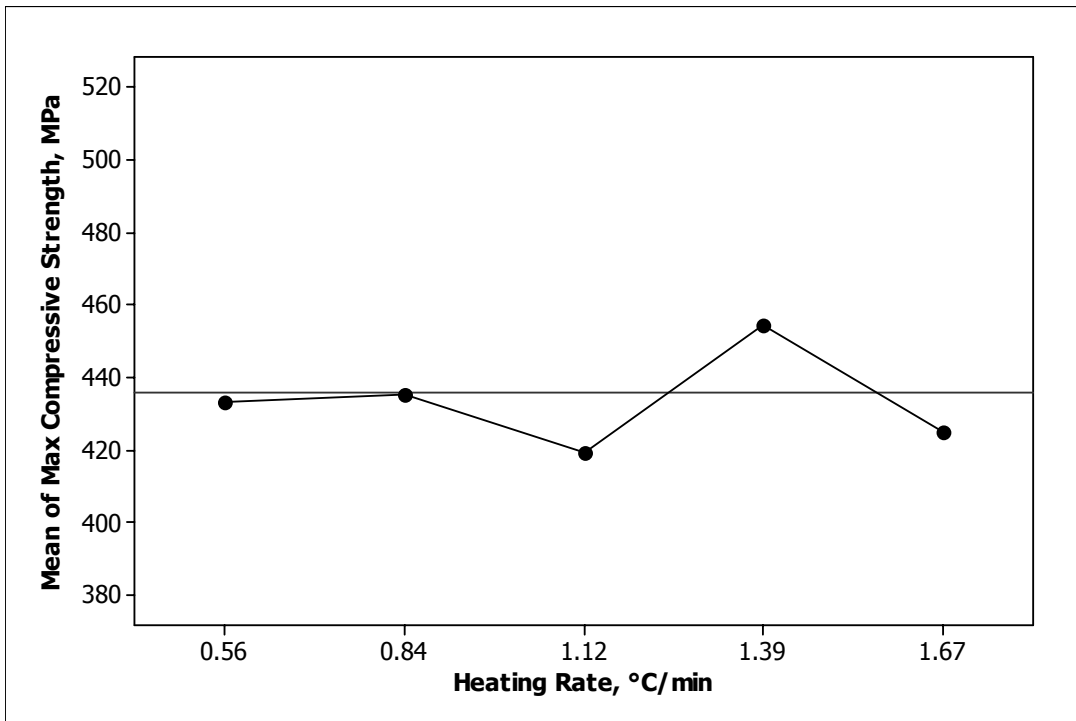


Figure 6-27. Average main effect of heating rate on compressive strength.

Analysis of variance (ANOVA) was performed for the obtained responses and summarized in Table 6-10. The analysis shows that post cure time in the range used in the experiments is a significant parameter. As shown in Tables 6-10 the p-value for post cure time, 0.003, is less than the percentage of confidence,  $\alpha$ -value, which is 0.05 and its F-ratio, 6.809, is greater than F-table, 2.90. Also, the analysis shows that the p-value for heating rate and maximum cure temperature are greater than the  $\alpha$ -value. Then, these two parameters in the range used in the experiment are statistically insignificant.

Table 6-10. Analysis of variance for compressive strength at high temperature-dry

Source	Sum Squares	DF	Mean Square	F	P
Max Cure Temp	8730.5	3	2910.18	2.072	0.138
Heating Rate	156.0	3	52.00	0.037	0.990
Post Cure Time	28694.9	3	9564.98	6.809	0.003
Error	26688.7	19	1404.67		
Total	118445.8	33			

Figures 6-28 to 6-30 show the average main effects of process parameters, which are maximum cure temperature, post cure time, and heating rate, on compressive modulus, respectively. Figure 6-28 shows that as the maximum cure temperature increases, in the range used in the experiment, the modulus slightly increases. As shown in Figures 6-29 and 6-30 the effects of post cure time and heating rate on compressive strength are not clear and the data is scattered around the average line.

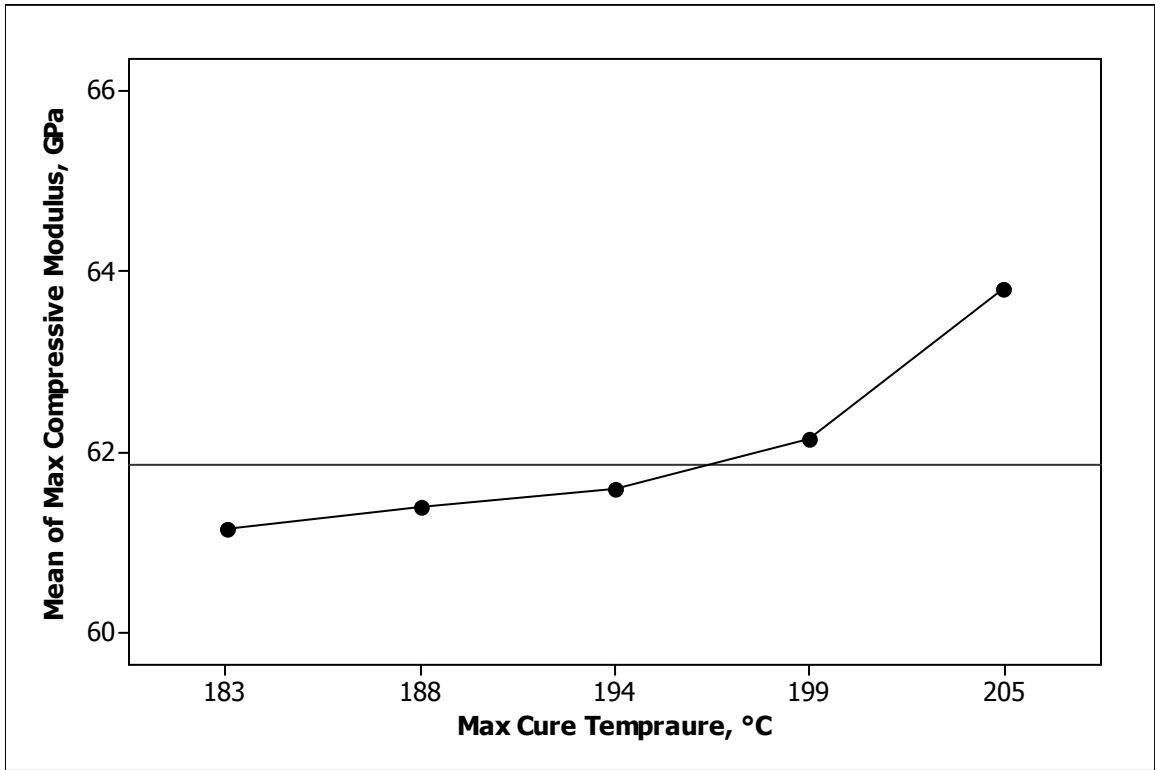


Figure 6-28. Average main effect of max cure temperature on compressive modulus.

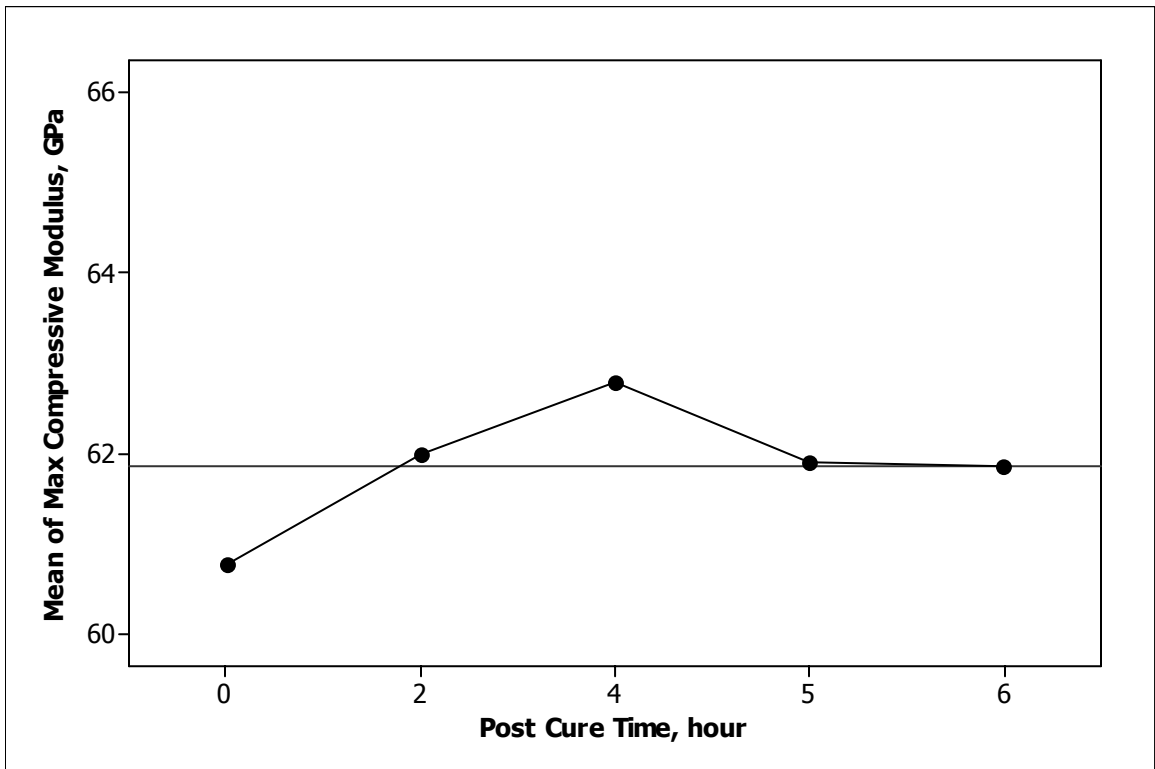


Figure 6-29. Average main effect of post cure time on compressive modulus.

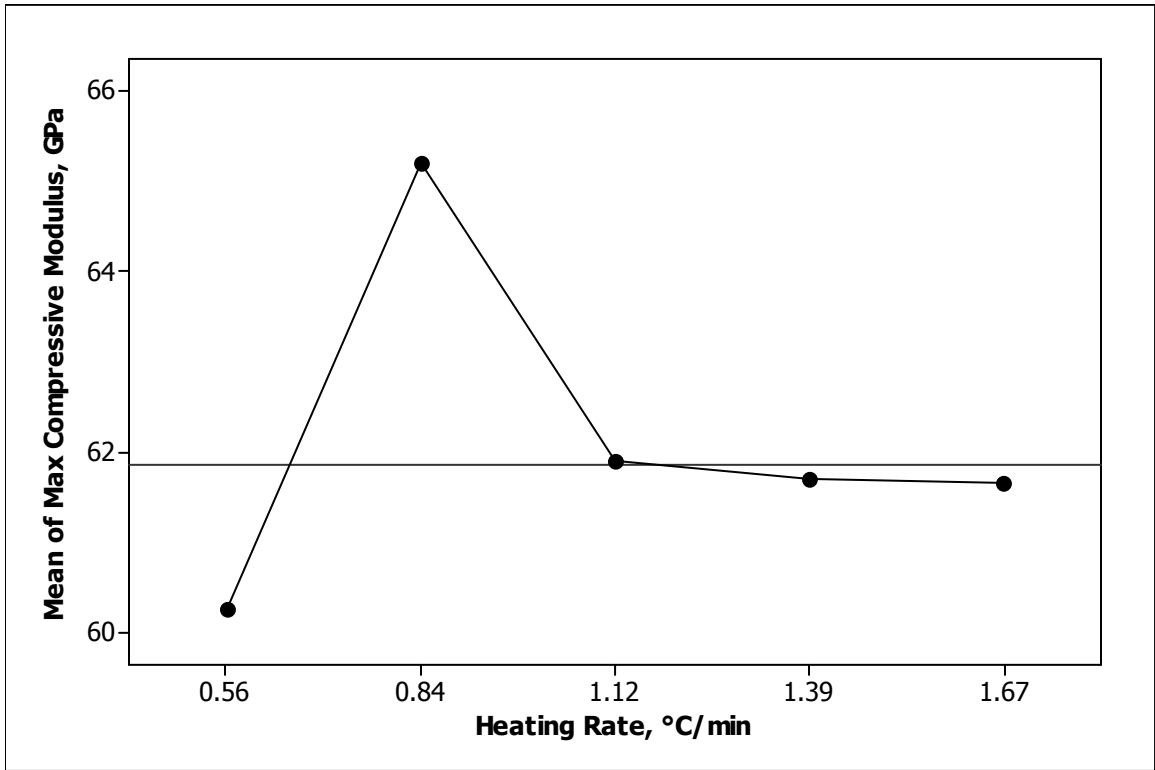


Figure 6-30. Average main effect of heating rate on compressive modulus.

The analysis of variance shown in Tables 6-11, shows that maximum cure temperature, heating rate, and post cure time, in the range used in the experiment, are statistically insignificant for this response (compressive modulus). As shown in the table, the p-values for these three parameters are less than  $\alpha$ -value, which is 0.05. The F-ratios for maximum cure temperature, heating rate, and post cure time are 1.336, 1.802 and 1.207 respectively as shown in Table 6-11. The F-ratios confirm the same results as before, since they are all less than F-table (2.91).

Table 6-11. Analysis of variance for compressive modulus at high temperature-dry

Source	Sum Squares	DF	Mean Square	F	P
Max Cure Temp	35.2	3	11.721	1.336	0.296
Heating Rate	47.4	3	15.813	1.802	0.185
Post Cure Time	31.8	3	10.592	1.207	0.337
Error	149.1	17	8.773		
Total	277.5	31			

### 6.4.3 High Temperature-Wet Compression Test

#### 6.4.3.1 Test Procedure

The same test procedure used in section 6.4.2 for high temperature-dry compression test was used for high temperature-wet compression test. The same specimen size was also used. But the main difference is the specimens in this test have been exposed to 100% relative humidity for 3400 hours (140 days) according to the procedure explained in section 5.6. The moisture weight gained during this period was found to be 1.05% of the specimen weight.

The specimen was heated, inside the compression fixture, from room temperature up to 177°C (350°F) and kept at this level for 10 minutes to reach to a homogeneous temperature distribution before applying the compression load.

A group of 15 specimens, one of each case tested, called “travelers” was conditioned at 100% relative humidity for the same period. These specimens went through the heating cycle inside the test fixture, but without applying any compression load. Then they were weighed to determine the actual percentage of moisture gained at the time of the test.

Table 6-12 shows the percentage of moisture gain after conditioning and at the time of test.

Table 6-12. Percentage of weight gain after condoning and at time of test

Specimen No.	Weight gain % after 3400 h at 100% RH	Weight gain % at time of test
1	1.06	0.88
2	1.07	0.88
3	1.05	0.92
4	1.03	0.85
5	1.04	0.89
6	1.04	0.89
7	1.05	0.87
8	1.07	0.88
9	1.05	0.87
10	1.05	0.87
11	1.06	0.86
12	1.06	0.91
13	1.06	0.87
14	1.04	0.84
15	1.07	0.88

### 6.4.3.2 Data Collection

The data was collected and recorded during the test form the MTS by LABVEIW. The data collected is the compressive load and the specimen temperature. The maximum compressive strength was calculated based on maximum load recorded and the dimension measured of the gage length of the sample (width and thickness).



Table 6-13 shows the effect of process parameters on the ultimate compressive strength. The average coefficient of variation for the 15 cases, every case repeated 3 times, was found to be 10.1 %. Table 6-13 also shows the standard deviation and the coefficient of variation for each case. Figure 6-31 shows the scatter plot for ultimate compressive strength for each case.

Table 6-13. Process parameters effect on the compressive strength for high temp-wet

Case No.	Maximum Cure Temp. (°C)	Heating Rate (°C/min.)	Post Cure Time at 227°C (h)	No of Samples Tested	Compressive Strength		
					Compressive Strength (MPa)	Standard Deviation	Coefficient of Variation %
1	188	1.67	0	3	219	28	12.7
2	188	1.67	4	3	286	3	0.9
3	188	1.12	0	3	175	4	2.5
4	188	1.12	4	3	250	33	13.3
5	199	1.67	0	3	307	36	11.7
6	199	1.67	4	3	240	41	17.2
7	199	1.12	0	3	242	15	6.4
8	199	1.12	4	3	300	33	10.9
9	183	1.39	2	3	283	22	7.9
10	205	1.39	2	3	255	24	9.4
11	194	0.56	2	3	259	48	18.6
12	194	0.84	2	3	240	21	8.7
13	194	1.39	6	3	225	13	5.9
14	194	1.39	5	3	301	32	10.6
15	194	1.39	2	3	225	34	15.0

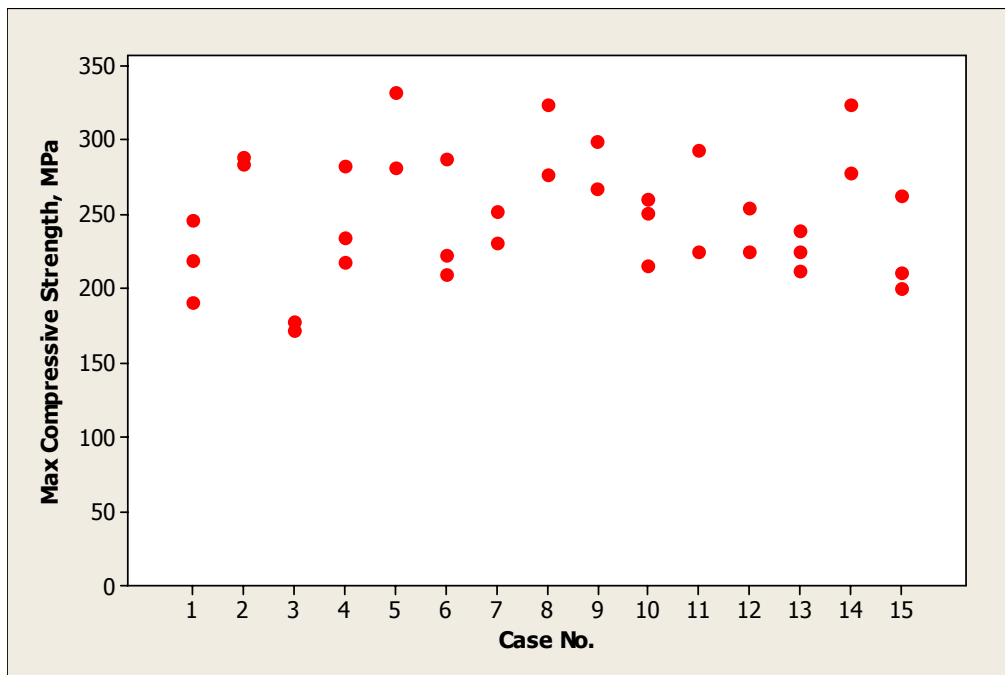


Figure 6-31. Scatter plot of compressive modulus for each case shown in table 6-13.

### 6.4.3.3 Response Analysis

The responses obtained from the 15 different cases as shown in Table 6-12 was analyzed using graphical representation of the mean effects of each parameter. Figures 6-32 to 6-34 show the average main effects of process parameters, which are post cure time, maximum cure temperature, and heating rate, on compressive strength, respectively. Figure 6-32 shows that the compressive strength increases as the post cure time increases from zero to 5 hours, and then it drops sharply at post cure time of 6 hours. Figure 6-31 shows that the maximum compressive strength is at cure temperature of 183°C (360°F). The heating rate, as shown in Figure 6-34, does not show a clear effect on compressive strength, since the data is scattered around and close to the average line.

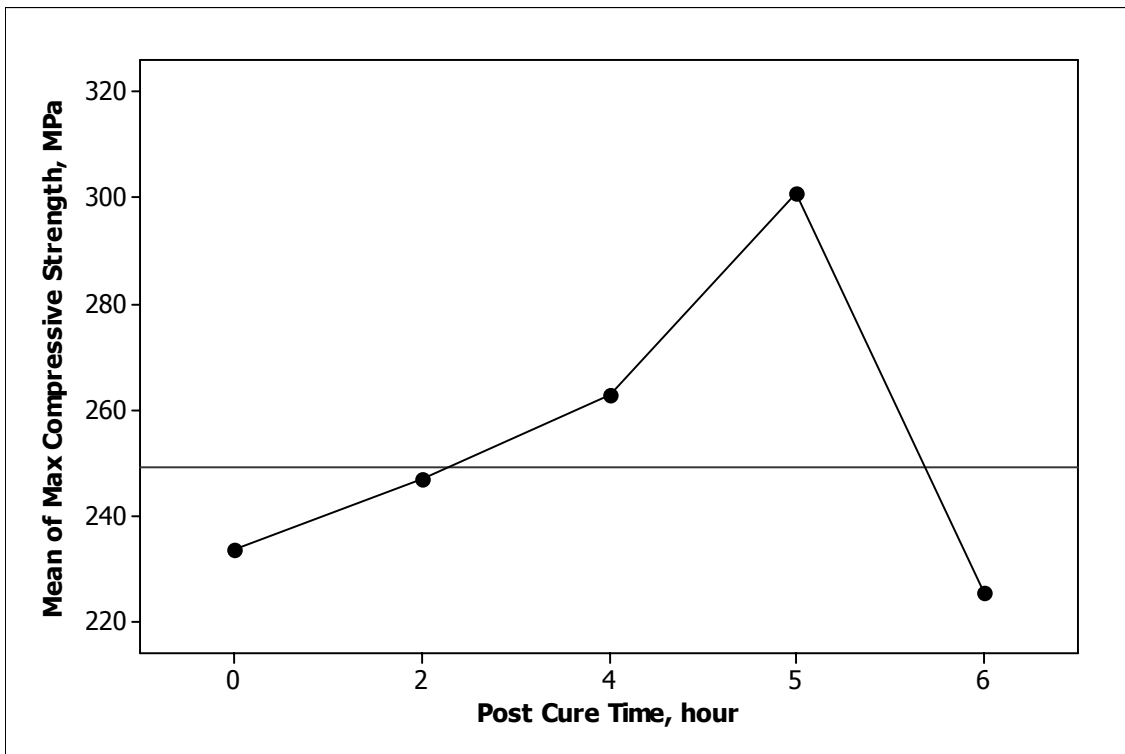


Figure 6-32. Average main effect of post cure time on compressive strength.

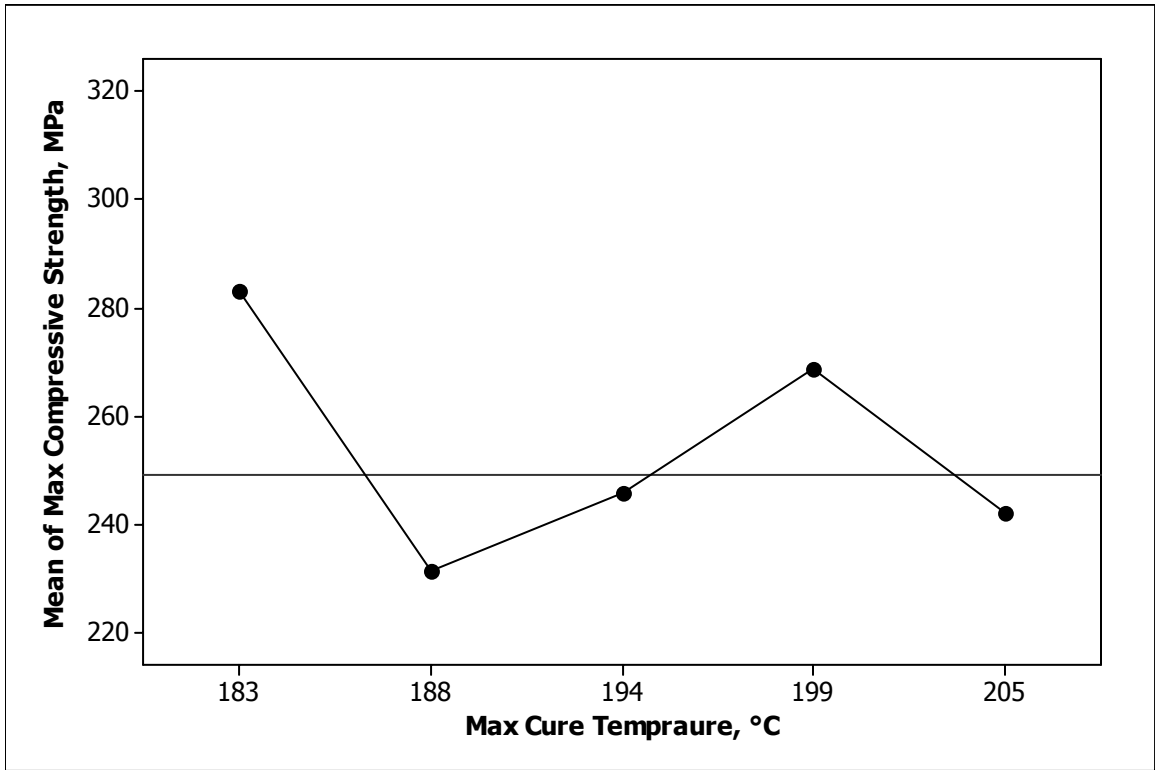


Figure 6-33. Average main effect of max cure temperature on compressive strength.

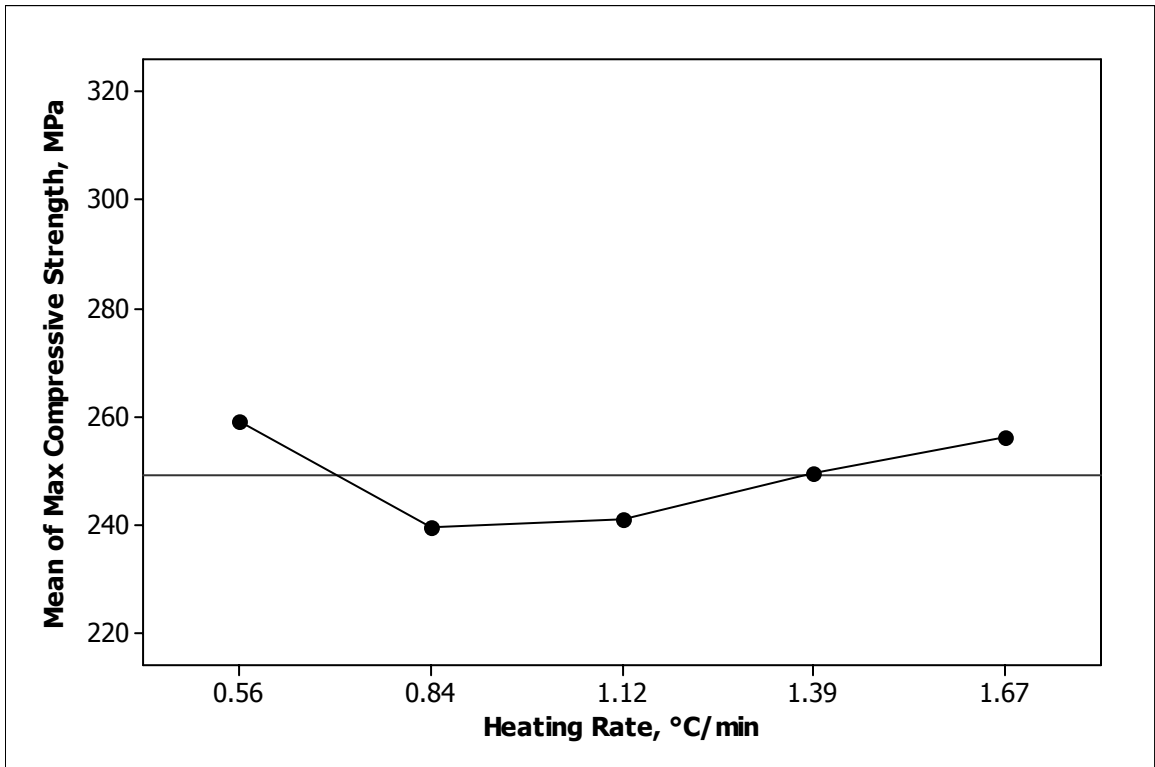


Figure 6-34. Average main effect of heating rate on compressive strength.

Table 6-14 summarizes the analysis of variance (ANOVA) conducted for the obtained responses. The p-values for maximum cure temperature, and post cure time are less than  $\alpha$ -value, which is 0.05. Then, these two parameters within the range used in the experiment are, statistically, significant parameters. F-ratios for maximum cure temperature and post cure time are 4.648 and 5.278 respectively as shown in Table 6-14. The F-ratios confirm the same results as before, since they are greater than F-table (2.88). Post cure time is the most significant parameters, as it has the highest F-ratio and the lowest p-value. The analysis of response, as shown before in Figures 6-32 and 6-33, showed that these two parameters have strong effect on compressive strength. The ANOVA shows also that heating rate, with F-ratio less than F-table and p-value greater than  $\alpha$ -value, is an insignificant parameter.

Table 6-14. Analysis of variance for compressive strength at high temperature-wet

Source	Sum Squares	DF	Mean Square	F	P
Max Cure Temp	11851.0	3	3950.34	4.648	0.012
Heating Rate	3704.9	3	1234.97	1.453	0.256
Post Cure Time	13456.2	3	4485.39	5.278	0.007
Error	17846.7	21	849.841		
Total	58329.0	35			

## **6.5 Discussion of Experimental Results**

One of the objectives of this study is to experimentally investigate the effects of the major process parameters on mechanical properties for composite materials molded by VARIM. This experimental investigation helps to build a science based technology for VARIM process to produce composite materials free of defects with the highest possible mechanical properties suitable for high temperature applications. The major process parameters, that were investigated, are maximum cure temperature, post cure time, and heating rate. Mechanical properties were tested under tensile and compressive loads. Tests were conducted at room temperature and at elevated temperature. A group of specimens tested were first conditioned at 100% relative humidity to simulate the actual working condition.

The findings of room temperature tensile and compressive load tests show that post cure time and maximum cure temperature plays the most significant role in VARIM process. The response analysis for both tension and compression test confirms that as post cure time increases, in the range used in the experimental design, the material strength decreases. The highest strength at room temperature was obtained without a post cure stage. The effect of maximum cure temperature on room temperature tensile test shows that as maximum cure temperature decreases in the range used in the experimental design, tensile strength increases. Also, the highest compressive strength was obtained at a low cure temperature (188°C). So, both tensile and compressive load test confirms that a low cure temperature, within the range used in the experimental design, leads to a high strength.

Heating rate, in the range used in the experimental design, does not show a significant effect on both tensile and compressive strength at room temperature. However, the response analysis shows that as heating rate increases the strength slightly increases. The highest heating rate used in this study, which is 1.67°C/min, led to the highest strength.

The findings of room temperature tensile and compressive load tests show that the compressive strength is about 32% less than the tensile strength. In fact this difference was explored by Li [55] using composite materials with a different type of carbon fiber. In his study, there is a 37% reduction in the compressive strength from the tensile strength. It was found that the most likely damage in the tested specimens is the intra-ply delamination, which was also observed in this study. It's obvious that the intra-ply delamination has a greater effect on compressive strength rather than on tensile strength.

During Cure and post cure stages, the cross linking mechanism involves two main steps, as explained in section 3.2.1. These two steps are carbon-carbon double bonds (C=C) opening, and dehydration of hydroxyl groups. First step improves the composite mechanical properties, while the second step deteriorates the mechanical properties. As the maximum cure temperature increases the effects of the rate of dehydration becomes more pronounced as compared with the mechanism of carbon-carbon double bonds (C=C) opening. Since curing the resin at a high temperature, for the same time as at a low temperature, increases the possibility of water molecules diffusion out of the polymer, which leads to more defects. While at a low maximum cure temperature, within the range used in the experimental design, the carbon-carbon double bonds (C=C) opening

dominates the mechanism of cross linking, which improves the composite mechanical properties.

So, curing time, which is 4 hours in this study, at a low maximum cure temperature, within the range used in the experiments, is enough to reach the maximum degree of cure based on carbon-carbon double bonds (C=C) opening mechanism, which improves the properties. A post cure stage after that leads to increase the degree of cure based on dehydration, which deteriorates the properties. That explains why the strength, tensile and compressive, decreases as post cure time increases.

In the high temperature-wet compressive load test, the specimens were conditioned at 100% relative humidity and 80°C for 3400 hours (140 days) to reach moisture absorption steady state. Then the specimens were tested at 177°C with a high heating rate of 15°C/min. The experimental investigation of high temperature-high humidity compressive load test shows that post cure time is a dominant parameter in VARIM process followed by maximum cure temperature. As post cure time increases the composite compressive strength increases until it reaches a peak at 5 hours post cure time. At a one hour further post cure time, the strength shows a sharp drop.

In high temperature-dry compressive load test, the specimens were dried at 163°C for two hours and half and were tested at 177°C with a high heating rate of 15°C/min. As in the high temperature-wet, the compressive strength shows a peak at 5 hours of post cure time and then a sharp drop at post cure time of 6 hours. So, the effect of post cure time on



compressive strength is the same at both high temperature-dry and high temperature-wet tests.

Maximum cure temperature shows the same effect on compressive strength at high temperature (wet and dry) tests as well as at room temperature tests. The highest compressive strength, for both high temperature dry and wet, was obtained at the lowest maximum cure temperature used in the experimental design. Also, as in room temperature tests, heating rate has a little significance effect on compressive strength at high temperature test, dry and wet.

High humidity and high temperature are the major factors in damaging composite materials [68-74]. The problem arises when a composite with absorbed moisture is heated suddenly with a high heating rate. Moisture absorbed in composite materials reduces glass transition temperature and deteriorates the mechanical properties of fiber/matrix interfacial adhesion [55]. The response analysis, conducted in this study, shows that, for high temperature application, post cure time can play a great role to improve the mechanical properties of molded composites by VARIM. Increasing post cure time from zero to five hours helped to increase the compressive strength. Increasing the time to 6 hours resulted in less compressive strength. As post cure time increase composite mechanical properties decreases, but glass transition temperature increases. As glass transition increases, the molded material attains more chemical and physical stability. This stability helps the material to become less reactive, and to resist the effects of high humidity to certain limit, as shown in the previous results. As post cure time increases

further, glass transition temperature increases, but defects increases more and more, which makes the strength to drop.

It's obvious from the previous discussion that one of the three major parameters investigated in this study, within the range used in the experimental design, which is heating rate, has a little effect on the strength of the molded composite by VARIM. However, it was found that a heating rate of  $1.67^{\circ}\text{C}/\text{min}$  helped to increase the strength. Also it was found that decreasing maximum cure temperature to the lowest value used in the experiments, which is  $183^{\circ}\text{C}$ , helped to increase the strength. So a maximum cure temperature of  $183^{\circ}\text{C}$  and a heating rate of  $1.67^{\circ}\text{C}/\text{min}$  are the optimum conditions for room temperature and high temperature applications at tension and compression modes. Post cure time has different effects on room temperature application than on high temperature (dry and wet) application. For room temperature application, using the previous optimum maximum cure temperature and heating rate, excluding post cure stage from molding process resulted in increasing the material strength. On the other hand, for high temperature applications, with high humidity or without, adding a time of 5 hours of post cure time at  $227^{\circ}\text{C}$  increased the material strength.

## 6.6 Empirical Model of VARIM Process

An empirical relationship between process parameters and the evolved properties (responses) can help in determination of the optimum process window for the required properties. Response can be represented as a function of the process parameters, so it can be written as follows:

$$y = f(x_1, x_2, x_3) \quad (4)$$

The response can be modeled based on a regression model approach in the form

$$y = a_0 + \sum_{i=1}^k a_i x_i + \sum_{i=1}^k a_{ii} x_i^2 + \sum_{\substack{ij \\ i < j}} a_{ij} x_i x_j \quad (5)$$

Equation (5) can be written as an empirical model as follows:

$$y = a_0 + a_1 x_1 + a_2 x_2 + a_3 x_3 + a_{11} x_1^2 + a_{22} x_2^2 + a_{33} x_3^2 + a_{12} x_1 x_2 + a_{13} x_1 x_3 + a_{23} x_2 x_3 \quad (5)$$

Where:

$y$  : response, maximum strength (MPa)

$x_1$  : maximum cure temperature ( $^{\circ}\text{C}$ )

$x_2$  : heating rate ( $^{\circ}\text{C}/\text{min}$ )

$x_3$  : post cure time (h)

$a_0$  : average response

$a_1, a_2, \dots$  : regression coefficients.

The regression coefficients for the model that best represents the experimental data for room temperature tensile strength are shown in Table 6-15. Table 6-16 shows the effect of process parameters on the ultimate tensile strength and their corresponding predicted value for each case of the experimental design. The average percent error of model for the 15 cases was found to be 1.6%. As shown in the table, the maximum percent error of model is 3.8% for case number eight, while the minimum one is 0.1% for case number three. Figure 6-35 shows the comparison between the measured and the predicted value for maximum tensile strength. The model prediction is plotted in Figure 6-36 versus the average of the experimentally measured tensile strength for the 15 different cases of the experimental design. The diagonal solid line represents the ideal fit. Based on the response analysis in section 6.3.3, the optimal process parameters are specified in Table 6-17 with the predicted maximum tensile strength. The accuracy of the model cannot be guaranteed for parameters outside the range of the experimental design used in this study.

Table 6-15. Analysis of variance for compressive strength at high temperature-wet

Coefficient	Value
$a_0$	5397.15
$a_1$	-48.63
$a_2$	753.66
$a_3$	-152.32
$a_{11}$	0.13
$a_{22}$	-1.83
$a_{33}$	3.64
$a_{12}$	-3.80
$a_{13}$	0.64
$a_{23}$	-2.69

Table 6-16. Predicted strength and the corresponding percent error of model for each case

Case No.	Maximum Cure Temp. (°C)	Heating Rate (°C/min.)	Post Cure Time at 227°C (h)	Max Tensile strength, MPa	Predicted Max Tensile strength, MPa	Percent Error of Model, %
1	188	1.67	0	917	910	0.8
2	188	1.67	4	828	822	0.7
3	188	1.12	0	892	891	0.1
4	188	1.12	4	804	809	0.7
5	199	1.67	0	847	859	1.3
6	199	1.67	4	786	799	1.6
7	199	1.12	0	841	863	2.5
8	199	1.12	4	778	809	3.8
9	183	1.39	2	884	866	2.1
10	205	1.39	2	817	817	0.0
11	194	0.56	2	825	819	0.7
12	194	0.84	2	828	822	0.7
13	194	1.39	6	838	815	2.9
14	194	1.39	5	808	806	0.2
15	194	1.39	2	856	826	3.7

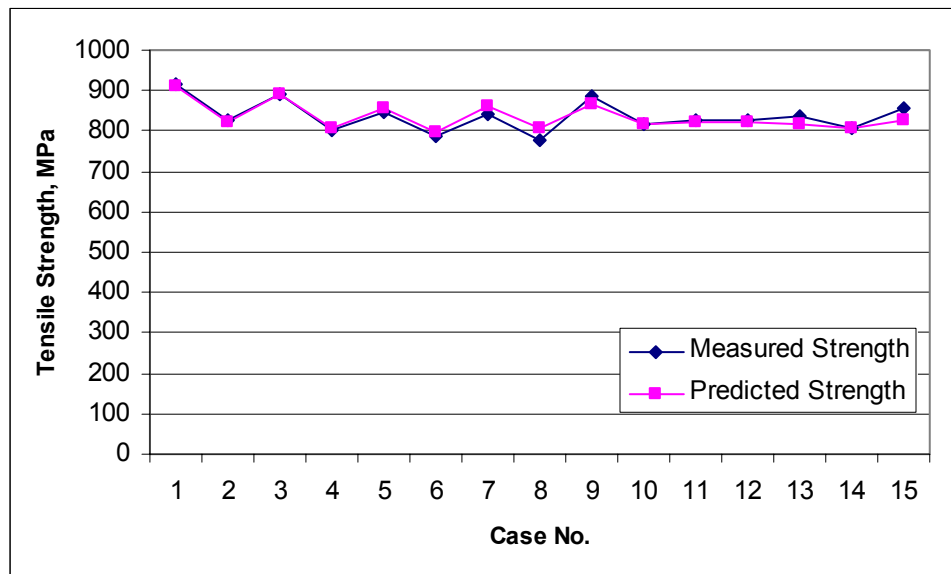


Figure 6-35. Comparison between the measured and the predicted tensile strength.

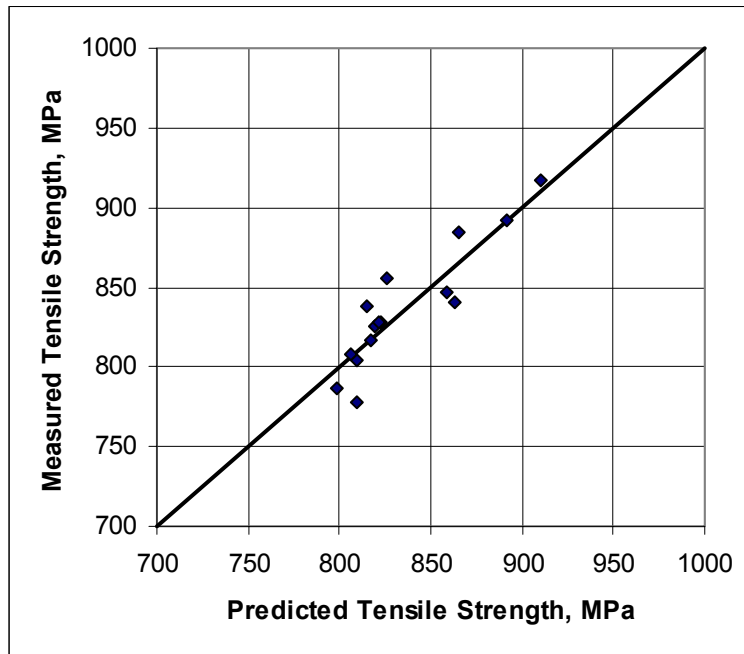


Figure 6-36. Predicted tensile strength versus measured tensile strength.

Table6-17. Optimum process parameters and the model predicted response

Maximum Cure Temp. (°C)	Heating Rate (°C/min.)	Post Cure Time at 227°C (h)	Predicted Max Tensile strength, MPa	Average Percent Error of Model, %
183	1.67	0	944	1.6

The regression coefficients for the model that best represents the experimental data for room temperature compressive strength are shown in Table 6-18. Table 6-19 shows the effect of process parameters on the ultimate tensile strength and their corresponding predicted value for each case of the experimental design. The average percent error of model for the 15 cases was found to be 3.3%. As shown in the table, the maximum percent error of model is 10.7% for case number fifteen, while the minimum one is 0.4% for case number nine. Figure 6-37 shows the comparison between the measured and the predicted value for maximum compressive strength. The model prediction is plotted in Figure 6-38 versus the average of the experimentally measured compressive strength for the 15 different cases of the experimental design. The diagonal solid line represents the ideal fit. Based on the response analysis in section 6.4.1.3, the optimal process parameters are specified in Table 6-20 with the predicted maximum compressive strength.

Table 6-18. Response polynomial coefficients for maximum compressive strength

Coefficient	Value
$a_0$	-6205.00
$a_1$	56.54
$a_2$	2053.18
$a_3$	-176.18
$a_{11}$	-0.11
$a_{22}$	57.14
$a_{33}$	6.20
$a_{12}$	-11.18
$a_{13}$	0.66
$a_{23}$	2.60

Table 6-19. Predicted strength and the corresponding percent error of model for each case

Case No.	Maximum Cure Temp. (°C)	Heating Rate (°C/min.)	Post Cure Time at 227°C (h)	Max Compressive strength, MPa	Predicted Max Compressive strength, MPa	Percent Error of Model, %
1	188	1.67	0	620	615	0.8
2	188	1.67	4	538	523	3.0
3	188	1.12	0	564	554	1.9
4	188	1.12	4	476	456	4.3
5	199	1.67	0	555	563	1.5
6	199	1.67	4	495	500	1.1
7	199	1.12	0	557	570	2.2
8	199	1.12	4	481	501	4.0
9	183	1.39	2	501	500	0.4
10	205	1.39	2	477	492	2.9
11	194	0.56	2	480	508	5.5
12	194	0.84	2	523	500	4.7
13	194	1.39	6	498	529	5.9
14	194	1.39	5	507	506	0.2
15	194	1.39	2	455	509	10.7

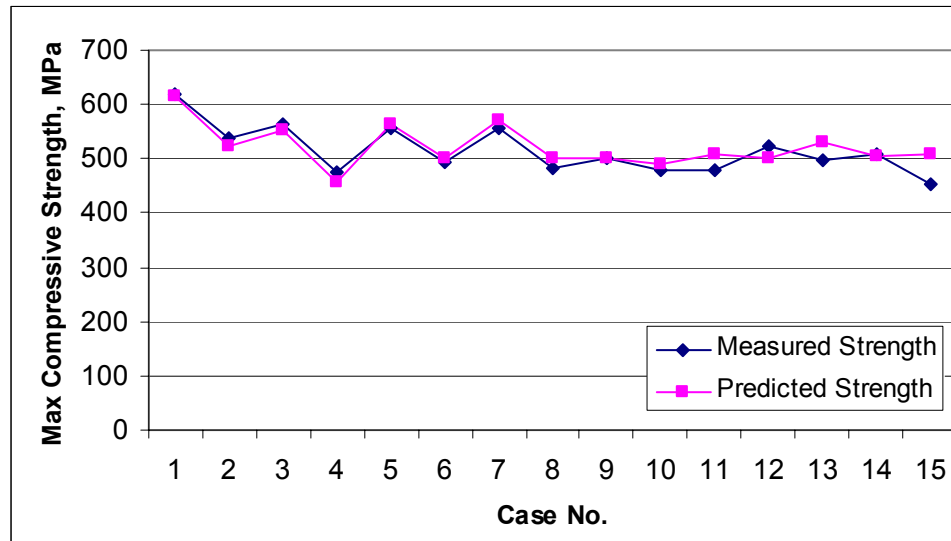


Figure 6-37. Comparison between the measured and the predicted compressive strength.



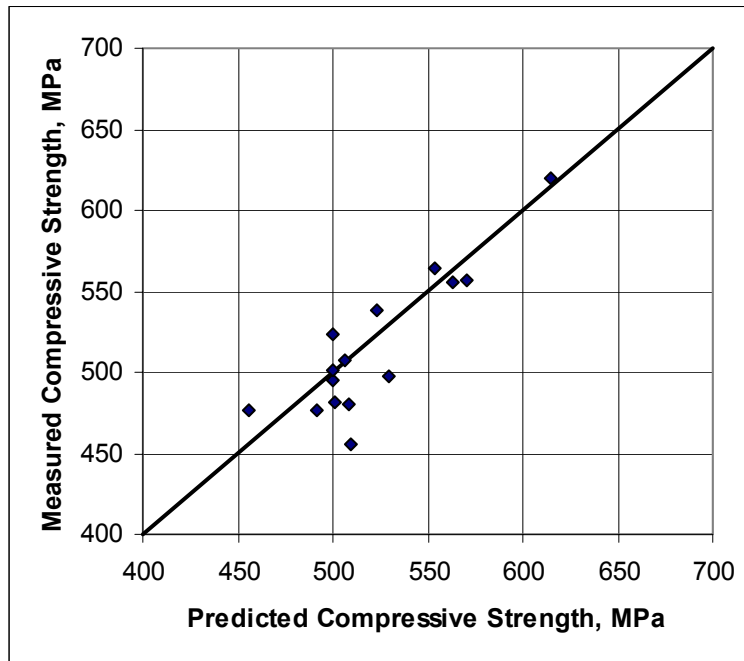


Figure 6-38. Predicted compressive strength versus measured compressive strength.

Table6-20. Optimum process parameters and the model predicted response

Maximum Cure Temp. (°C)	Heating Rate (°C/min.)	Post Cure Time at 227°C (h)	Predicted Max Compressive strength, MPa	Average Percent Error of Model, %
183	1.67	0	629	3.3

The regression coefficients for the model that best represents the experimental data for high temperature-wet compressive strength are shown in Table 6-21. Table 6-22 shows the effect of process parameters on the ultimate tensile strength and their corresponding predicted value for each case of the experimental design. The average percent error of model for the 15 cases was found to be 8.4%. As shown in the table, the maximum percent error of model is 17.6% for case number fourteen, while the minimum one is 0.3% for case number ten. Figure 6-39 shows the comparison between the measured and the predicted value for maximum compressive strength. The model prediction is plotted in Figure 6-40 versus the average of the experimentally measured compressive strength for the 15 different cases of the experimental design. The diagonal solid line represents the ideal fit. Based on the response analysis in section 6.4.3.3, the optimal process parameters are specified in Table 6-23 with the predicted maximum compressive strength.

Table 6-21. Response polynomial coefficients for maximum compressive strength

Coefficient	Value
$a_0$	560.00
$a_1$	-15.28
$a_2$	1130.67
$a_3$	365.71
$a_{11}$	0.07
$a_{22}$	67.95
$a_{33}$	-1.97
$a_{12}$	-6.34
$a_{13}$	-1.63
$a_{23}$	-23.85

Table 6-22. Predicted strength and the corresponding percent error of model for each case

Case No.	Maximum Cure Temp. (°C)	Heating Rate (°C/min.)	Post Cure Time at 227°C (h)	Max Compressive strength, MPa	Predicted Max Compressive strength, MPa	Percent Error of Model, %
1	188	1.67	0	219	249	12.0
2	188	1.67	4	286	295	3.1
3	188	1.12	0	175	178	1.7
4	188	1.12	4	250	277	9.7
5	199	1.67	0	307	262	17.1
6	199	1.67	4	240	237	1.4
7	199	1.12	0	242	230	5.1
8	199	1.12	4	300	257	16.9
9	183	1.39	2	283	259	9.3
10	205	1.39	2	255	255	0.3
11	194	0.56	2	259	260	0.4
12	194	0.84	2	240	246	2.5
13	194	1.39	6	225	251	10.1
14	194	1.39	5	301	256	17.6
15	194	1.39	2	225	248	9.5

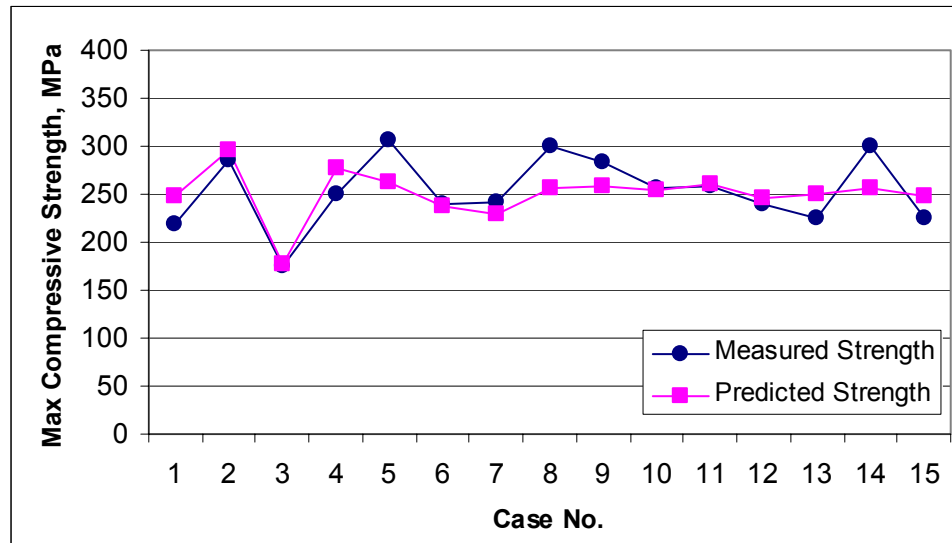


Figure 6-39. Comparison between the measured and the predicted compressive strength.

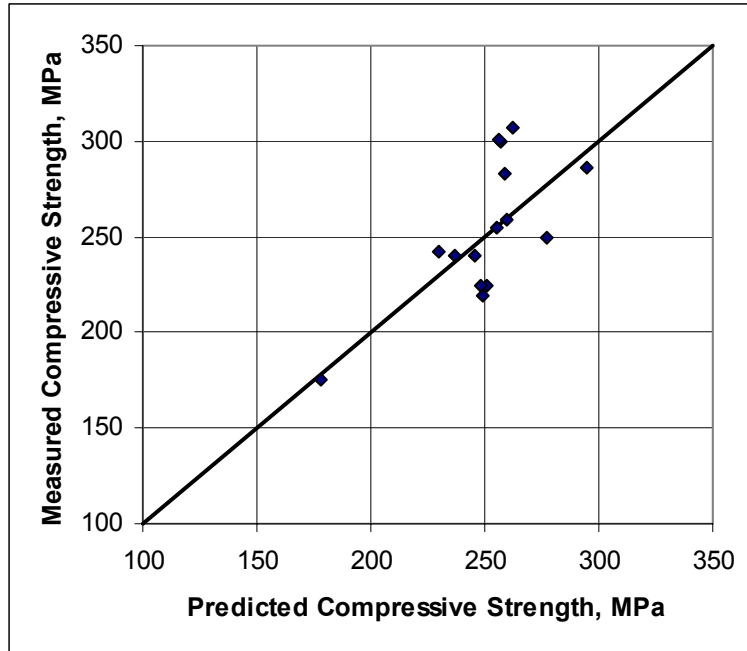


Figure 6-40. Predicted compressive strength versus measured compressive strength.

Table6-23. Optimum process parameters and the model predicted response

Maximum Cure Temp. (°C)	Heating Rate (°C/min.)	Post Cure Time at 227°C (h)	Predicted Max Compressive strength, MPa	Average Percent Error of Model, %
183	1.67	5	337	8.4

## **6.7 Comparison of Properties of Composites Produced by VARIM and other Molding Techniques**

A comparison of the strength of composite materials produced by vacuum assisted resin infusion molding (VARIM), which is the focus of this research, resin transfer molding (RTM), and prepreg molding techniques is shown in Figure 6-41. The VARIM data used in the comparison was collected experimentally during this study. The RTM, and prepreg data for the same material system, carbon fiber and 5250-4 RTM, and the same carbon fiber volume fraction 58%, are available by the company produces the polymer (Cytec Engineered Materials).

It's obvious from Figure 6-41 that the tensile strength at room temperature of the composite materials molded by VARIM gives 917 MPa, which is higher than those molded by RTM and autoclave/prepreg molding techniques by 21% and 8.5% respectively. Comparison of compressive strength at room temperature shows that the composites produced by VARIM have higher strength than the material produced by RTM. The material produced by VARIM gives 620 MPa compressive strength, at room temperature, which is 4.5% higher than the material produced by RTM. A compression test for samples conditioned at 100% relative humidity and test at 177 oC shows that VARIM produces materials with higher compressive strength than those produced by RTM. The molded material by VARIM has a higher compressive strength than the material produced by RTM by 21%. So the comparison shows that, it's clear that the properties of the materials produced by VARIM, both in room temperature and high temperature-wet, are superior to those produced by RTM.

On the other hand, the comparison between the compressive strength of molded composites by VARIM, and the published data, available by the manufacturer of the resin, for composites molded by autoclave/prepreg technique shows that compressive strength of those produced by VARIM have less strength than those produced by autoclave/prepreg molding technique. Nevertheless, the composites produced by VARIM shows a superior tensile strength over the composite materials molded by autoclave/prepreg technique. However, the prepreg molding technique is not a cost effective process, and is limited to a small size structure. Uneven distribution of pressure and temperature during consolidation and curing of large parts are typical problems of autoclave technique.

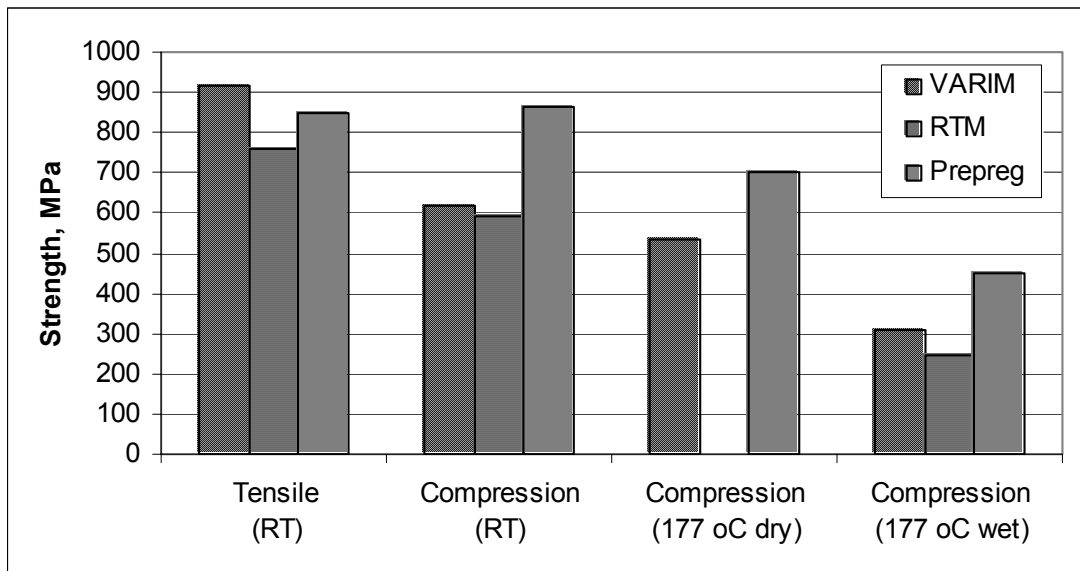


Figure 6-41. Comparison between the VARIM, RTM and prepreg molding technique.

## CHAPTER 7

### CONCLUSIONS AND RECOMMENDATIONS

#### 7.1 Introduction

This research focuses on an exploratory development of Vacuum Assisted Resin Infusion Molding (VARIM) process for manufacturing high temperature polymer matrix composites. The present study involves development of a comprehensive process virtual model and a physical model to relate the process conditions to the evolved properties and defects in vacuum assisted resin infusion molding of polymer composites. The virtual model consists of three modules: resin infusion stage; resin cure stage; and cure dependant mechanical properties. The physical model investigates the feasibility of VARIM for fabricating high temperature polymer composites and the behavior of the process with the change in its parameters. Characterization of properties, defects, and internal structure of produced composites is the major thrust in this study.

The findings of this research will help in developing a science based technology for the VARIM process for understanding of the process behavior and the effects of various process parameters on the properties and integrity of the produced composites. The numerical-experimental investigation provides capability for robust process and tooling design, prediction, and characterization of process induced damage and properties of high

temperature polymer composites molded by VARIM. The developed virtual models provide effective means for identifying process window for defects-free composite structures with the desired properties.

## **7.2 Conclusions**

From the results and discussion of this research, the following conclusions can be stated:

- With appropriate mold design based on the developed virtual model, sound panels with high fiber volume fraction (58%) were successfully molded. Thus, vacuum assisted resin infusion molding (VARIM) process was found to be feasible for fabrication of high temperature polymer composites.
- The developed process (VARIM) is a closed one, offering an environmentally benign manufacturing through the reduction of VOC emission.
- A virtual model for simulating the polymer flow behavior during the infusion stage was developed and verified experimentally, with capabilities for prediction of flow pattern, inside the mold, and evolved defects in vacuum assisted resin infusion molding operation. This model is a useful tool for process and mold design.
- A post processor visual mode involves combination of geometric reconstruction scheme and graphic interchange format (GIF) was introduced in the flow model in order to provide for effective visual presentation of the results and to create a simple animation of the process.



- Several case studies using the developed model show the effect of race-tracking on the formation of macro-voids and the importance of inlet ports location and the proper ventilation for elimination of these defects.
- The process virtual model should help advance the manufacturing technology for the production of affordable polymer composites for high temperature (up to 250°C) applications.
- The mechanical properties of panels produced by VARIM match the properties obtained on a similar material system using other molding techniques.
- The developed empirical relationship between VARIM process parameters, within the range of the experimental design used in this study, and the evolved properties helps in the determination of the optimum process window for the required properties.
- The experimental investigation shows that post cure time and maximum cure temperature are the most significant parameters in VARIM process for manufacturing high temperature composites. Heating rate, with the range used in the experimental design, has a little effect on VARIM process.
- This study shows that, within the range used for each parameter in the experimental design, a maximum cure temperature of 183°C, a post cure time of 5 hours, and a heating rate of 1.67°C/min are the optimum process conditions for high-temperature and high-humidity applications. These curing conditions would maximize the mechanical properties of composites molded by VARIM.

- There is a very good agreement between the developed model predictions and the experimental observations.

### **7.3 Recommendations**

Based on the observations from the current research, the following recommendations are suggested for future work:

- Construction of neural networks using the results obtained experimentally and numerically, in the current research, in order to represent the relationships between the process parameters and the evolved properties of the molded composites by vacuum assisted resin infusion molding (VARIM) over a wider range of process conditions.
- More complex shapes should be tested using VARIM process with multiple resin inlets and vacuum ports.
- Numerical optimization techniques should be integrated with the developed virtual models to define more global optimization process designs under given constraints.

## Appendix A

### Room Temperature Tensile Test Results

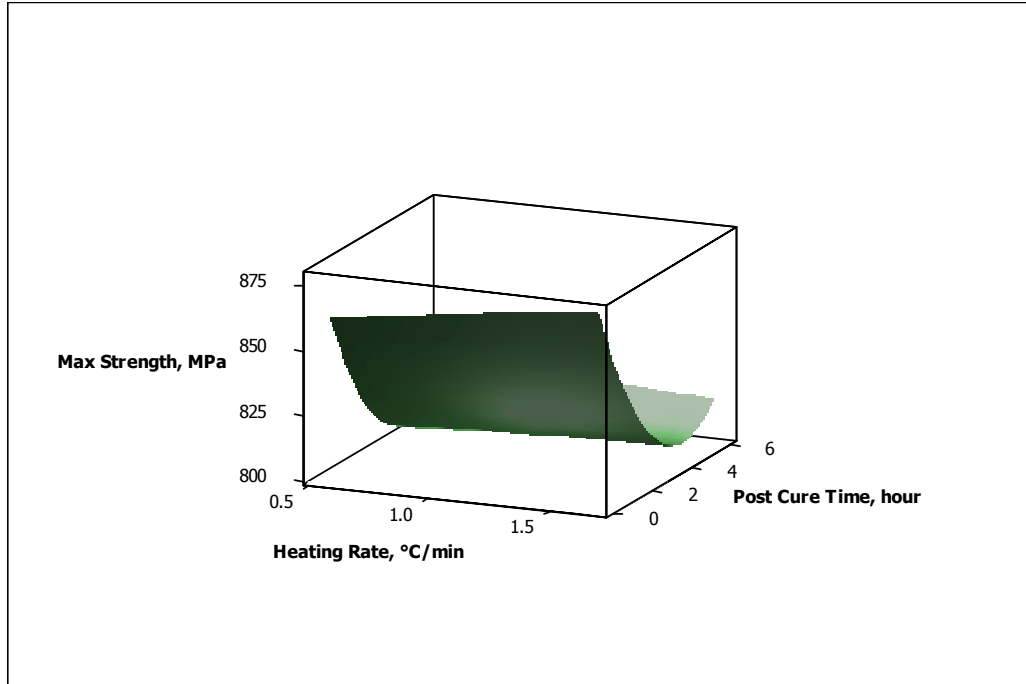


Figure A1. Surface plot of ultimate tensile strength vs. post cure time and heating rate.

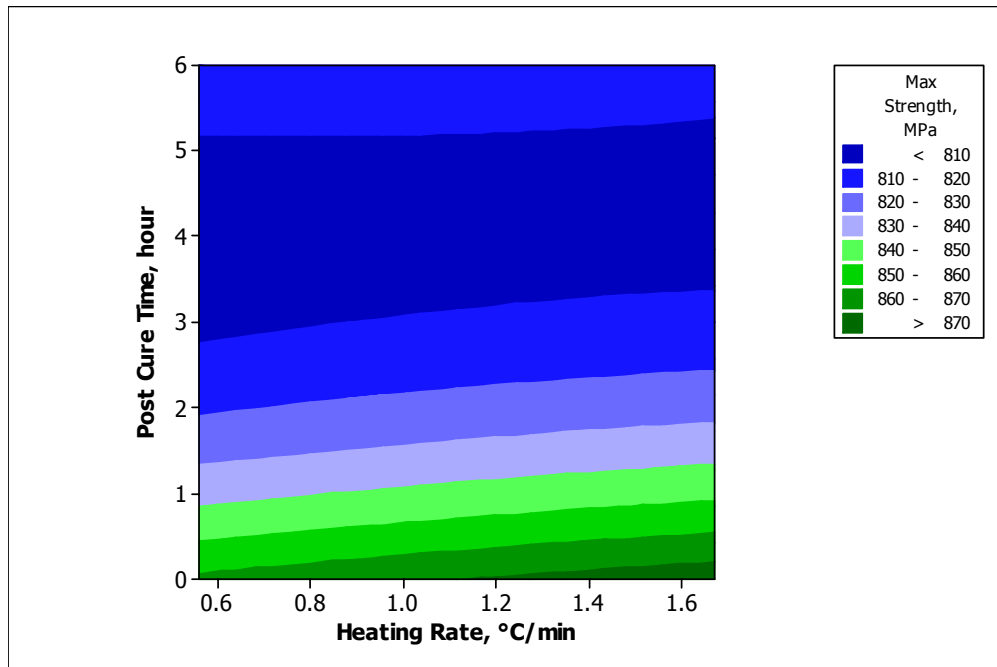


Figure A2. Contour plot of ultimate tensile strength vs. post cure time and heating rate.

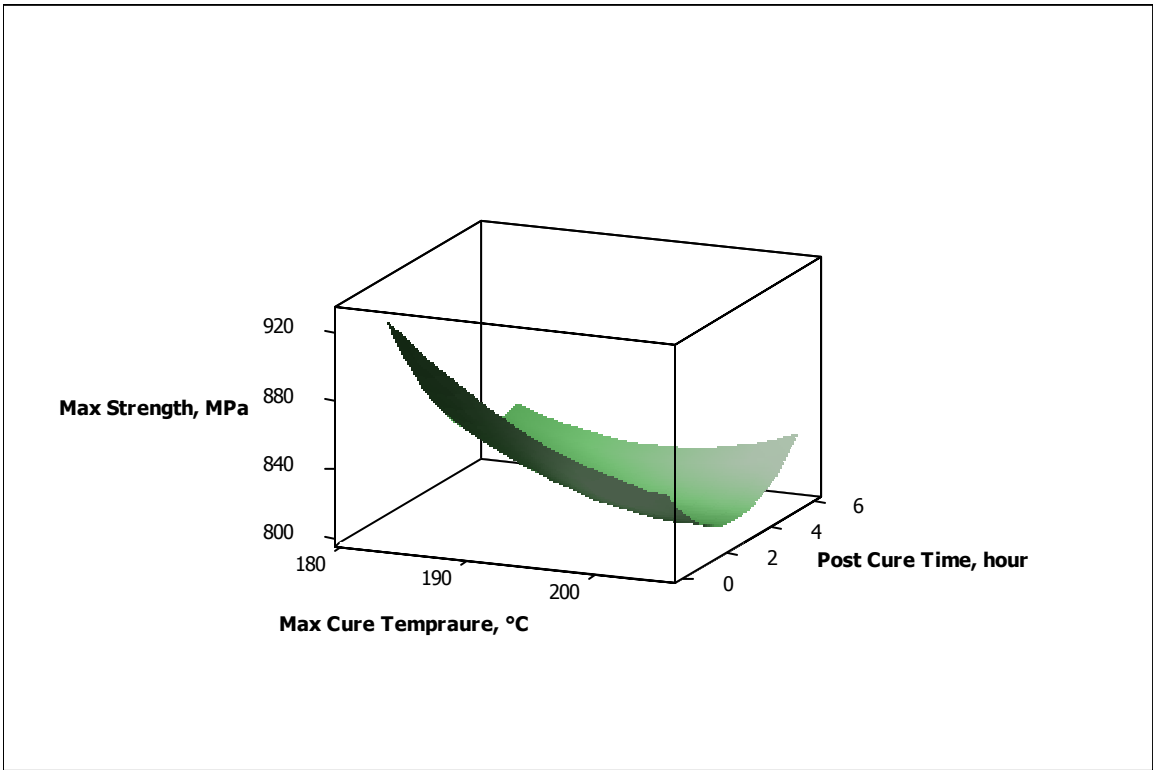


Figure A3. Surface plot of tensile strength vs. post cure time and max cure temp.

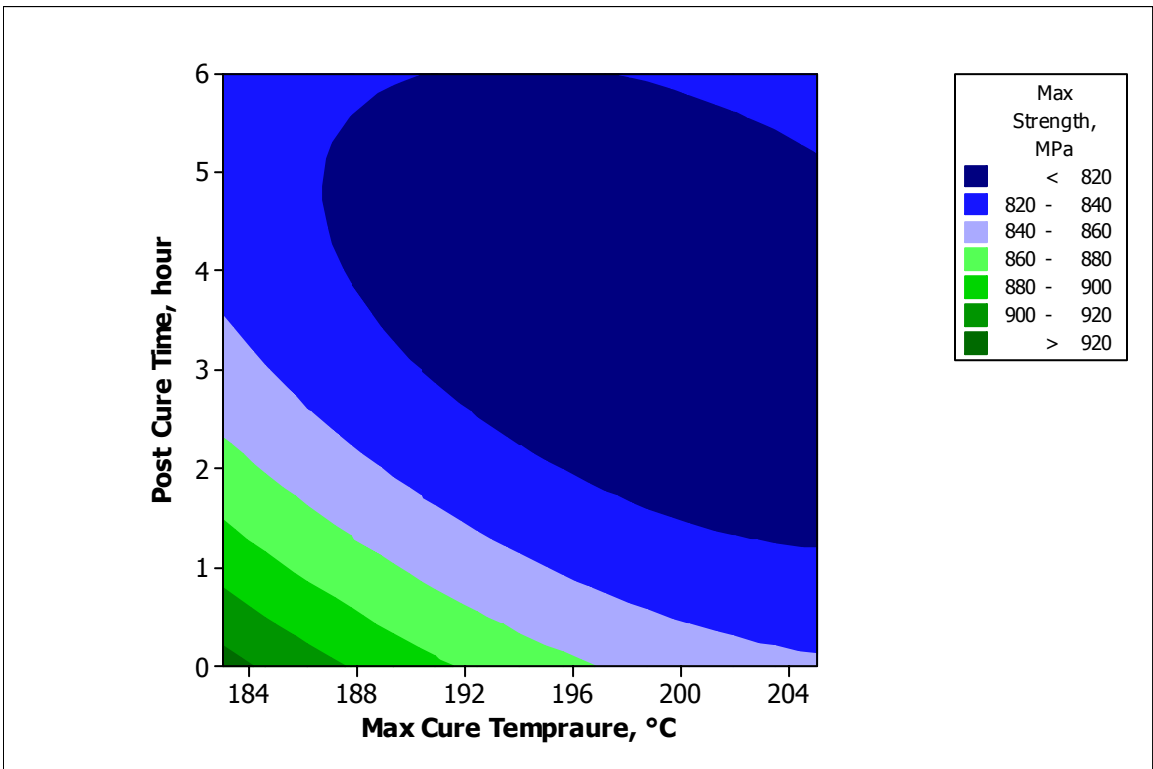


Figure A4. Contour plot of tensile strength vs. post cure time and max cure temp.

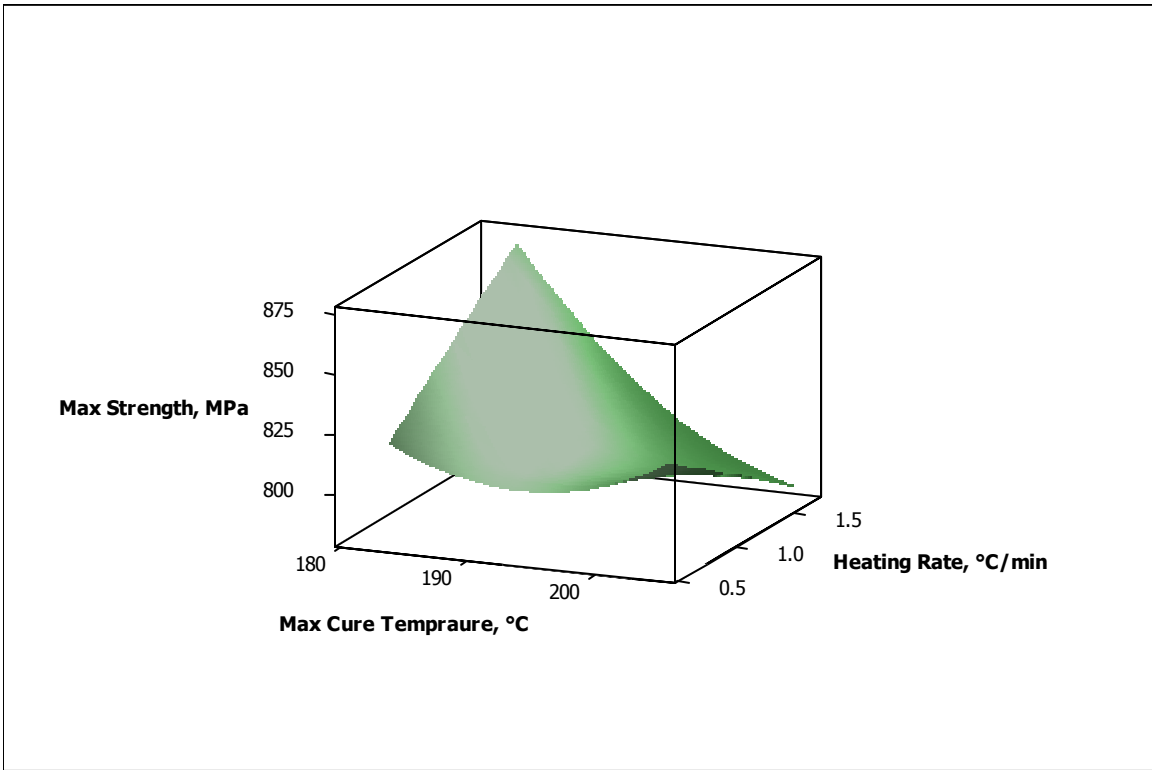


Figure A5. Surface plot of ultimate tensile strength vs. post cure time and heating rate.

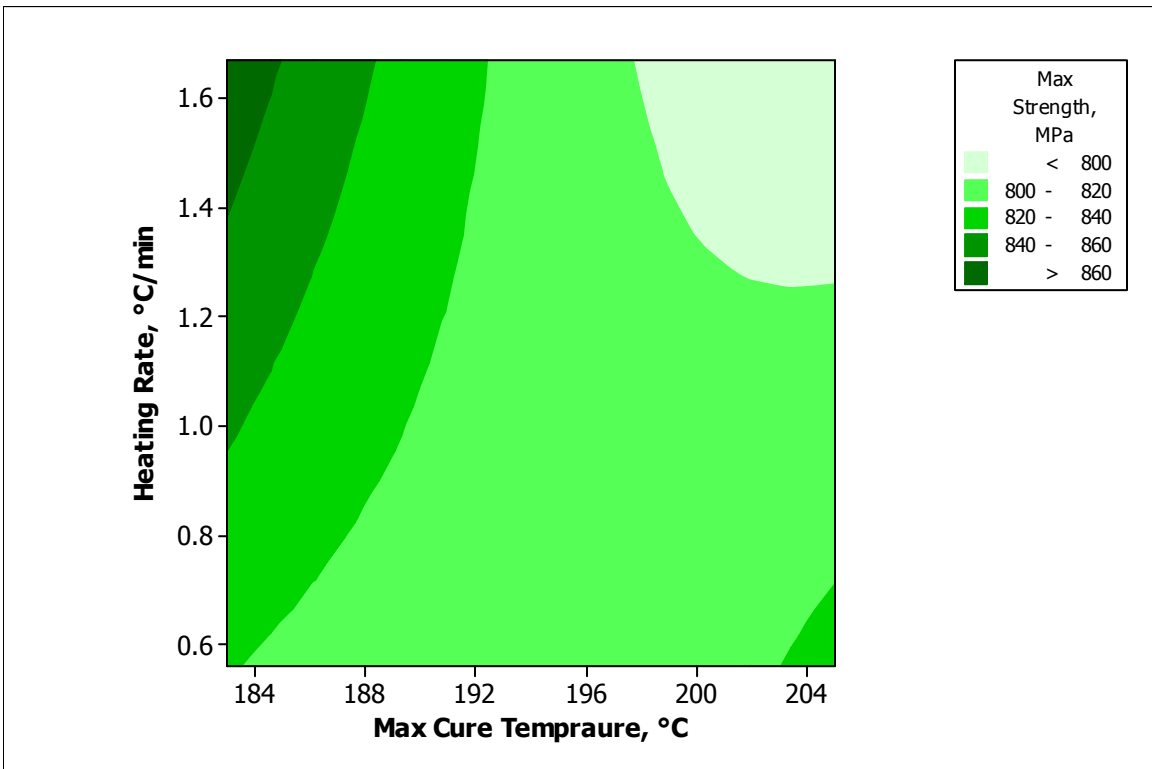


Figure A6. Contour plot of ultimate tensile strength vs. max cure temp and heating rate.

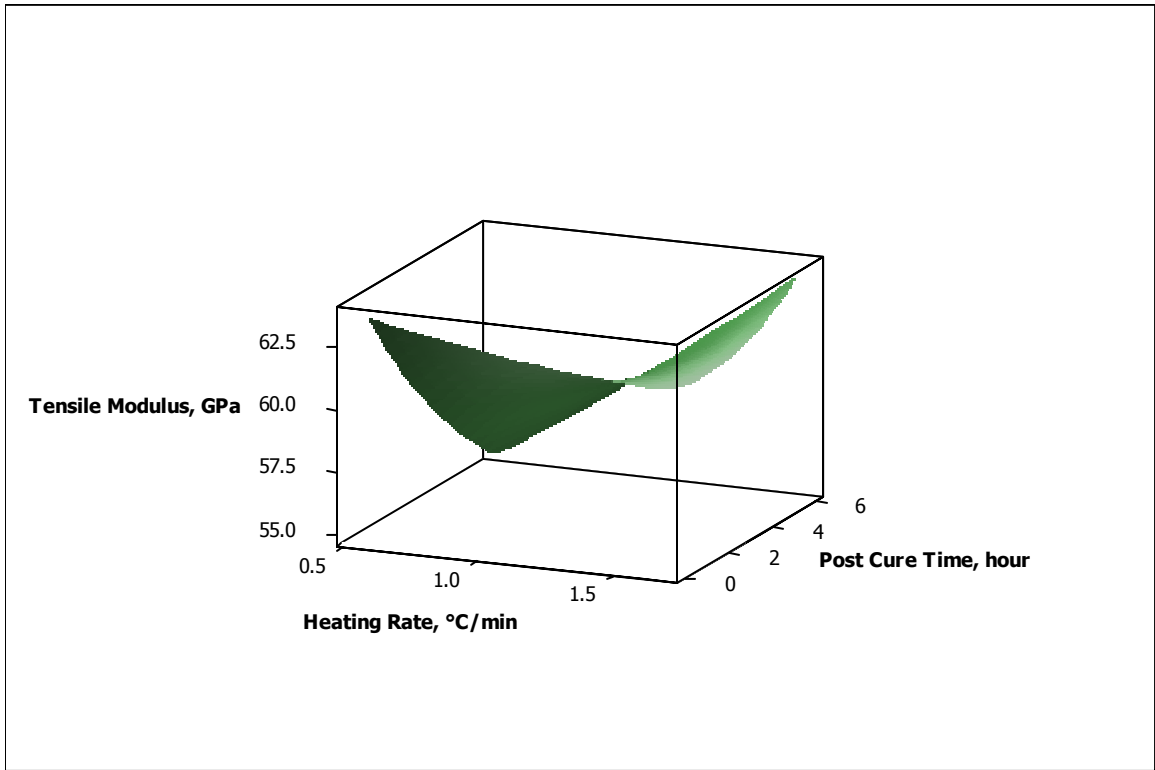


Figure A7. Surface plot of tensile modulus vs. post cure time and heating rate.

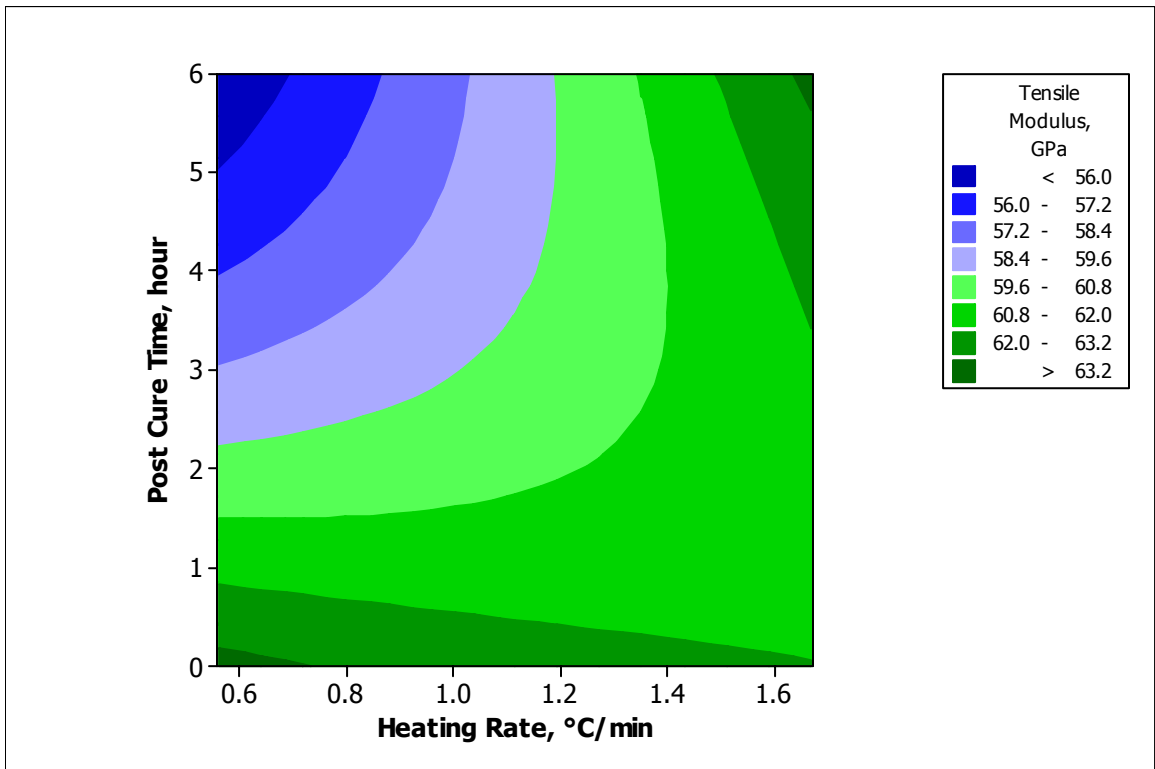


Figure A8. Contour plot of tensile modulus vs. post cure time and heating rate.

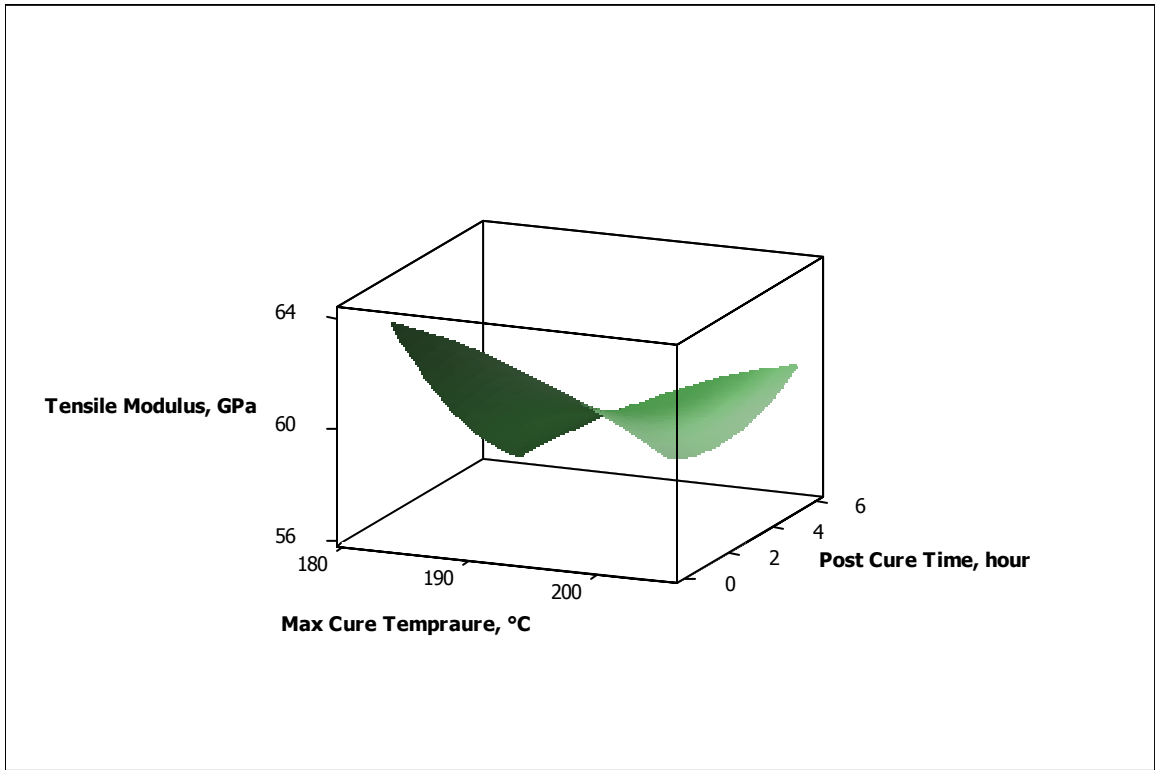


Figure A9. Surface plot of tensile modulus vs. post cure time and max cure temp.

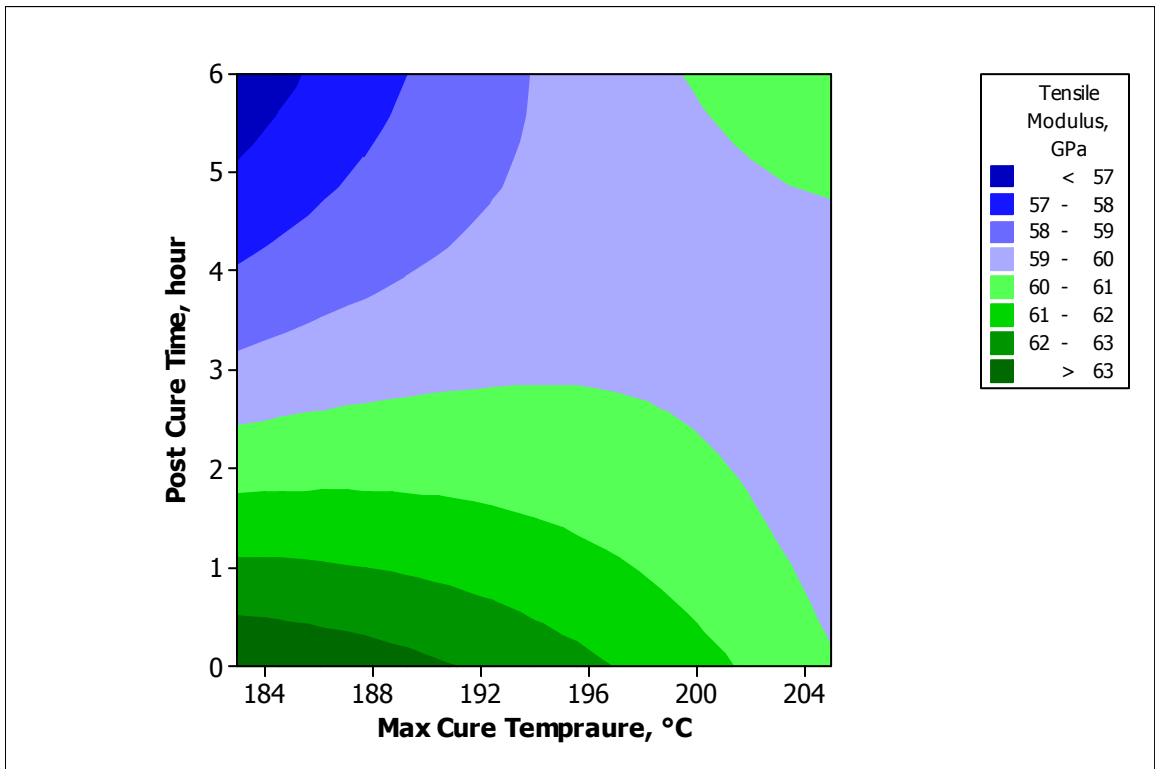


Figure A10. Contour plot of tensile modulus vs. post cure time and max cure temp.

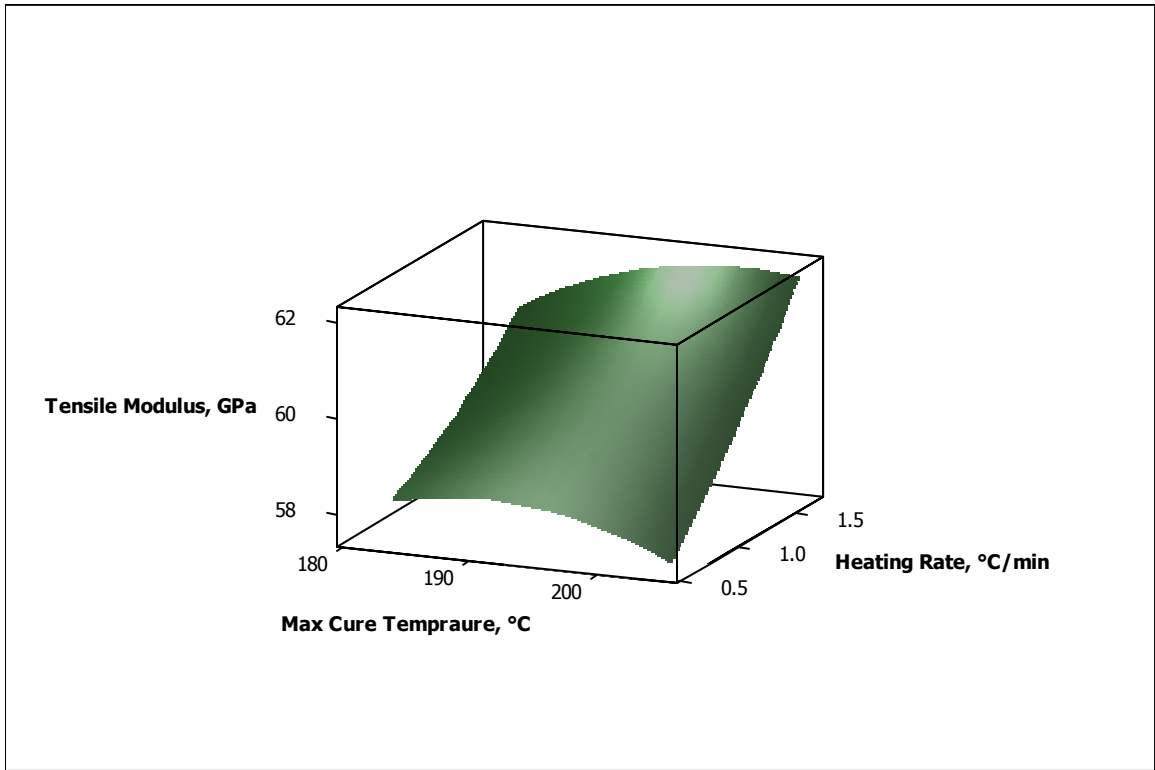


Figure A11. Surface plot of tensile modulus vs. heating rate and max cure temp.

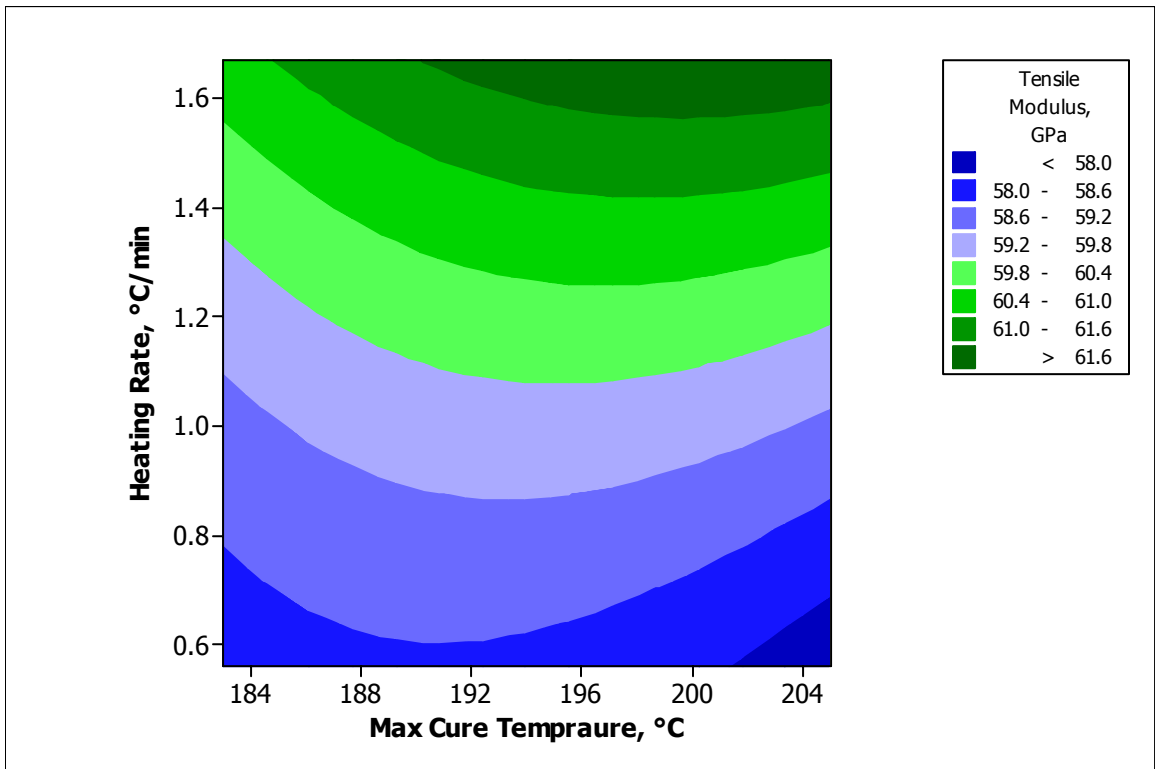


Figure A12. Contour plot of tensile modulus vs. heating rate and max cure temp.



## Appendix B

### Room Temperature Compressive Load Test Results

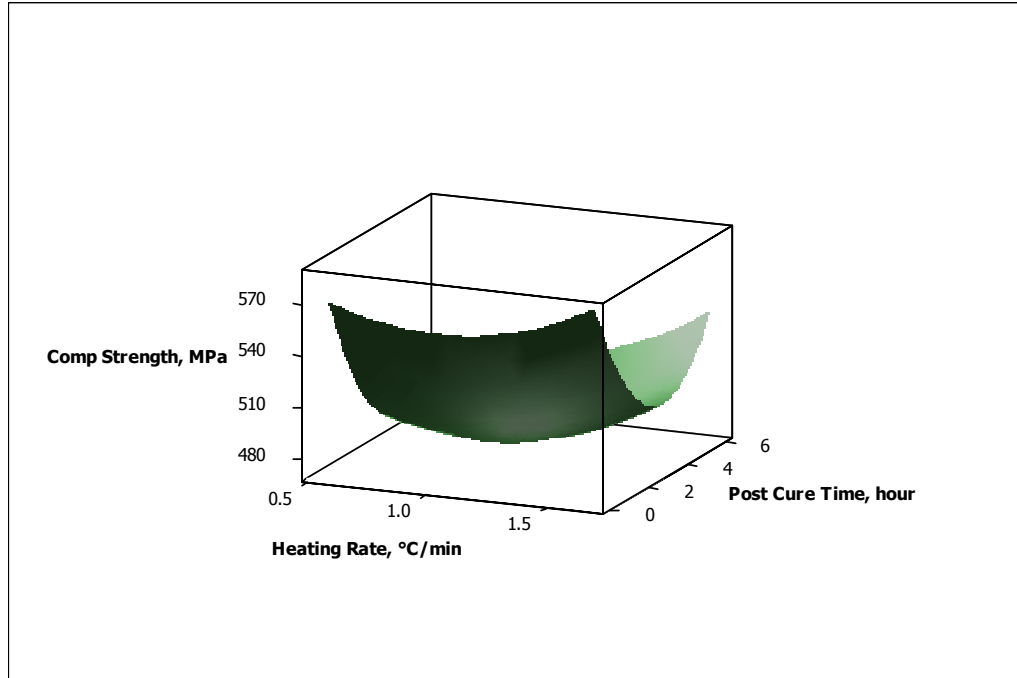


Figure B1. Surface plot of compressive strength vs. post cure time and heating rate.

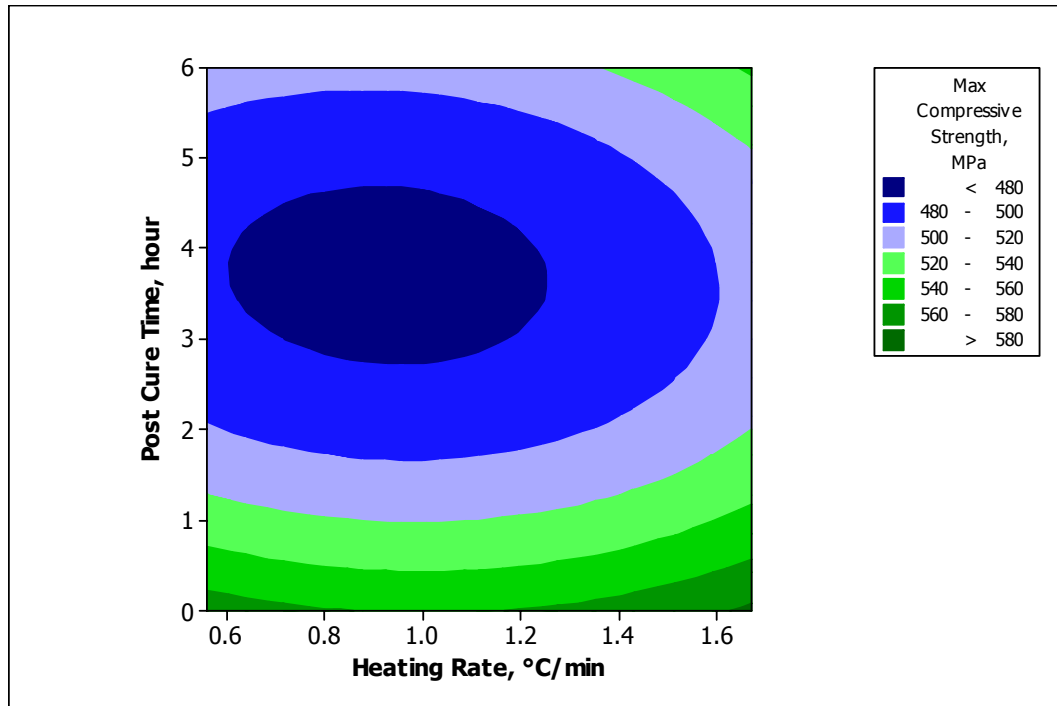


Figure B2. Contour plot of compressive strength vs. post cure time and heating rate.

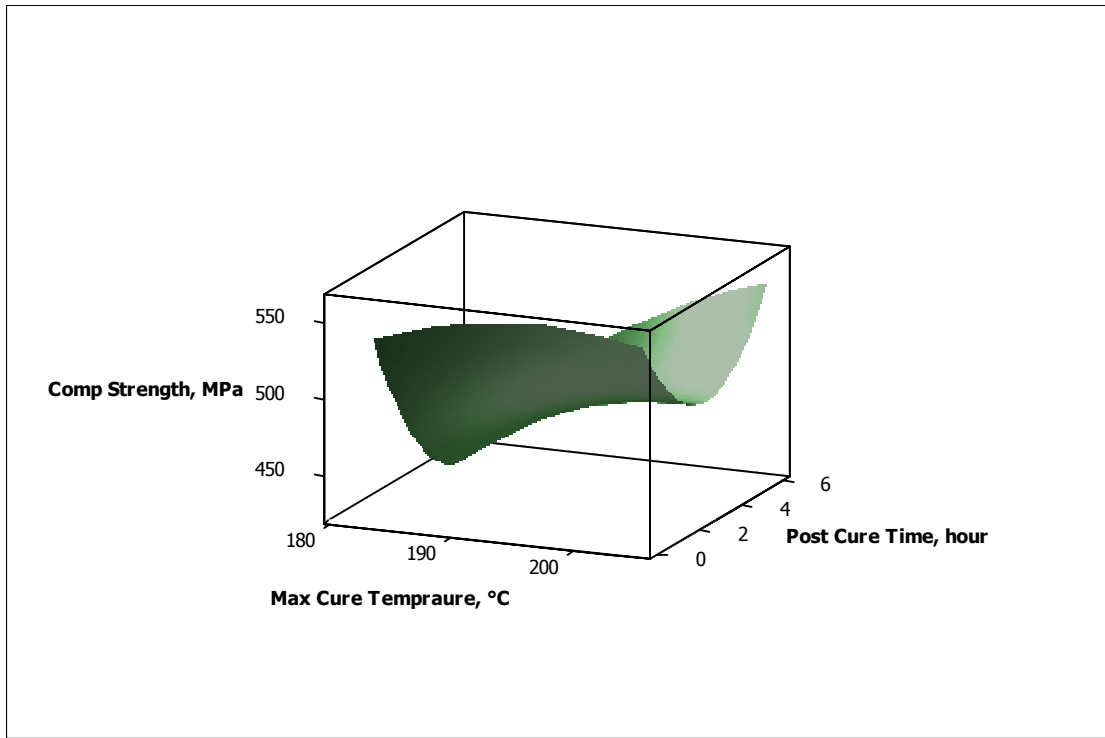


Figure B3. Surface plot of compressive strength vs. post cure time and max cure temp.

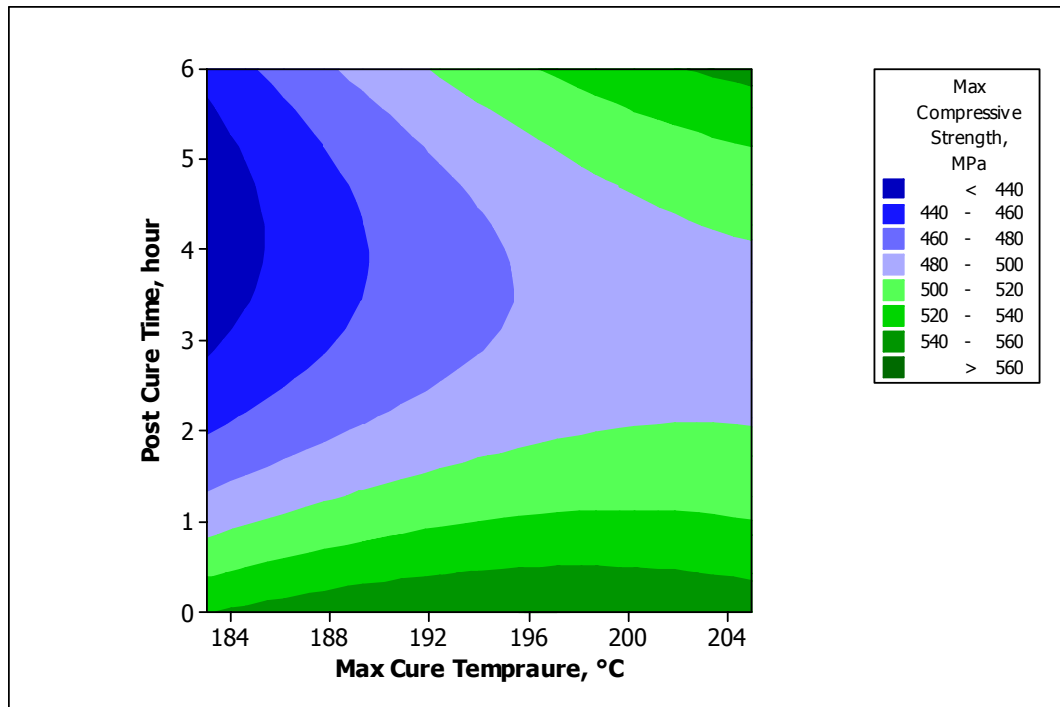


Figure B4. Contour plot of compressive strength vs. post cure time and max cure temp.

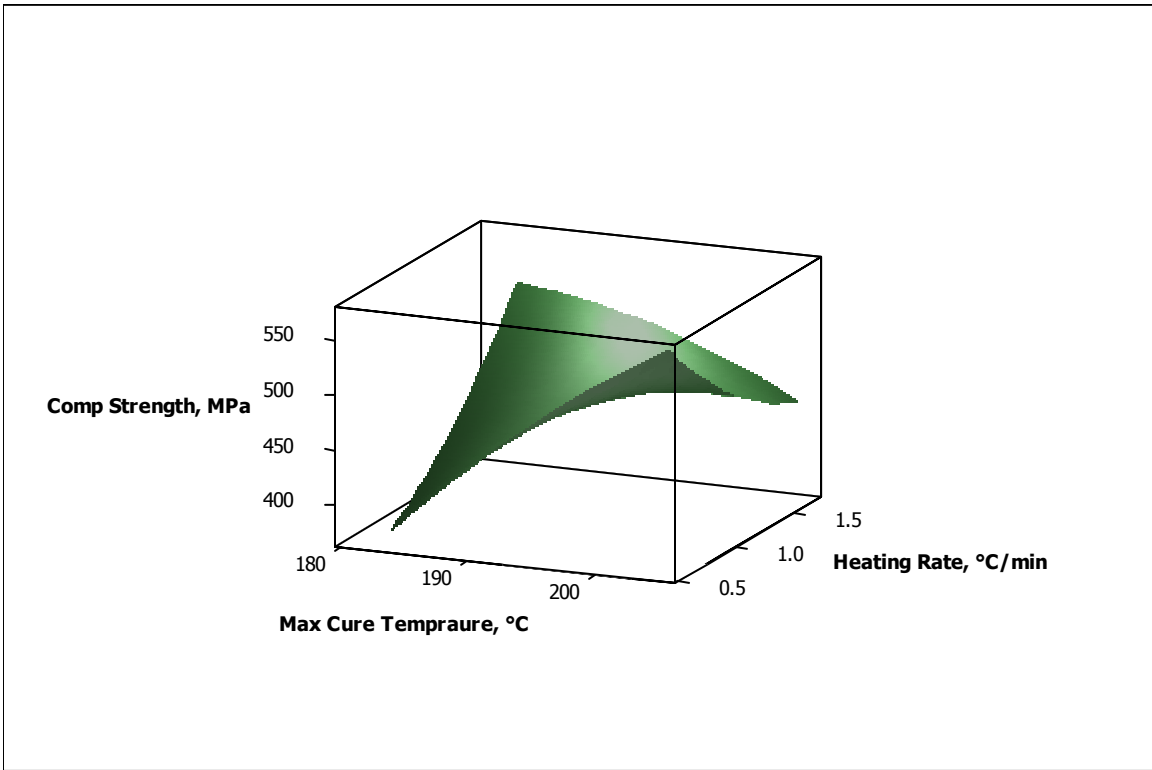


Figure B5. Surface plot of compressive strength vs. heating rate and max cure temp.

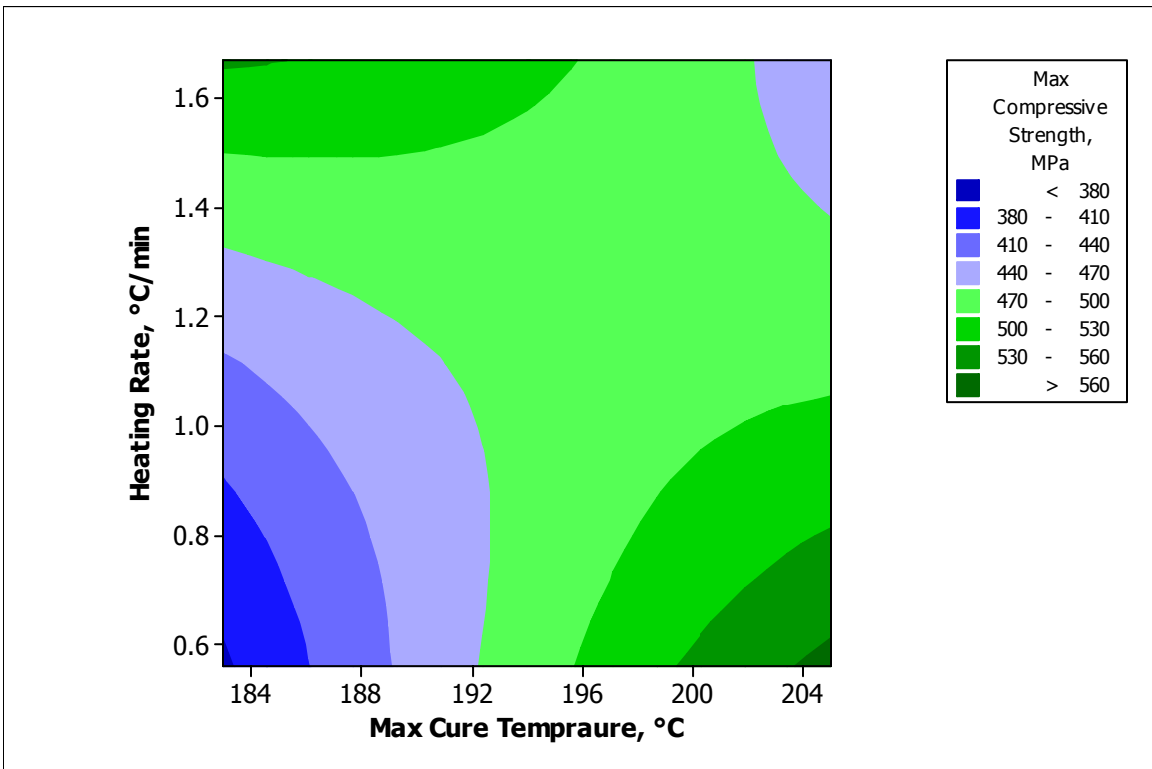


Figure B6. Contour plot of compressive strength vs. heating rate and max cure temp.

## Appendix C

### High Temperature-Dry Compressive Load Test Results

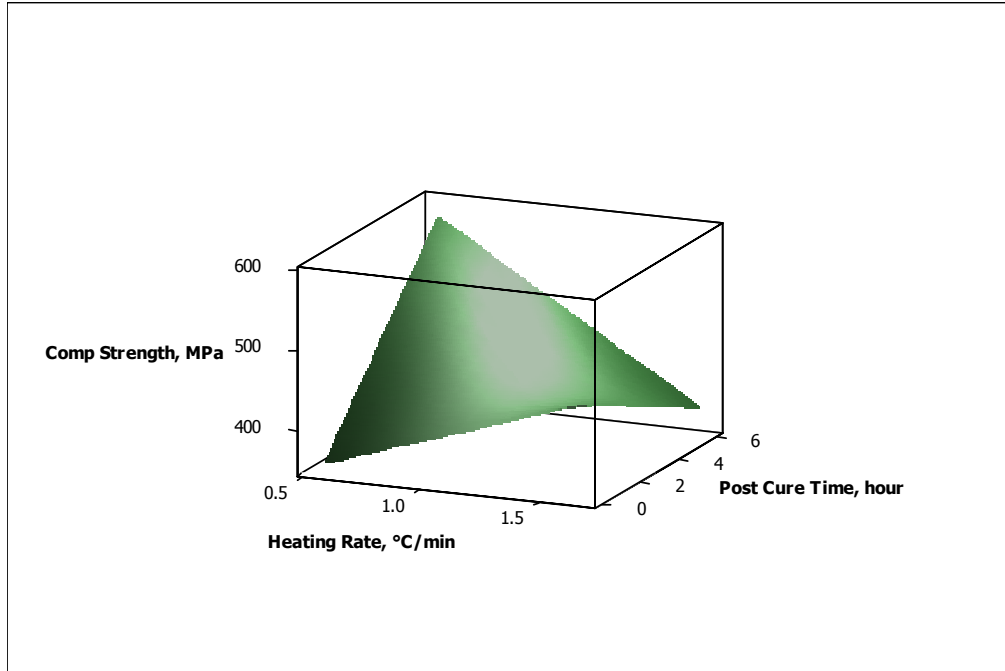


Figure C1. Surface plot of compressive strength vs. post cure time and heating rate.

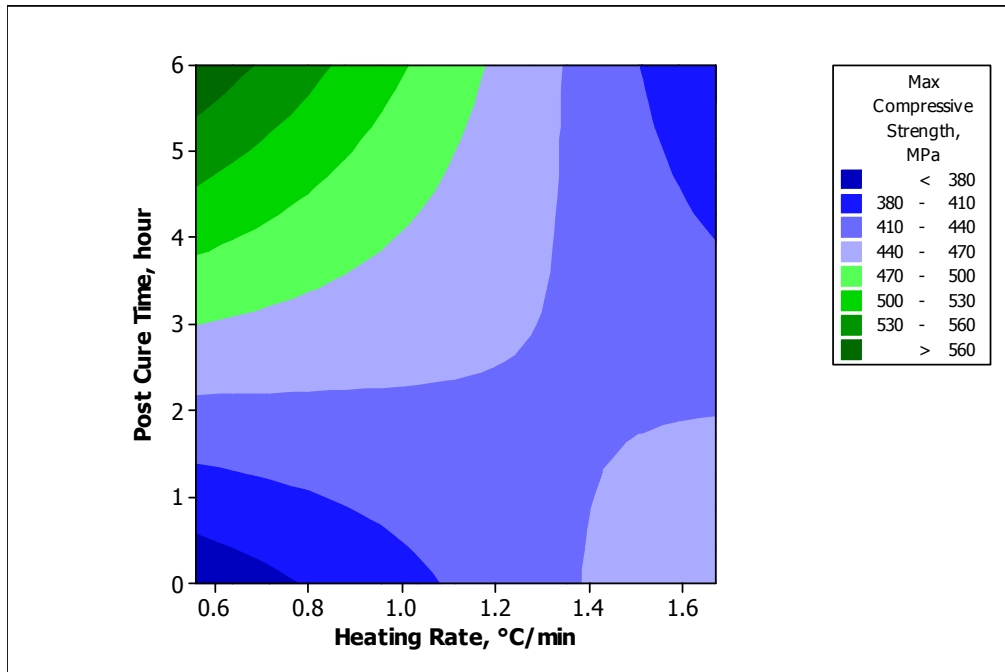


Figure C2. Contour plot of compressive strength vs. post cure time and heating rate.

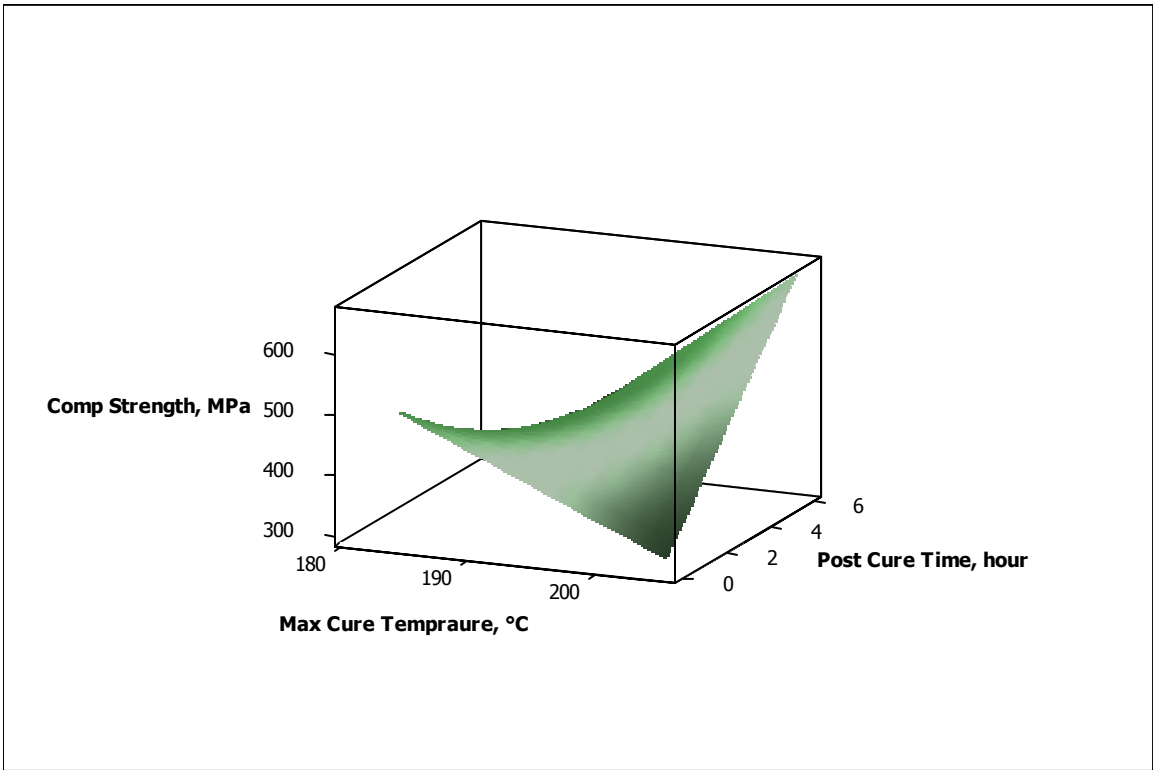


Figure C3. Surface plot of compressive strength vs. post cure time and max cure temp.

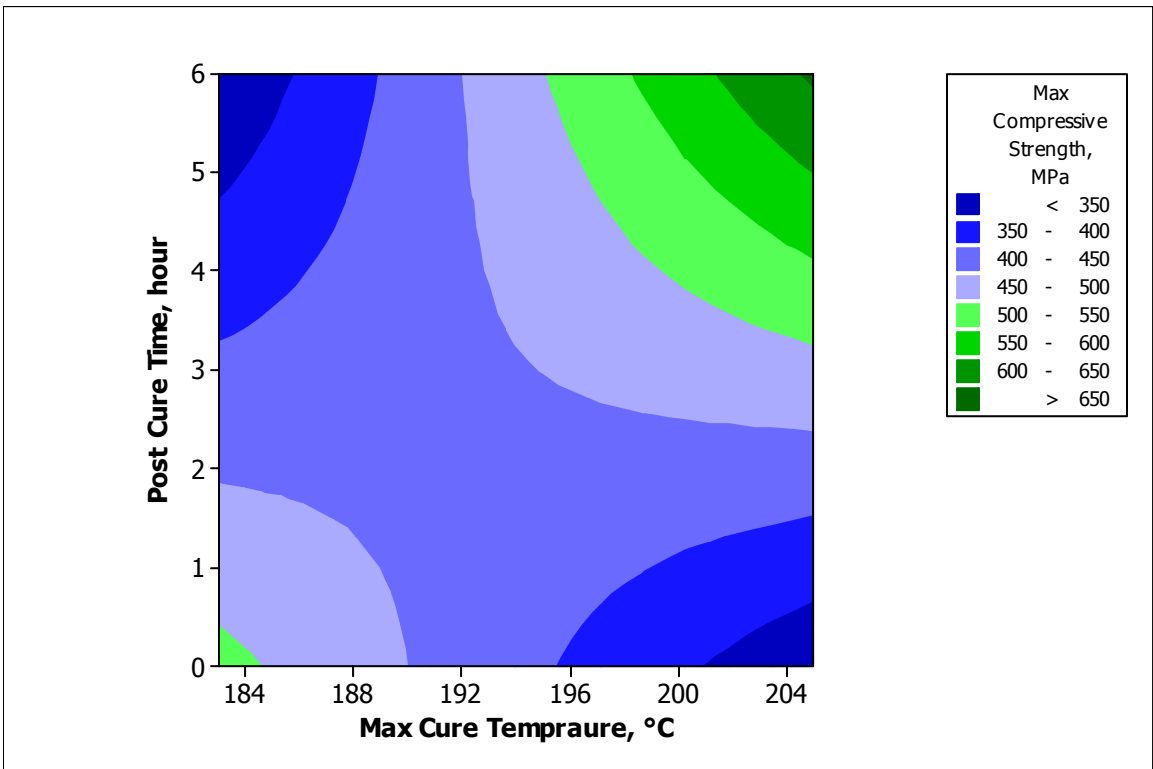


Figure C4. Contour plot of compressive strength vs. post cure time and max cure temp.

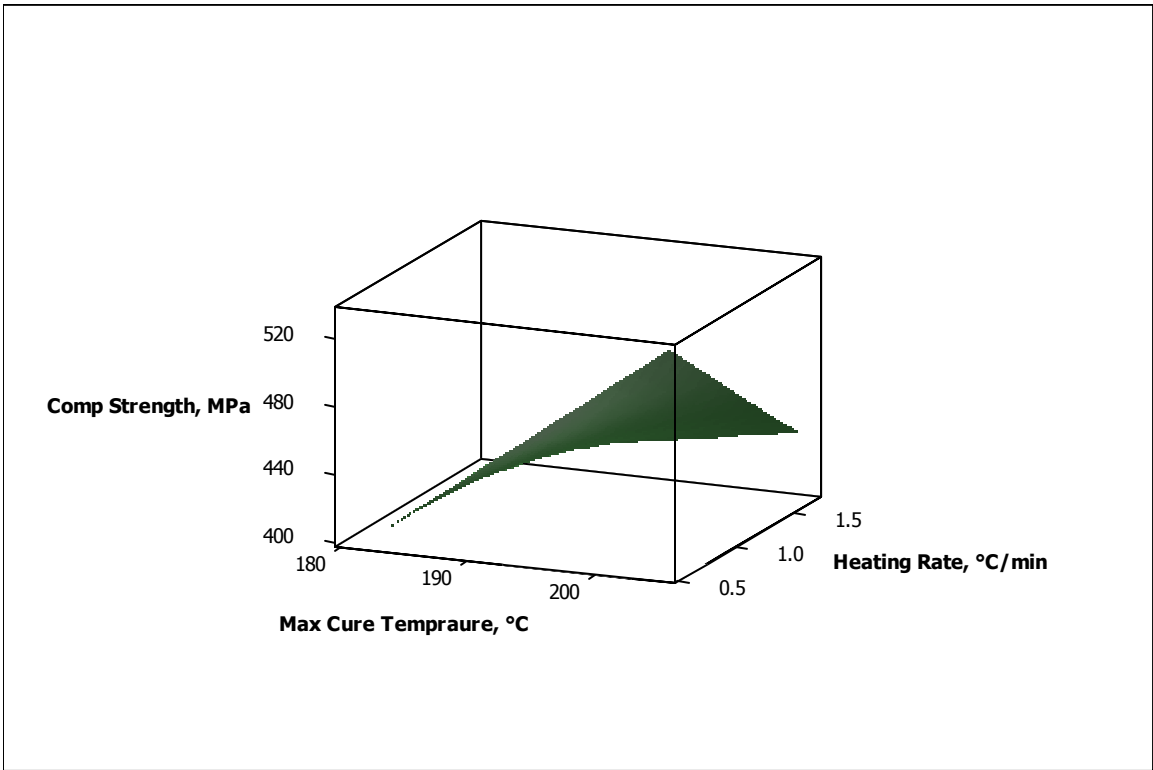


Figure C5. Surface plot of compressive strength vs. post cure time and heating rate.

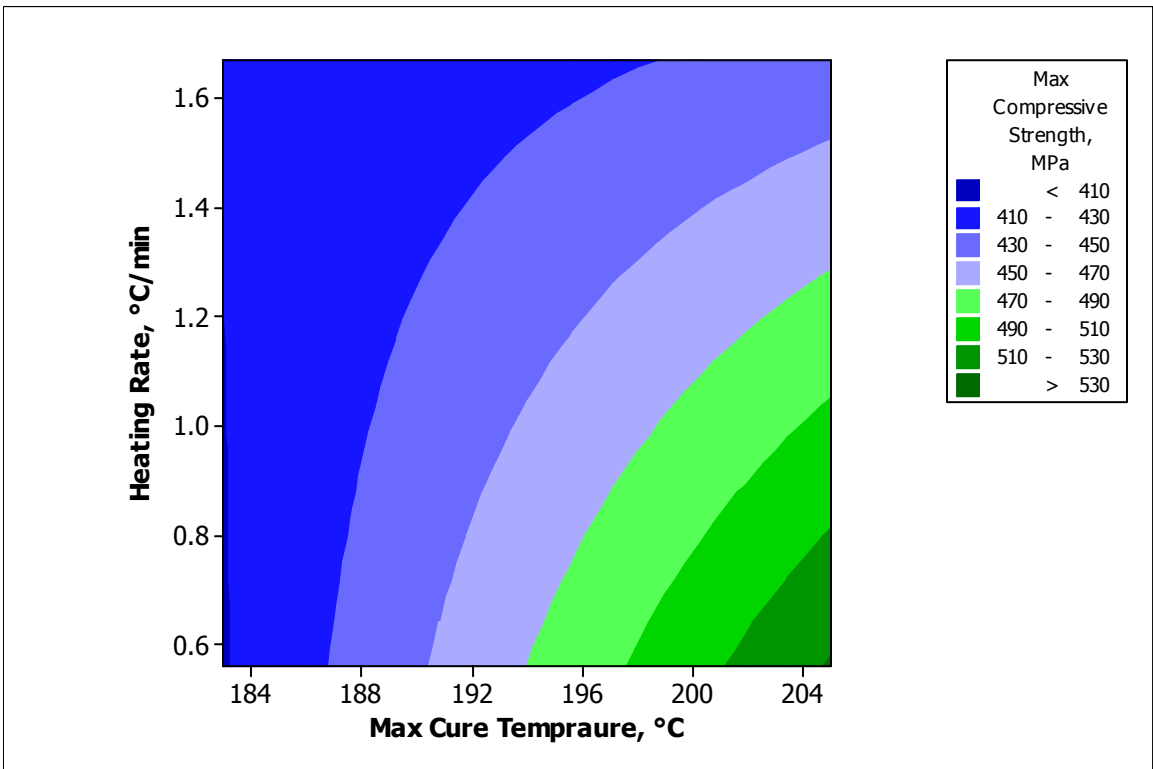


Figure C6. Contour plot of compressive strength vs. max cure temp and heating rate.

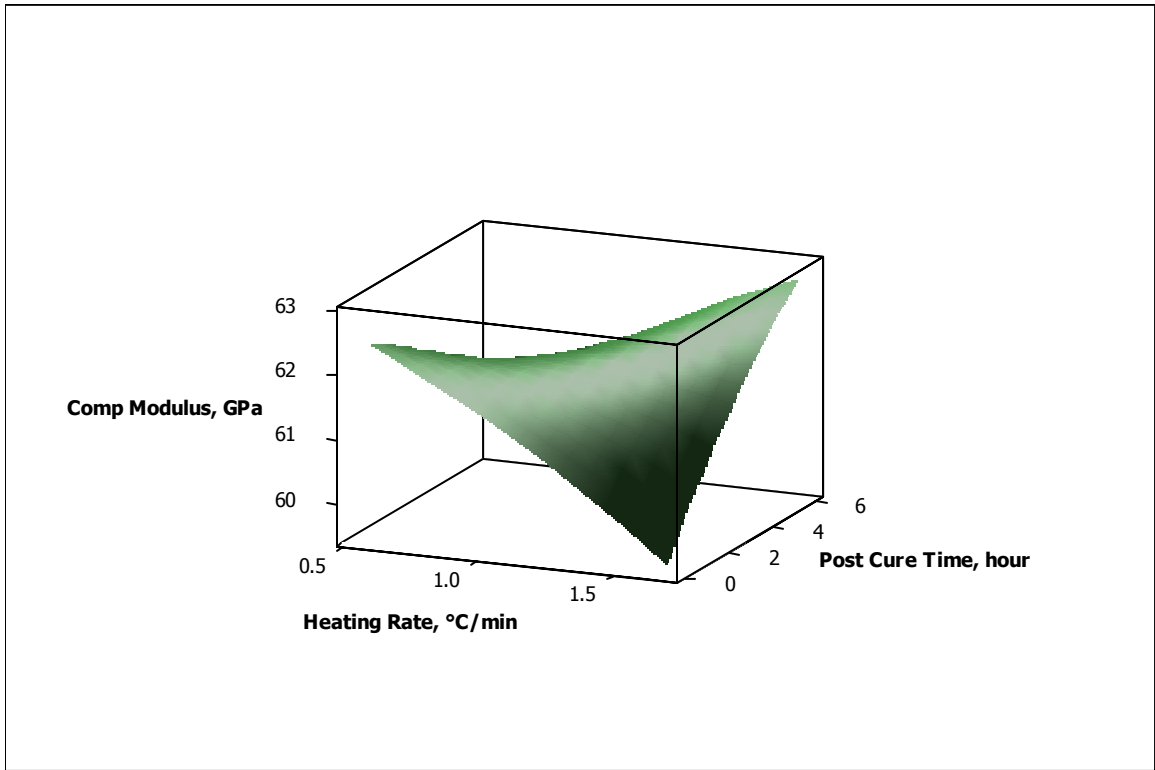


Figure C7. Surface plot of compressive modulus vs. post cure time and heating rate.

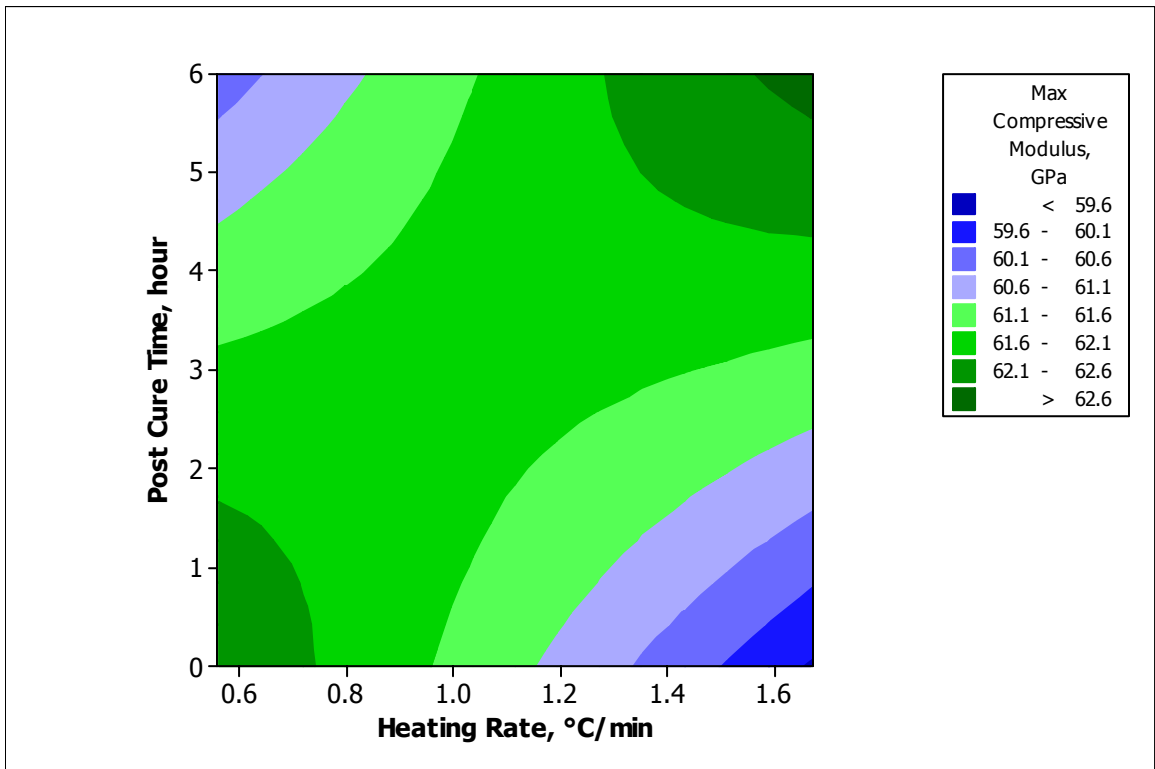


Figure C8. Contour plot of compressive modulus vs. post cure time and heating rate.

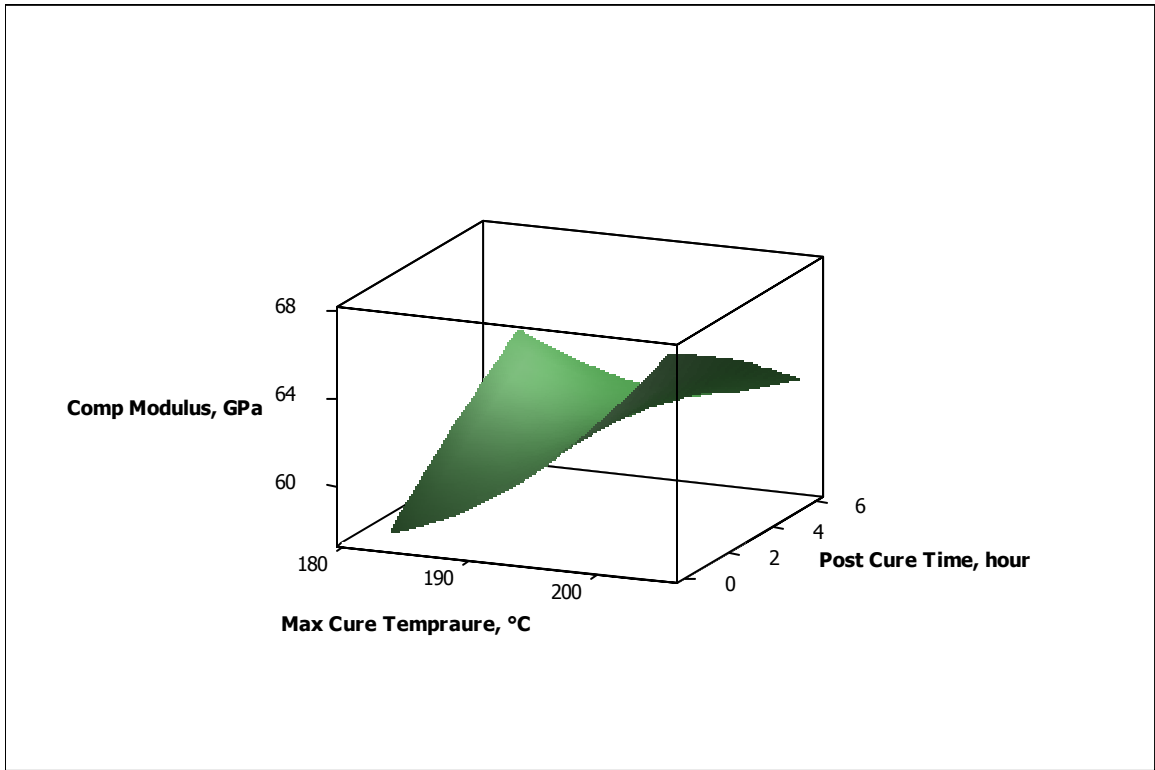


Figure C9. Surface plot of compressive modulus vs. post cure time and max cure temp.

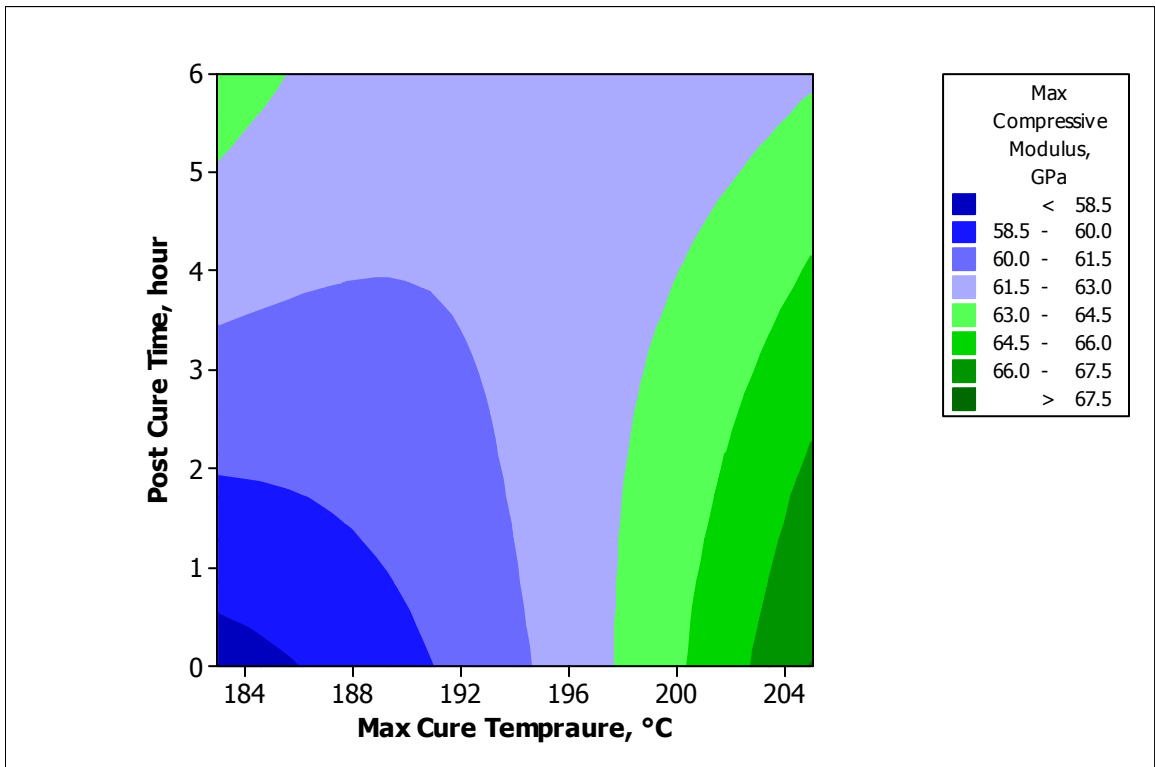


Figure C10. Contour plot of compressive modulus vs. post cure time and max cure temp.



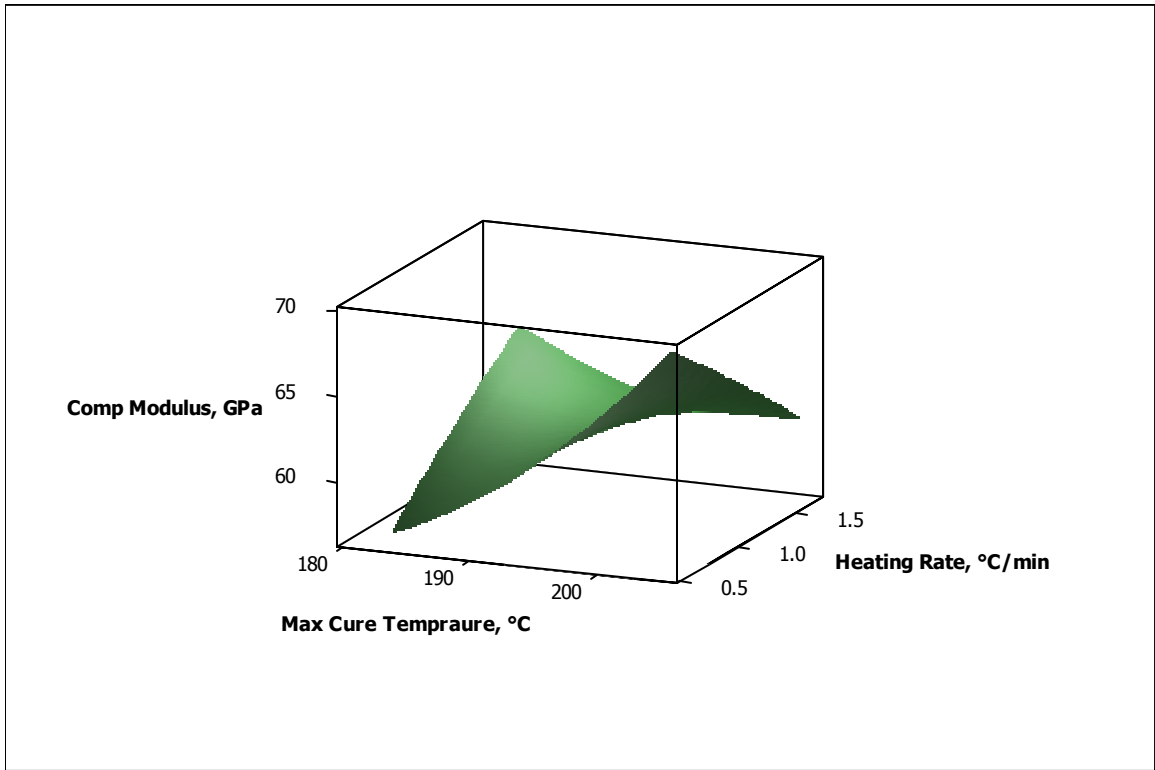


Figure C11. Surface plot of compressive modulus vs. heating rate and max cure temp.

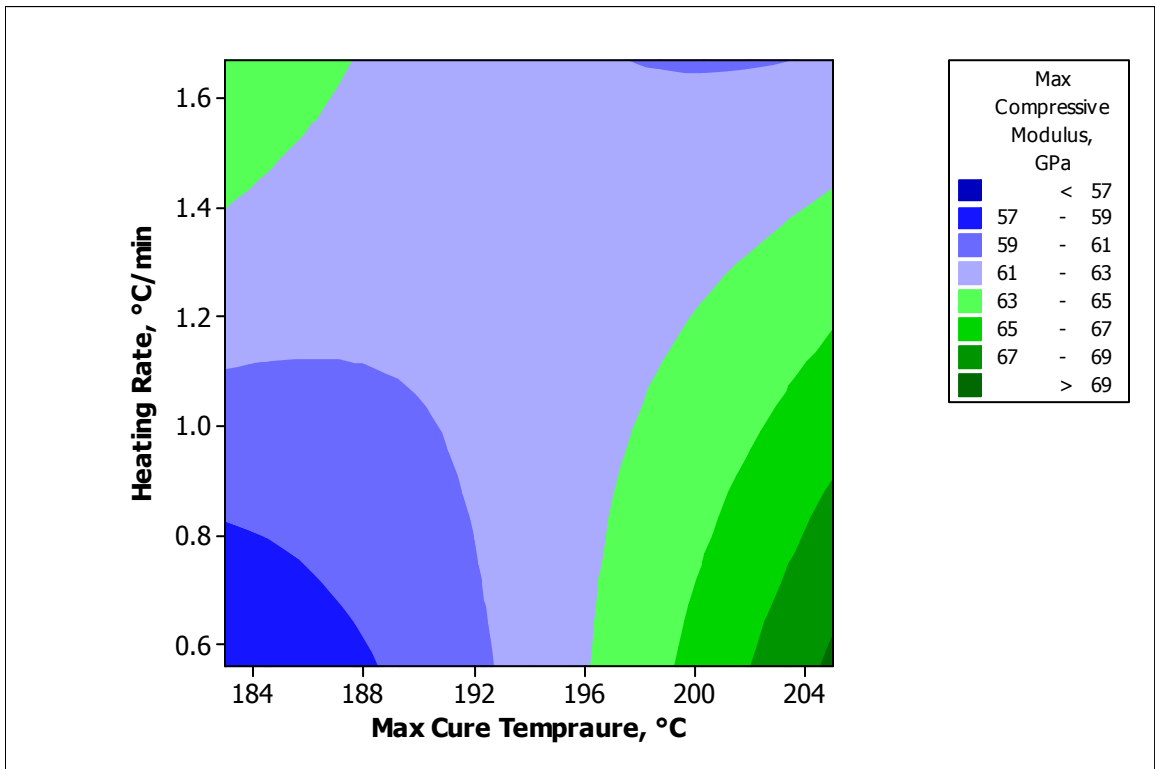


Figure C12. Contour plot of compressive modulus vs. heating rate and max cure temp.

## Appendix D

### High Temperature-Wet Compressive Load Test Results

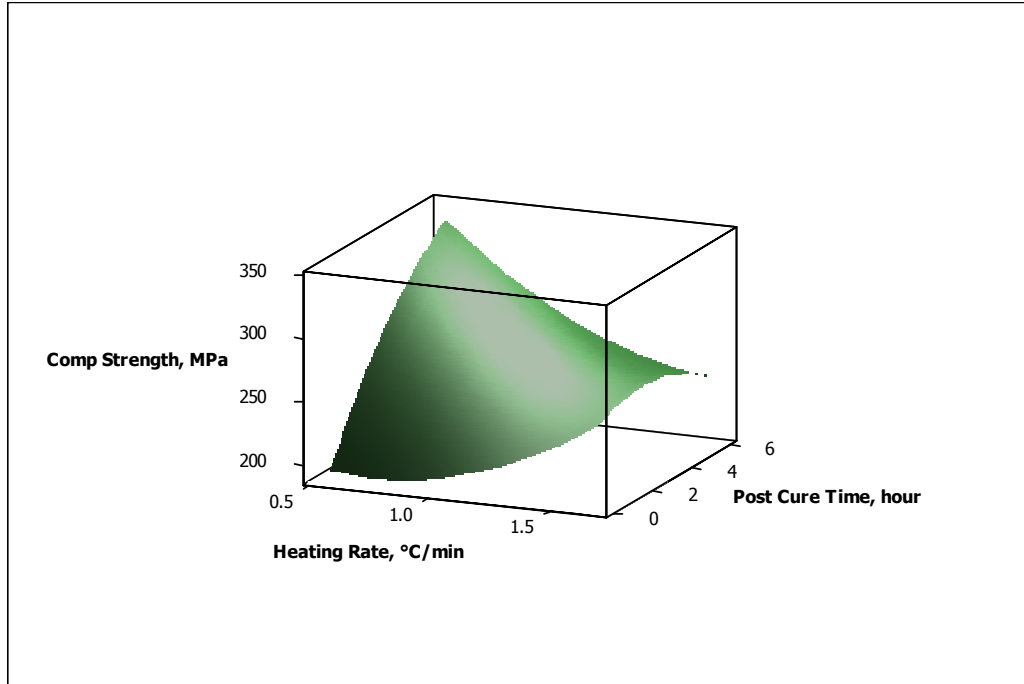


Figure D1. Surface plot of compressive strength vs. post cure time and heating rate.

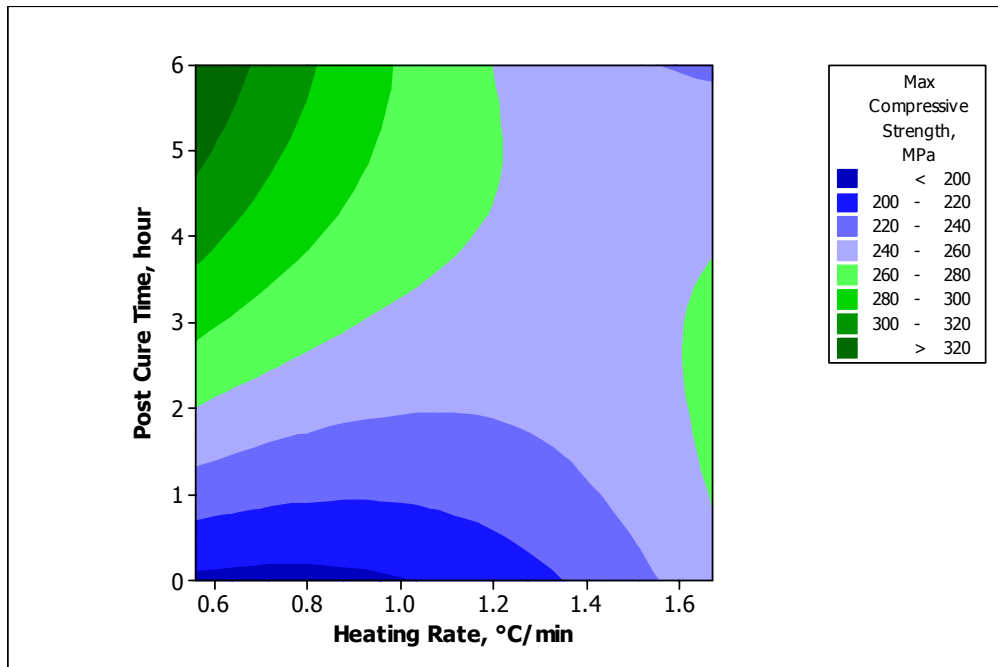


Figure D2. Contour plot of compressive strength vs. post cure time and heating rate.

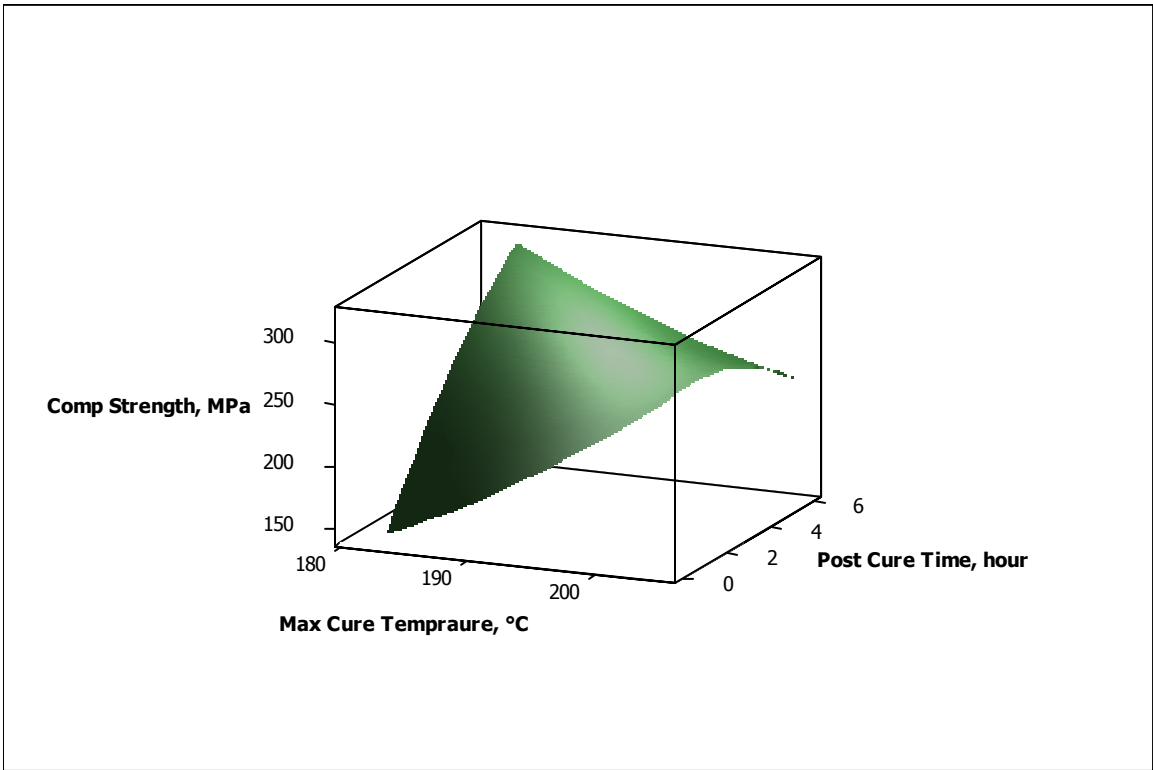


Figure D3. Surface plot of compressive strength vs. post cure time and max cure temp.

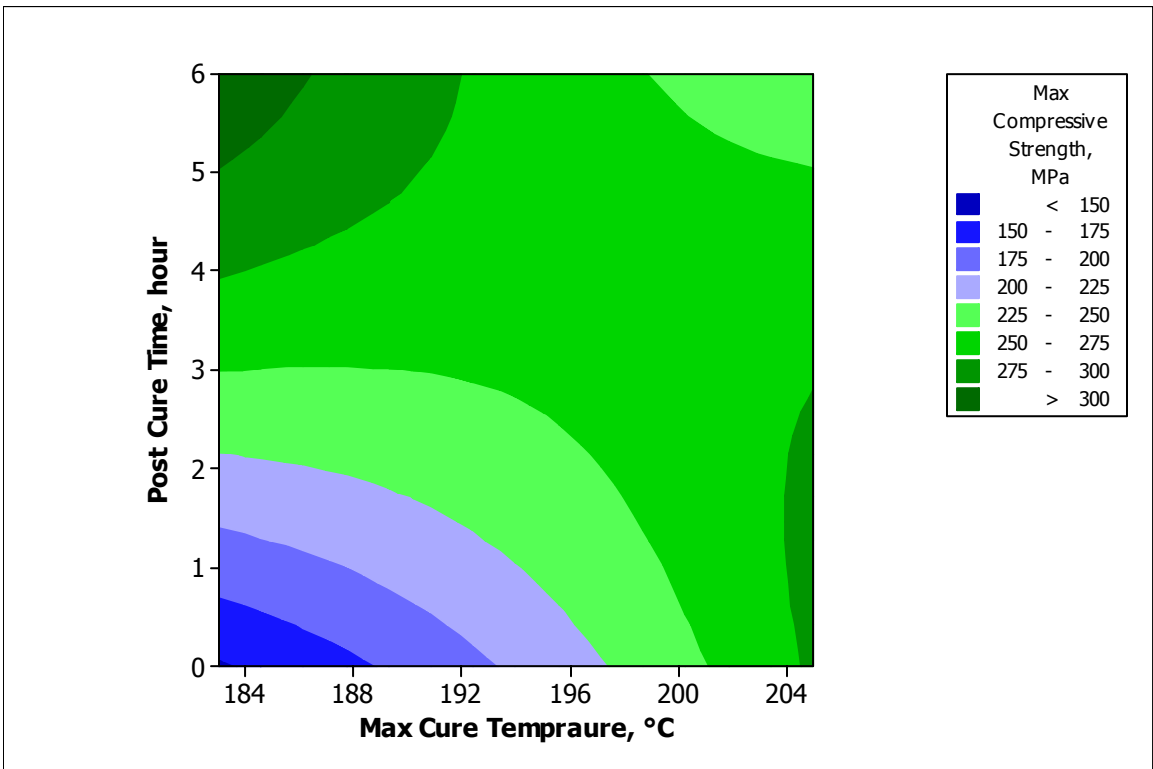


Figure D4. Contour plot of compressive strength vs. post cure time and max cure temp.

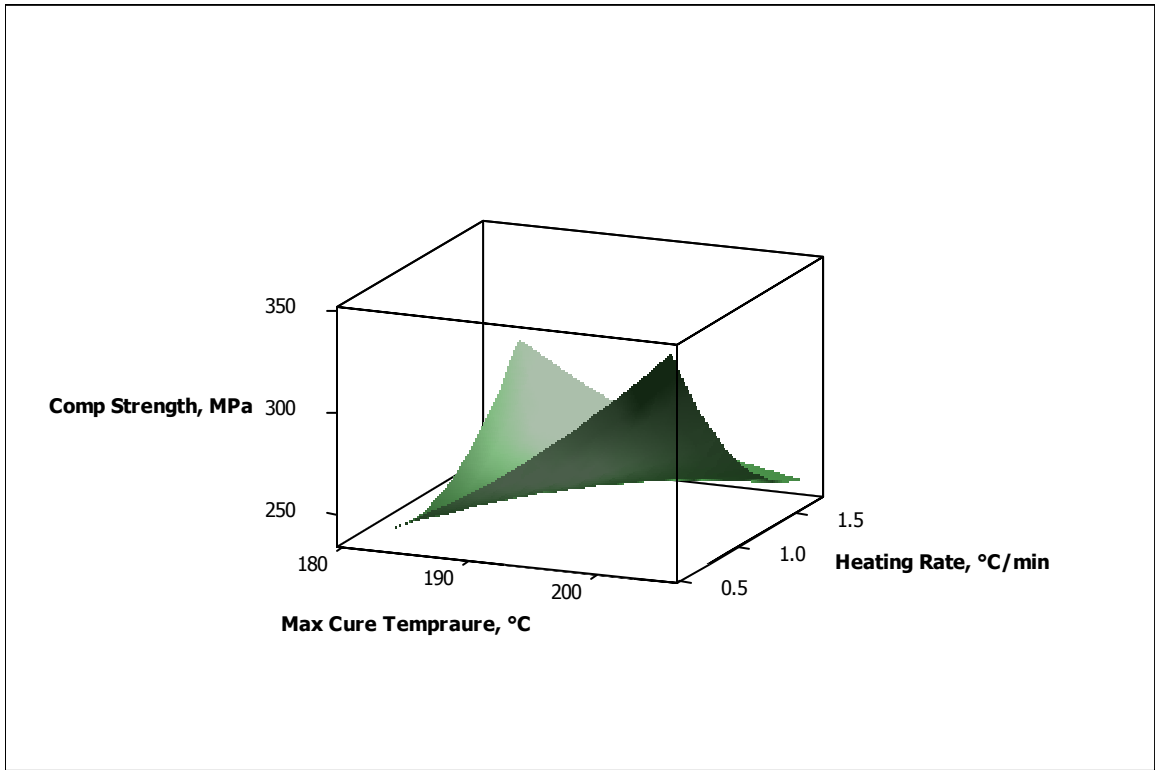


Figure D5. Surface plot of compressive strength vs. post cure time and heating rate.

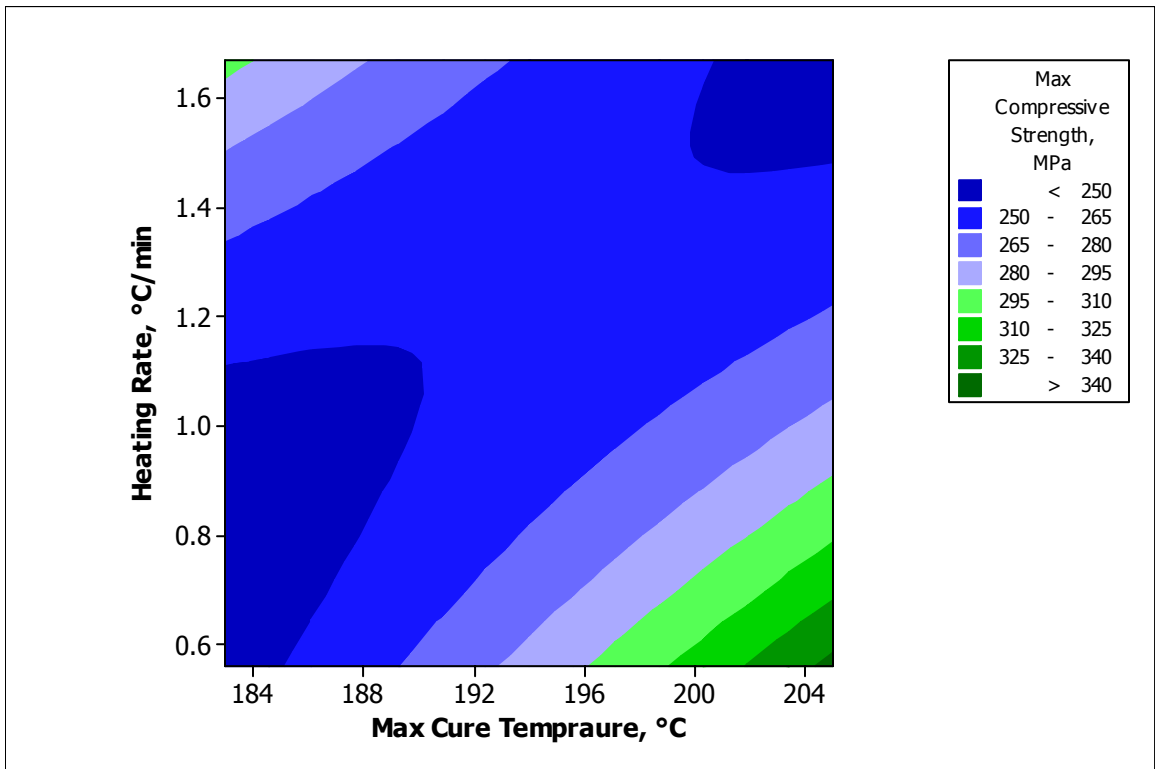


Figure D6. Contour plot of compressive strength vs. max cure temp and heating rate.

## REFERENCES

1. Pike, T., McArthur, M., Schade, D., "Vacuum Assisted Resin Transfer Molding of a Layered Structural Laminate for Application on Ground Combat Vehicles," International SAMPLE Technical Conference, Vol. 28, 1996, pp.374-380.
2. Lewit, S., Jakubowski, J., "Low Cost VARTM Process for Commercial and Military Applications," International SAMPLE Symposium, Vol. 42, 1997, pp.1173-1187.
3. Lazarus, Paul, "Resin Infusion of Marine Composites," International SAMPLE Symposium, Vol. 41, 1996, pp.1447-1458.
4. Gillio, E, Advani, S.G., Fink, B.K., and Gillespie, J.W., "Investigation of the Role of Transfer Flow in Co-injection Resin Transfer Molding," Polymer Composites, Vol. 19, 1998, pp738-749.
5. Wu, T. and Hahn, T., "Mechanical Properties of E-Glass/Vinyl Ester Composite Fabricated by VARTM," International SAMPLE Symposium, Vol. 42, 1997, pp.1-12.
6. Heider, D., Hofmann, C., and Gillespie, Jr., "Automation and Control of Large – Scale Composite Parts by VARTM Processing," International SAMPLE Symposium, Vol. 45, 2000, pp.1567-1574.
7. Advani, S.G., and Sozer, E.M., "Process Modeling in Composite Manufacturing," Marcel Dekker, Inc., New York, NY, 2003.
8. Golestanian H., and El-Gizawy, A.S., "Modeling of Process Induced Residual Stresses in Thin Molded Composites with Woven Fiber Mats," Journal of Composite Materials, Vol.35, No. 17, 2001, pp.1513-1528.
9. El-Gizawy, A. S., and Kuan, Yean-Der "Evolution and Management of Process-induced Damage in Polymer Composites", Proceedings, Global Symposium on Innovation in Materials Processing and Manufacturing, TMS Annual Meeting, New Orleans, Louisiana, February, 2001, pp.125-135.
10. Meador, M., "High Temperature Polymer-Matrix Composites", In Flight Vehicle Materials, Structure and Dynamics-Assessment and future Directions, Vol. 2, Ahmed Noor and Samuel Venneri, editors, American Society of Mechanical Engineers, 1994, pp.406-415.
11. Dillon, G., Mallon, P., and Monaghan, M., "The Autoclave Processing of Composites" In Gutowski, T.G., editor, Advanced Composites Manufacturing, John Wiley and Sons, New York, NY, 1997.

12. Lee, L.J., "liquid Composite Modeling," In Gutowski, T.G., editor, *Advanced Composites Manufacturing*, John Wiley and Sons, New York, NY, 1997.
13. A. H. Tullo, *Chem. Eng. News*, May 28, 2001, pp16.
14. Cycom 5250-4-RTM Resin System Description, Private Communication, Cytec Fiberite, Inc., July, 2002.
15. Criss, J. and Koon, R., "High temperature VARTM of phenylethynyl terminated imide composites," 33<sup>rd</sup> International SAMPE Technical Conference, 2001, pp1009-1021.
16. C. Williams, J. Summerscales, and S. Grove, "Resin infusion under flexible tooling: a review," *Composites*, 27A, 1996, pp 517-524.
17. Macro method, US patent No. 2495640, 1950.
18. W.H. Seemann, "Plastic transfer molding techniques for the production of fiber reinforced plastic structures," US patent No. 4902215, 1989.
19. Trochu, F. Gauvin, R.Gao, D –M., "Numerical Analysis of the Resin Transfer Molding Process by the Finite Element Method," *Advances in Polymer Technology*. Vol. 12, No. 4, 1993, pp.329-342.
20. A. Hammami, R. Gauvin, and F. Trochu, "Modeling the edge effect in liquid composites molding," *Composites, Part A* 29A, 1198, pp 603-609.
21. Pillai, K.M. and Advani, S.G., "Numerical Simulation of Unsaturated Flow in Woven Fiber Performs During the Resin Transfer Molding Process," *Polymer Composites*, Vol. 19, No. 1, Feb. 1998, pp.71-80.
22. Diallo, M.L., Gauvin, R., and Trochu, F., "Experimental Analysis and Simulation of Flow through Multi-layer Fiber Reinforcements in Liquid Composite Molding", *Polymer Composites*, vol. 19, No. 3, June 1998, PP.246-256.
23. Golestanian, H., and El-Gizawy, A.S., "Experimental and Numerical Modeling of Mold Filling in Resin Transfer Molding," *Polymer Composites Journal*, No.4, Vol. 19, August, 1998, pp. 359-406.
24. El-Gizawy, A.S., and Kuan, Year-Dear, "Numerical Characterization of Mold Injection in Resin Transfer Molding Process," *Advances in Polymer Technology*, Vol. 19, No. 3, Septemeber 2000, pp.173-179.
25. Hsiao, Kuang-Ting., Gillespie and Avani, S.G., "Numerical Simulation of Unsaturated Flow in Woven Fiber Performs During the Resin Transfer Molding Process," *Polymer Composites*, Vol. 19, No. 1, Feb. 1998, pp.71-80.

26. Kang, M.K., Lee, W.I., and Hahn, "Analysis of Vacuum Bag resin Transfer Molding Process," Composites, Part A: Applied Science and Manufacturing, Vol. 32, 2002, pp.1553-1560.
27. S. Jiang, C. Zhang, and B. Wang, "Optimum arrangement of gate and vent for RTM process design using a mesh distance based approach," Composites: part A33, 2002, pp 471-481.
28. B. Kim, G. J. Nam, and J. W. Lee, "Optimization of filling process in RTM using a genetic algorithm and experimental design method," Polymer composites, Vol. 23, No. 1, Feb., 2002, pp 72-86.
29. A. Gokce, K.T. Hsiao, and S. G. Advani, "Branch and bound search optimization injection gate locations in liquid composite molding processes," Composites: part A33, 2002, pp 1263-1272.
30. B. Miaie, Y.F. Chen, and A.M. Mescher, "A methodology to obtain a desired filling patten during resin transfer molding," Journal of composite materials, Vol. 36, No. 14, 2002, pp 1677-1692.
31. Jun H. Choi and C.K.H. Dharan, "Mold fill time and void reduction in resin transfer molding achieved by articulated tooling," Journal of composite materials, Vol. 36, No. 19, 2002, pp 2267-2285.
32. Jun H. Choi and C.K.H. Dharan, "Enhancement of resin transfer molding using articulated tooling," Polymer composites, Vol. 23, No. 4, August 2002, pp 674-681.
33. P. de Luca, Y. Benoit, and J. Trochon, "Coupled pre-forming/injection simulations of liquid composite molding progresses," 47<sup>th</sup> International SAMPLE symposium, 2002, pp 1307-1316.
34. L. Joubaud, and F. Trochu, "Simulation of the manufacturing of an ambulance roof vacuum assisted resin infusion (VARI)," Composites-2002, Composites fabricators association, 2002.
35. Adel Hammami, "Key factors affecting permeability measurement in the vacuum infusion molding process," Polymer composites, Vol. 23, No. 6, 2002, pp 1057-1067.
36. White, S. R. and Hahn, H.T., "Process Modeling of Composite Materials: Residual Stress Development During Cure. Part I. Model Formulation," Journal of Composite Materials, vol. 26, No. 16, 1992, pp.2402-2422.

37. White, S. R. and Hahn, H.T., "Process Modeling of Composite Materials: Residual Stress Development During Cure. Part II. Experimental Validation," *Journal of Composite Materials*, vol. 26, No. 16, 1992, pp.2423-2453.
38. White, S. R. and Hahn, H.T., "Cure Cycle Optimization for Reduction of Processing-Induced Residual Stresses in Composite Materials," *Journal of Composite Materials*, vol. 27, No. 14, 1993, pp.1352-1378.
39. Golestanian, H., and El-Gizawy, A.S., "Cure Dependent Lamina Stiffness Matrices of Resin Transfer Molded Composite Parts," *Journal of Composite Materials*, No. 23, Vol. 31, 1997, pp.2402-2423.
40. Osswald, Tim A., Sun, Esther M., and Tseng, Shi-Chang, "Experimental Verification on Simulation Shrinkage and Warpage of Thin Compression Molded SMC Parts," *Polymers & Polymer Composites*, Vol. 2, No. 3, 1994, pp. 187A-198A.
41. Bogetti, Travis A. and Gillespie, John W. Jr., "Process-Induced Stress and Deformation in Thick-Section Thermosetting Composite Laminates," *Journal of Composite Materials*, Vol. 26, No. 5, 1992, pp.626-658.
42. Tseng, Shi-Chang and Osswald, Tim, A., "Prediction of Shrinkage and Warpage of Fiber Reinforced Thermoset Composite Parts," *Journal of Reinforced Plastics and Composites*, Vol. 13, 1994, pp.698-721.
43. Loos.A.C., Sayer, J., McGrane, R., and Grimsley, B., "VARTM Process Model Development," *International SAMPLE Symposium*, Vol. 461, 2001, pp. 1049-1060.
44. Y.K. Kim and I.M. Daniel, "Cure cycle effect on composite structures manufactured by resin transfer molding," *Composite materials*, Vol. 36, No. 14, 2002, pp 1725-1743.
45. Dillon, G., Mallon, P., and Monaghan, M.: *Advanced Composites Manufacturing*, John Wiley and Sons, New York, NY, 1997.
46. Meyers, R.H., Montgomery, D.C., "Response Surface Methodology: Process and Product Optimization Using Designed Experiments," John Wiley and Sons, New York, Ny, 1995.
47. Y. Luo, I. Verpoest, K. Hoes, M. Vanheule, H. Sol, and A. Cardon, "Permeability measurement of textile reinforcements with several test fluids," *Composites-part A: applied science and manufacturing*, v32, 2001, pp 1497-1504.
48. D. L. Youngs, "Time Dependant Multi Material Flow Distortion," In K. W. Morton and M. J. Baines, *Academic Press*, 1982.



49. Srinivasan, R., Wang, T., and Lee, L., "Chemorheology of High Temperature RTM Resins," 53<sup>rd</sup> Society of Plastics Engineers, ANTEC Technical Conference, 1995, pp3016-3029.
50. Ito, Makoto, and Chou, Tsu-Wei, "An Analytical and Experimental Study of Strength and Failure Behavior of Plain Weave Composites," *Journal of Composite Materials*, Vol. 32, No. 1, 1998, pp.2-30.
51. Jones, Robert M., "Mechanics of Composite Materials," Taylor & Francis, Philadelphia, PA, 1999, pp. 151-157.
52. Kaw, K., "Mechanics of Composite Materials," CRC Press, New York, 1997, pp.174-178.
53. Patanakar, S. V., "Numerical Heat Transfer and Fluid Flow," McGraw-Hill, New York, 1980, pp.59-61.
54. Product data sheet of Magmamite AS4 Carbon Fiber, provided by Hexcel Schwebel, 2005.
55. Li, Chao, "Experimental and Analytical Investigation of Failure Behavior in Satin-Weave Composites and Uni-Weave Satin-Weave Hybrid Composites," Dissertation, Texas A&M University, 2001.
56. Loos, C., and Springer, S., "Moisture Absorption of Graphite-Epoxy Composites Immersed in Liquid and in Humid Air," *Journal of Composite Materials*, v13, 1979, pp.131-147.
57. Collings, T.A., "The Effect of Observed Climatic Conditions on the moisture Equilibrium Level of Fiber-Reinforced Plastics," *Composites*, Jan 1986, pp.33-41.
58. Shen, Chi, and Springer, S. "Moisture Absorption and Desorption of Composite Materials," *Journal of Composite Materials*, v10, 1976, pp.2-20.
59. Lincoln, E., and Morgan, J., Shin, E., "Moisture Absorption-Network Structure Correlations in BMPM/DABPA Bismaleimide Composite Matrices," *Journal of Advanced Materials*, v32, No. 4, 2000, pp.24-34.
60. Springer, S., and Tang, Jian-Mao, "Accelerated Environmental Testing of Composites," *Journal of Composite Materials*, v21, 1987, pp.225-242.
61. Ju, J. and Morgan, R.J., "Characterization of Microcrack Development in BMI-Carbon Fiber Composite under stress and Thermal Cycling," *Journal of Composite Materials*, v38, 2004, pp. 2007-2024.

62. He, Y., Zhong, Y. and Zhou, J., "Post-Curing Effects on Physical and Mechanical Properties of IM7/5250-4 Composites," 30<sup>th</sup> International SAMPE Technical Conference, 1998, pp. 226-233.
63. Antony, Jiju, "Design of Experiments for Engineers and Scientists," Butterworth-Heinmann, Burlington, MA, 2003.
64. Montgomery, C., "Introduction to Statistical Quality Control," John Wiley & Sons, New York, 1996.
65. Hodgkinson, J.M., "Mechanical Testing of Advanced Fiber Composites," Woodhead Publishing Limited, Cambridge, England, 2000.
66. Adams, D.F. and Welsh, J.S., "The Wyoming Combined Loading Compression Test Method," Journal of Composites Technology and Research, JCTRE, 19(3), 197, pp. 123-133.
67. Li, R.B., "Moisture Absorption and Hygrothermal Aging in a Bismaleimide Resin and its Carbon Fiber Composites," Dissertation, Univ. of Michigan, 2001.
68. Wright, W.W., "The Effect of Diffusion of Water into Epoxy Resins and their Carbon-Fiber Reinforced Composites," Composites, July 1981, pp.201-205.
69. Biney, O. and Zhong, Y., "Hydrolytic Effects on the Properties of Graphite/BMI Composites," 43<sup>rd</sup> International SAMPE Symposium, 1998, pp.120-129.
70. Biney, O. and Wilson, E., "Hygrothermal Effects on the Thermal and Mechanical Properties of IM7/5250-4 Composites," 44<sup>th</sup> International SAMPE Symposium, 1999, pp.734-740.
71. Zhong, Yang, and He, Yu, "Short-Term aging effects on Thermal and Mechanical Properties of IM7/5250-4 Composites," 44<sup>th</sup> International SAMPE Symposium, 1999, pp.741-747.
72. Bechel, T., and Fredin, B., "Combined Cryogenic and Elevated temperature cycling of Carbon/polymer Composites," 47<sup>th</sup> International SAMPE Symposium, 2002, pp.808-819.
73. Morgan, J., and Ju, Jaehyung, "Characterization of BMI-Carbon Fiber Composite Microcrack Development Under Thermal Cycling," Society of Plastics Engineers, ANTEC Technical Conference, 2003, pp.2059-2063.
74. Walker, Sandra, "Thermal Effects on the Compressive Behavior of IM7/PETI5 Laminates," Journal of Composites Materials, v38, No. 2, 2004, pp.149-162.

## VITA

Ahmed Khattab was born on November 27, 1966 in Alexandria, Egypt. He received his B.S. degree in Mechanical Engineering from Faculty of Engineering-Alexandria University, Egypt in 1990. He joined CATERPILLAR Inc. dealer in Egypt for one year as a Maintenance Engineer. Then he worked as a Researcher for nine years at the Research Center of Arab Academy for Science and Technology, Alexandria-Egypt. He earned his Master degree in Mechanical Engineering from Faculty of Engineering-Alexandria University, Egypt in 1998.

In summer 2000, he went to the United States of America to pursue his Ph.D. from University of Missouri-Columbia. Ahmed is married to Eman Matter and he is a father of two boys, Karim and Khaled.